



HAL
open science

Collective behaviour of active colloids

Isaac Theurkauff

► **To cite this version:**

Isaac Theurkauff. Collective behaviour of active colloids. Soft Condensed Matter [cond-mat.soft].
Universite Claude Bernard Lyon 1, 2013. English. NNT: . tel-01370597

HAL Id: tel-01370597

<https://theses.hal.science/tel-01370597>

Submitted on 23 Sep 2016

HAL is a multi-disciplinary open access archive for the deposit and dissemination of scientific research documents, whether they are published or not. The documents may come from teaching and research institutions in France or abroad, or from public or private research centers.

L'archive ouverte pluridisciplinaire **HAL**, est destinée au dépôt et à la diffusion de documents scientifiques de niveau recherche, publiés ou non, émanant des établissements d'enseignement et de recherche français ou étrangers, des laboratoires publics ou privés.

THÈSE DE L'UNIVERSITÉ DE LYON

Délivrée par

L'UNIVERSITÉ CLAUDE BERNARD LYON 1

ÉCOLE DOCTORALE DE PHYSIQUE ET D'ASTROPHYSIQUE DE LYON

DIPLÔME DE DOCTORAT

(arrête du 7 aout 2006)

Soutenue Publiquement le 29 novembre 2013

par

ISAAC THEURKAUFF

Collective Behavior of active colloids.

Directeurs de Thèse :

CÉCILE COTTIN-BIZONNE et LYDERIC BOQUET

JURY : M. ROBERTO DI LEONARDO (rapporteur)

M. LUDOVIC BERTHIER (rapporteur)

M. DENIS BARTOLO

M. JULIEN TAILLEUR

M. OLIVIER DAUCHOT

M. FRÉDÉRIC CAUPIN

M. CHRISTOPHE YBERT

This thesis is licensed under the Creative Commons Attribution-Share Alike 2.0 Generic license. You are free:

- to share – to copy, distribute and transmit the work
- to remix – to adapt the work

Under the following conditions:

- attribution – You must attribute the work to its author.
- share alike – If you alter, transform, or build upon this work, you may distribute the resulting work only under the same or similar license to this one.

All figures reproduced in this thesis from other sources are not released under the creative commons license, and remain under the license in their respective sources.

This pdf document was compiled with pdflatex, MikteX 2.9. It contains transparency info and modern formatting parameters, It requires a modern pdf viewer, such as Foxit versions 6.0.6 and up, or adobe reader versions 11 and up. Hyperlinks for various videos and web resources are embedded in the text, however, they will probably only work for a limited period of time, as they point to non long-term maintained websites.

Introduction

A curious observer might spend hours watching the hypnotic flights of swallows above the roofs of our cities. Beyond their showmanship at acrobatic flying, their twittering calls distorted by the Doppler effect, a most striking feature of these flights is the presence of collective effects, especially before the autumn migrations. As the days become shorter and temperatures decrease, the swallows regroup to form clouds containing up to hundreds of thousands swallows. The behavior of an individual swallow inside such a cloud is very different from its behavior alone. It follows its neighbors, and has a much more directed flight. On the scale of the cloud of swallows itself mesmerizing waves propagate. These features have a size comparable to the size of the cloud, up to hundreds of meters, but the individual is only able to see the other birds when they are close.

Hiking in the Pyrenees offers many observations of the collective behavior of herds of sheep. While grazing sheep are very randomly oriented, as the herding dogs gather them for the daily milking, they spontaneously organize in an oriented herd. Similarly to the previous example, the sheep only sees its neighbors, but the collective orientation spans hundreds or thousands of individuals.

Ants, Bees, Fish, Humans; all social species present on the planet demonstrate collective behavior. An assembly of individuals undergoes collective behavior when the behavior of an individual in the assembly is very different from the behavior of the individual alone. Scientists alone in the coffee room, fortunately behave very differently from the same scientists mosh-pitting during heavy-metal concerts. The interaction between individuals is often short-ranged, but the collective behavior, waves, vortices, flocks, can have sizes comparable to the whole assembly. We wish to limit the study of collective effects to effects that are not linked to the social structure, but rather emergent behavior, in which all individuals have equivalent or almost equivalent roles. Indeed, the ordered march of battalions on July 14th is by no means a spontaneous emergent behavior. Similarly, horse or cattle herds, when called by presenting food, have a behavior that is defined by external constraint and hierarchy in the herd rather than an emergent behavior. Although

the interplay between external constraints and activity is very interesting, we limit ourselves to the study of systems where the ordering comes from interparticle interactions rather than external constraints.

All these systems present strikingly similar features: oriented assemblies, dense clusters, lanes formation, long range positional, polar, or nematic order. By the nature of interactions, the physical causes of collective effects are very different. Bacteria interact through hydrodynamics and chemical signals, while birds only see and hear each other. This suggests that underlying fundamental principles exist that describe and predict the emergence of collective effects based not on a specific description of the interactions, but on general systematic properties, whose nature still has to be determined. Conserved quantities such as number density¹, or total kinetic energy, or other more system-specific observables, probably play a key role.

The key question is then to find the *generic observables*² and the *simplest theory*³ based on those observables that gives rise to collective effects. What we are searching for are therefore the *sufficient conditions* for the emergence of collective effects.

The first step might be similar to what was done in statistical physics. In this branch of physics the large number of particles and a very schematic view of their interactions is enough to model the equilibrium behavior of very different systems, e.g. ultra-cold atomic gas, electrons in semiconductors, or liquids close to a critical point. All collective effects share similar properties. The first is that, being collective, a large assembly of individuals is required. Then all individuals are active in the sense that they dissipate energy, either stored internally, or harvested in the environment. Hence the generic term “active matter” proposed for this class of systems. A theory of active matter based on statistical physics ideas could be possible, however, new observables should be introduced to take into account the activity.

In order to find those generic parameters, for a first approach, we have to restrict our very broad objectives, and will study in this thesis active matter at the colloidal scale, while of course keeping in mind that we seek the most generic conclusions. Biological systems are complicated,

¹Which is not always a constant, for example in systems of multiplying cells or bacterias

²As mentioned before we want generic observables, such as individual velocities, polarity, or energy dissipation, rather than an accurate description of a system. Thus specific descriptions such as flagella description, a description of chemical signaling, and the specific biologic pathways, for a bacterial system; or a description of flight mechanics and response to neighbors for a system of birds, are ruled out as being too specific to have any easy generalization.

³The simplicity criterion is known as Occam’s razor: the simplest theory, in the sense of that which makes as few assumption as possible is the best.

in the sense that their behavior can be difficult to predict; bacteria have a complex biological response to the chemical signals they send in the medium. We thus need simpler systems, physical model systems. The interaction between individuals in physical system is often simpler, and better known than that of biological systems. Active systems such as vibrated granular at the macroscopic scale, or active colloids⁴ at the colloidal scale, have been used since the beginning of the century as active model systems, and macroscopic systems have recently shown collective behavior. In this thesis, we present the development of a new active system made of gold-platinum active colloids, and the observations of their collective effects.

These colloids have interesting and novel collective behavior. When active, that is self propelled by the addition of peroxide fuel in the observation chamber, they form dynamic clusters that continuously exchange particles with one another, that move and collide, that spontaneously divide, and fuse with other clusters⁵. Our goal with this system is first and foremost to observe and quantify collective effects, since this has not yet been achieved for colloidal systems. Then it is to find the most basic observables that describe the system, and to compare these with the wealth of theoretical and numerical knowledge that has been developed in the past decade. We will follow an approach similar to what is done in numerical simulations, by tracking individual particles and resolve the individual dynamics to measure, from the microscopic level, macroscopic observables.

This thesis comprises four chapters, which are as independent from each other as possible.

In a first chapter, I will present the state of the art at the beginning of my PhD, pertaining to collective effects, both macro- and microscopic; a brief and partial review of the experimental and theoretical work that predates this thesis. It will be a sort of snapshot of the state of research on active matter circa 2010. We try to focus on observables and theoretical frameworks that are widely used, and I will always present theories as emerging from experiments, trying to answer experimental questions.

The second chapter is mostly technical, and presents the experimental developments performed during this thesis, from chemical synthesis of gold colloids, to camera interfacing, from particle tracking to differential dynamic microscopy. It contains as much as possible, all details necessary to reproduce the experiments whose results are described in the next

⁴Asymmetric micrometer-scale colloids in an isotropic energy field, such as chemical fuel, have spontaneous directional motion along the asymmetry axis.

⁵You can already watch Sup Mat movies 5-7. Do not yet take care about the length and time scales, simply observe at different speeds the formation, and destruction of clusters.

chapters.

The third chapter describes the static and dynamic properties of the cluster phase. The static properties are its structure, the size of the clusters, and especially the way these quantities change with respect to activity. The dynamical properties are translation and rotation velocities, who also change with activity.

The last chapter presents a generic thermodynamical approach. We try to measure an equation of state for a system of active colloids undergoing a phase transition in a sedimentation experiment. We use the low density gas phase as a thermometer, and describe the system using very generic observables, such as pressure, temperature, and density.

Supplemental material: our experiment produces beautiful movies that really help the reader understand the behavior of our system. Although the paper version has no embedded movies, we give links to experimental movies to illustrate the dynamics of our system.

At this address you should find the following movies:

This Dropbox archive contains low resolution movies

This Btsync key opens a folder with high resolution movies :

B2TE6B5SJP36B7EQ3NFI3FF6MRSJDIDEV

The file contains 9 movies totaling ~ 2 GB of data. Please bear in mind that my server only has 300kB/s upload speeds.

A web-server should be up at some point to offer high quality service.

Résumé

Il peut sembler étrange de résumer en dix pages un projet de recherche s'étalant sur trois années. Ce résumé ne peut se substituer à la thèse elle-même, ni à son introduction. Il faut plutôt le considérer comme un guide de lecture, dont le but est d'aider le lecteur à naviguer parmi les chapitres afin de picorer les informations qui l'intéressent.

Cette thèse s'intéresse à deux grandes questions, auxquelles nous tenterons d'apporter quelques éléments de réponse. La première motivation, assez simple à comprendre est l'étude des effets collectifs. Considérons un ensemble d'éléments autonomes, par exemple, un troupeau de moutons ou un banc de poissons ou encore un biofilm⁶ bactérien. Lorsque l'interaction entre les individus devient suffisamment forte, le comportement de l'individu devient déterminé par ses voisins. Le mouton dans un troupeau, l'hirondelle lors de la migration, l'humain entrant dans un métro à l'heure de pointe, se comportent très différemment en assemblée que lorsqu'ils sont seuls.

Pourquoi l'étude des effets collectifs est-elle importante ? La beauté des formes que prend un vol d'oiseaux pourrait être une motivation suffisante, mais des motivations plus applicatives existent, car comprendre les foules humaines pourrait permettre d'organiser les transports de manière plus efficace, ou d'évacuer plus rapidement les bâtiments en cas d'incendies. Comprendre les effets collectifs à l'échelle du micron pourrait faciliter les cultures des micro-algues qui synthétisent les biocarburants, ou des bactéries qui fabriquent nos médicaments.

Comment cette thèse s'inscrit-elle dans cette étude ? L'observation d'effets collectifs semblables (formation de troupeaux⁷, arrangements or-

⁶Il s'agit d'une assemblée très dense de bactéries, leur comportement est souvent très différent, la reproduction bactérienne est ralentie, ce qui en fait une assemblée très résistante aux attaques externes.

⁷La plaine est vaste, mais pour se déplacer, les bisons se regroupent en assemblées denses, se touchant presque.

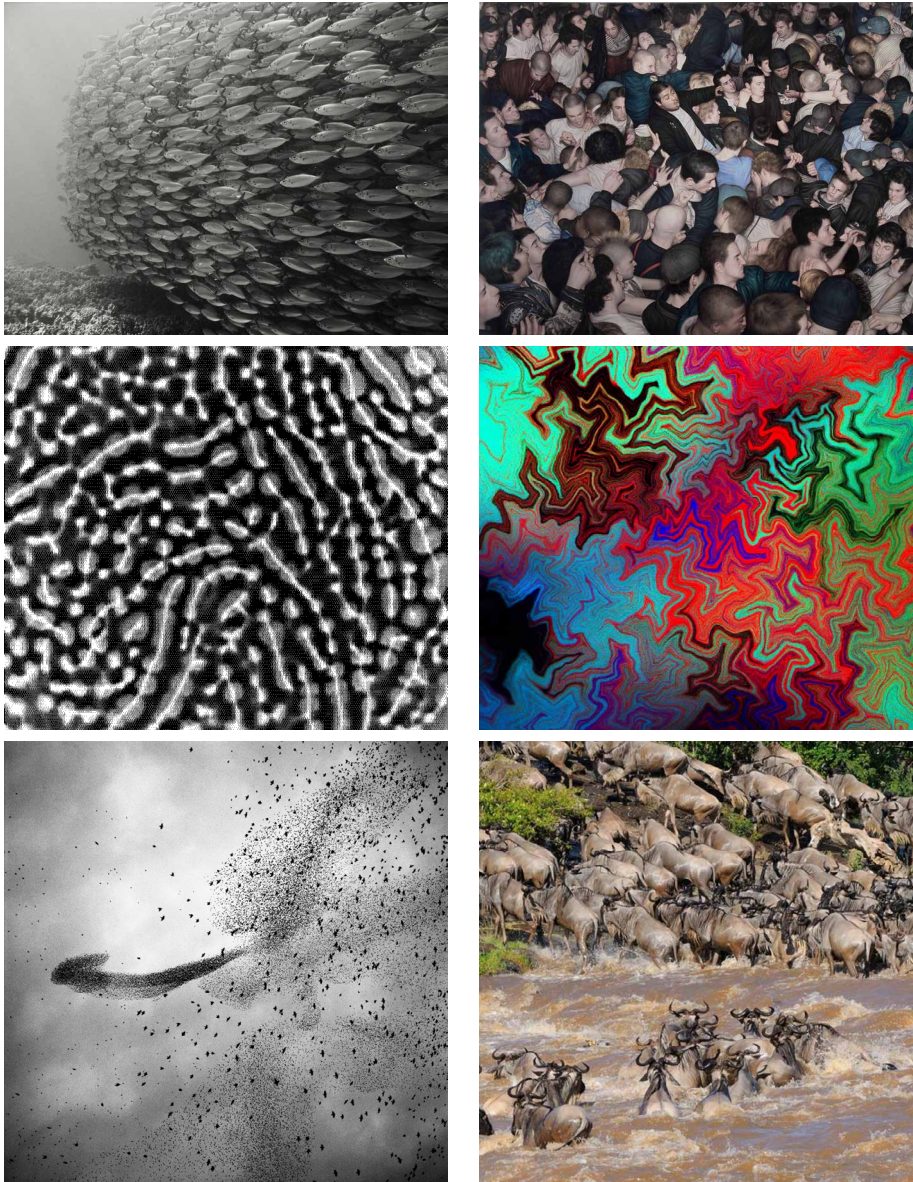


FIGURE 1 – Effets collectifs : Banc de poissons (SteveD/Wikipedia), foule dans un concert, probablement de musique baroque (Dan Witz), bioconvection dans une assemblée de bactéries [1], auto-organisation fractale dans une assemblée de cellules [2], vol de passereaux (Paolo Patrizi), Troupeau de gnous traversant une rivière, en bien meilleur ordre que les métallex ci-dessus (Gerard David).

donnés⁸, ordre nématique⁹, turbulence¹⁰) dans des systèmes très différents, permet de penser que les phénomènes physique permettant l'émergence de ces comportements collectifs sont universels, et communs à tous les systèmes. Il est donc nécessaire de trouver les paramètres génériques communs à tous ces systèmes, et de discriminer entre les paramètres spécifiques au système, et ceux qui sont communs entre les différents systèmes. L'étude de systèmes naturels, biologiques, se limite souvent à des observations¹¹, où il est difficile de contrôler les paramètres que l'on croit importants. Pas facile d'imposer aux oiseaux de ralentir ! Aussi est-il important de développer des systèmes physiques modèles, des systèmes pour lesquels on doit pouvoir contrôler facilement la vitesse, la densité... tous les paramètres qu'on estime entrer en compte dans les effets collectifs. Si de tels systèmes existent à l'échelle macroscopique, ils étaient encore inconnus au début de cette thèse à l'échelle micrométrique, particulièrement intéressante pour l'étude des bactéries ou des micro-algues. Cette thèse présente le développement de colloïdes auto-propulsés, et va ensuite décrire et analyser leur comportements collectifs.

Une seconde problématique qui est liée aux effets collectifs est celle, plus générale, de la thermodynamique hors équilibre, et plus spécifiquement, de la thermodynamique loin de l'équilibre. Replaçons rapidement cela dans son contexte. La thermodynamique est conçue par ses fondateurs¹² à la fin du 18^e siècle comme réellement dynamique : l'objectif est de rendre compte des transferts de chaleur et des transformations parfois rapides et brutales de la matière comme dans les machines à vapeur. Ces situations sont souvent très loin de l'équilibre, un état stationnaire idéal, de durée infinie qui par nature interdit tout changement. Dès la première moitié du 19^e siècle, les difficultés rencontrées¹³ font préférer une thermodynamique plus simple, qui se contente de donner les relations entre états d'équilibres. Pour rendre compte des transformations rapides, la notion de

⁸Colonnes de fourmis, vols d'oiseaux sauvages, des formes géométriques régulières sont utilisées par les animaux

⁹Les individus du système ont une orientation semblable, mais pas de position bien définie, c'est par exemple le cas pour un troupeau de moutons ; presque tous les moutons vont dans la même direction.

¹⁰Des tourbillons apparaissent dans le système, par exemple dans un banc de poissons, ou dans une assemblée de bactéries

¹¹En effet il est souvent possible d'étudier l'effet de l'environnement sur ces systèmes, mais la modification des acteurs, requise pour une compréhension fine des phénomènes en jeu est souvent difficile.

¹²Parmi lesquels nous ferons figurer en tête Lavoisier[3], Gay-Lussac, Biot, Fourier[4], qui s'intéressent à la nature de la chaleur bien avant Carnot ou Kelvin.

¹³D'après C. Truesdell[5, 6], historien des sciences et chercheur en physique statistique, c'est la paresse, la bêtise et l'incapacité mathématique des grands thermodynamiciens (Duheim, Carnot & Co), qui empêche la thermodynamique d'avancer. Si la méchanceté du propos déshonore son auteur, l'analyse historique qu'il présente est riche, et sa grossièreté, amusante.

transformation quasistatique, infiniment lente, et toujours arbitrairement proche de l'équilibre, est souvent utilisée. Ce modèle est très loin de ce qu'avaient imaginé les fondateurs, mais son efficacité lui fait dominer la thermodynamique pour de nombreuses années. Il est certain que la thermodynamique hors équilibre, c'est à dire l'étude des échanges d'énergie loin de l'équilibre est délicate, pourtant, c'est une question essentielle en physique. Depuis le début du 20^e siècle, de nombreux développements expérimentaux et théoriques ont permis d'avancer sur le sujet. L'approche physique statistique permet de construire des modèles dynamiques. On peut noter par exemple la théorie de la réponse linéaire[7][8], développée dans les années 50, qui permet d'expliquer, dans la plupart des cas pas trop loin de l'équilibre, la réponse d'un système à une perturbation extérieure¹⁴. Plus récemment, avec l'étude de systèmes biologiques, bactéries, mais aussi les réseaux cellulaires d'actine, on s'intéresse à une nouvelle classe de systèmes, ceux qui sont hors équilibre, non pas sous l'effet d'une perturbation extérieure, mais intrinsèquement hors équilibre. C'est à dire que les éléments constitutifs du système consomment de l'énergie, et génèrent donc de l'entropie, mais à l'échelle d'un individu. Ces systèmes sont très loin de l'équilibre, mais également très différents des systèmes usuels, puisque de l'ordre peut apparaître spontanément sans apport externe d'énergie¹⁵. Par exemple, une roue crantée dans un bain de bactéries se met spontanément à tourner sur elle même[9]. Un biofilm bactérien en milieu pauvre se structure de manière semblable à la vascularisation d'un tissu[10]. Les assemblées macroscopiques d'animaux sont également des exemples de systèmes mis hors équilibre par ses constituants. Dans ce cadre, cette thèse propose tout d'abord une réalisation expérimentale d'un système physique dans lequel les individus consomment de l'énergie à l'échelle de l'individu, et sont responsables de l'aspect hors équilibre du système. Nous proposons ensuite de chercher quelle sont les paramètres qui permettent de décrire efficacement ce système, par exemple en mesurant une température, ou une équation d'état.

Ces deux questions qui sont assez proches, sont présentes dans cette thèse, et pour y répondre, nous avons conçu un système physique modèle, non-biologique, de particules autopropulsées.

Pour comprendre ce système, j'en fait une description sommaire et qualitative, qui sera développée plus loin. Le système que nous étudions est une assemblée bidimensionnelle de colloïdes de 2 μ m. Ces colloïdes sont sphériques, mais sortent de l'ordinaire : Une de leurs faces est couverte

¹⁴On peut étudier par exemple la réponse d'un liquide ou d'un verre à un cisaillement, ou la réponse d'un matériau à un courant électrique ou un champ magnétique.

¹⁵Du moins en apparence, bien évidemment, les éléments actifs consomment une source d'énergie, qui n'est pas considérée dans cette analyse, et le second principe est toujours vérifié.

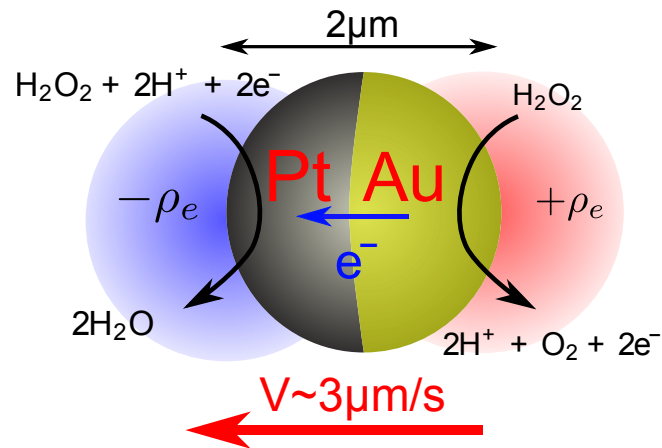


FIGURE 2 – Schéma représentant les réactions chimiques sur les électrodes d'or et de platine du colloïde Janus. Le champ électrique créé assure la propulsion du colloïde à des vitesses $v \sim 3\mu\text{m}\cdot\text{s}^{-1}$.

d'or tandis que la seconde est couverte de platine. Lorsqu'on plonge un tel colloïde (appelé Janus d'après la divinité romaine à deux faces¹⁶) dans un bain contenant de l'eau oxygénée, il dissout ce carburant de manière asymétrique, comme une pile, et se propulse grâce au champ électrique ainsi créé (voir fig. 2). Il atteint des vitesses de l'ordre de $3\mu\text{m}\cdot\text{s}^{-1}$, avec de faibles concentrations en eau oxygénée.

Ce système est bien hors équilibre, puisque les particules dissipent de l'énergie, et l'injection d'énergie dans le système se fait à l'échelle du colloïde. Les colloïdes interagissent via des interactions stériques, hydrodynamiques et chimiques (voir plus loin).

Si aux faibles concentrations le comportement de ces colloïdes est ordinaire, ils se comportent de manière semblable à celle d'une particule passive, le mouvement en plus. En revanche, lorsque la concentration augmente (voir la fig. 3), des troupeaux de colloïdes apparaissent. Ces troupeaux (nous les appellerons par la suite clusters) observés dans un système non-biologique pour la première fois durant cette thèse, ont un comportement fort amusant. Ils sont très mobiles, et bien qu'ils se déplacent plus lentement que les colloïdes individuels, ils tournoient sur eux-mêmes, échangent des colloïdes, se divisent, et entrent en collision, ce qui peut engendrer la fusion de deux clusters.

Maintenant que le système est décrit, on peut poser des questions physiques, et proposer des explications qui pourront être infirmées par l'expérience.

¹⁶Janus est le dieu des portes et ouvertures, mais aussi du passé du présent et du futur. Portefolio divin que je ne peux m'empêcher de trouver assez cool.

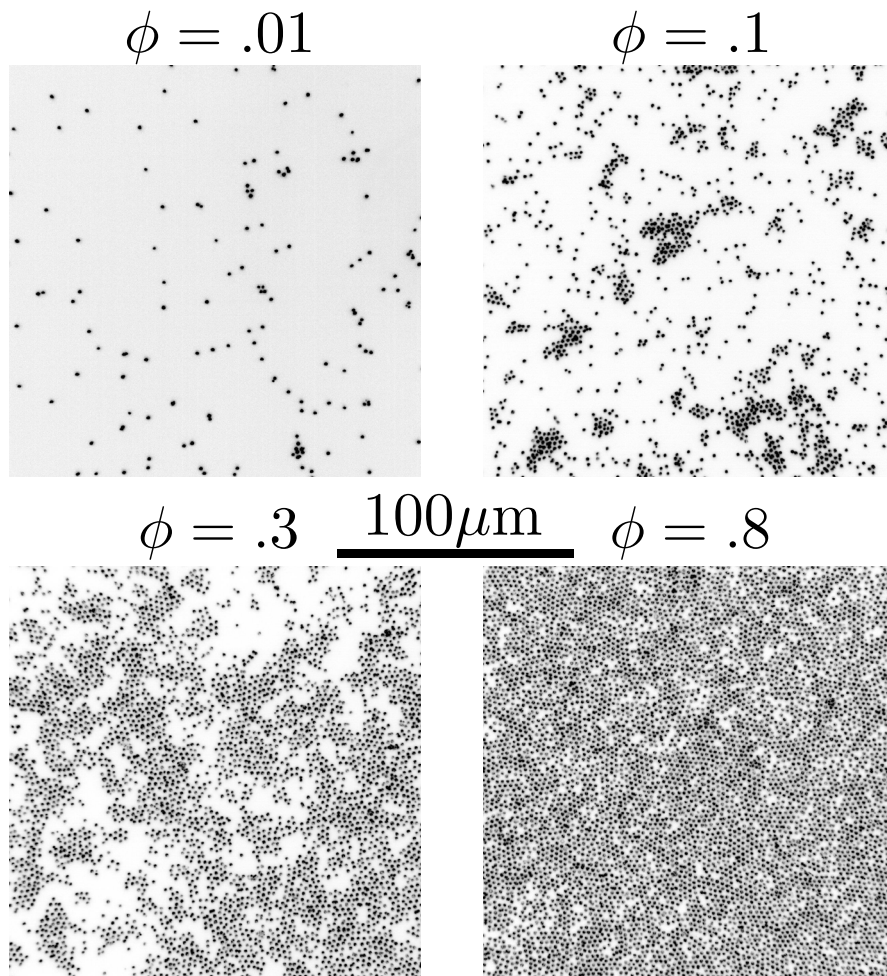


FIGURE 3 – Assemblées de clusters pour plusieurs concentrations. La taille des clusters croit avec la concentration, mais dépend également de l'activité. Voir les films n°4-7 des sup.mat.

Plan de la thèse

Très classique, la thèse s'articule en quatre parties. Je présente tout d'abord les travaux expérimentaux et théoriques qui ont précédé cette thèse. Ensuite, je décrirais, dans une partie assez technique, les développements expérimentaux réalisés durant ces trois années. Les deux chapitres suivants constituent le cœur de mon travail expérimental, avec tout d'abord une description avancée des clusters, qui s'intéresse à leurs propriétés statiques et dynamiques. Le quatrième chapitre propose de mesurer l'équation d'état pour une assemblée de nageurs.

Chapitre 1 : Bibliographie. Commençons par un très bref bilan des expériences et travaux théoriques qui précèdent cette thèse. Expérimentalement, de nombreux systèmes actifs ont été étudiés ; à l'échelle macroscopique : troupeaux de moutons, vols d'étourneaux, ainsi qu'à l'échelle microscopique : assemblées de bactéries ou d'algues. Dans tous les cas, des phénomènes similaires sont observés, regroupement, essaims, troupeaux, tourbillons...

Pour rendre compte de ces observations, les principaux outils théoriques utilisés appartiennent à trois grandes catégories. Tout d'abord, les modélisations inspirées des techniques de dynamique moléculaire : des particules pour lesquelles on choisit une interaction *ad hoc*. Les effets observés sur les assemblées permettent de mieux comprendre quels sont les ingrédients nécessaires pour observer des effets collectifs. Une seconde approche utilise la théorie cinétique. A partir de l'équation de Langevin pour une particule, qui contient l'interaction avec les autres particules, on détermine les équations de Fokker-Plank associées. On peut ainsi lier les interactions et les propriétés globales du système. Une dernière méthode est une description hydrodynamique, dont les propriétés dépendent des symétries du système.

Cette analyse bibliographique est un survol partiel et orienté, qui est un instantané de la recherche sur les systèmes actifs au début de ma thèse. De très nombreux articles ont été publiés durant ma thèse, et ces articles sont commentés en regard des expériences que nous avons réalisées.

Chapitre 2 : Description détaillée de l'expérience. Cette partie très technique décrit les développements expérimentaux réalisés durant ces trois ans. L'objectif du chapitre est de donner suffisamment d'informations au lecteur intéressé pour qu'il puisse reproduire les expériences. Dans un premier temps la synthèse des colloïdes est présentée en détails. Vient ensuite l'utilisation et les aménagements faits sur le microscope qui sert aux observations optique des colloïdes. Enfin, on présente le système

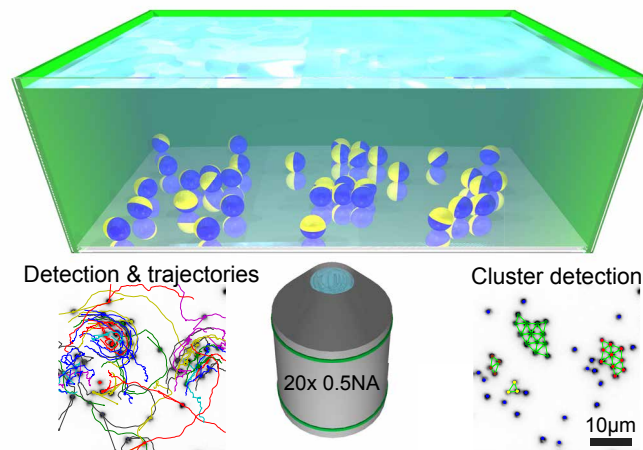


FIGURE 4 – Schéma de la cellule d’observation avec exemples de détection et de suivi des particules.

d’acquisition et de traitement des données, qui permet la détection et le suivi des particules.

Chapitre 3 : Dynamique de la phase de clusters Les clusters sont sans cesse en mouvement, tournoyant, échangeant des colloïdes fusionnant après une collision, ou encore se séparant spontanément, en se brisant en clusters plus petits.

L’analyse de l’évolution de la taille moyenne des clusters (le nombre de colloïdes par cluster), nous permet de proposer comme cause de la formation des clusters l’attraction d’origine chimique entre les colloïdes.

L’analyse fine de la structure des clusters permet d’observer une divergence de la compressibilité, qui rappelle les transitions de phase critiques, une loi de distribution des tailles de clusters $P(N) \sim 1/N^3$, en loi de puissance (cf figure 6), ce qui est assez surprenant.

Pour finir, l’analyse quantitative des vitesses de translation et de rotation des clusters donne quelques indices sur l’organisation des colloïdes à l’intérieur des clusters, mais permet surtout des comparaisons quantitatives avec les simulations numériques et les expériences les plus récentes qui observent également des clusters, dans des systèmes physiquement différents.

Chapitre 4 : Expériences de sédimentation. Pour terminer, nous étudions une expérience de sédimentation qui permet de mesurer la relation entre pression et densité dans un système. La phase à basse densité suit gentiment la loi des gaz parfaits $\Pi = \rho k_B T_{eff}$, ce qui permet de mesurer la “température” du système (voir fig. 8), formant ainsi un véritable thermomètre à gaz, tel qu’il était utilisé au 17^e siècle.

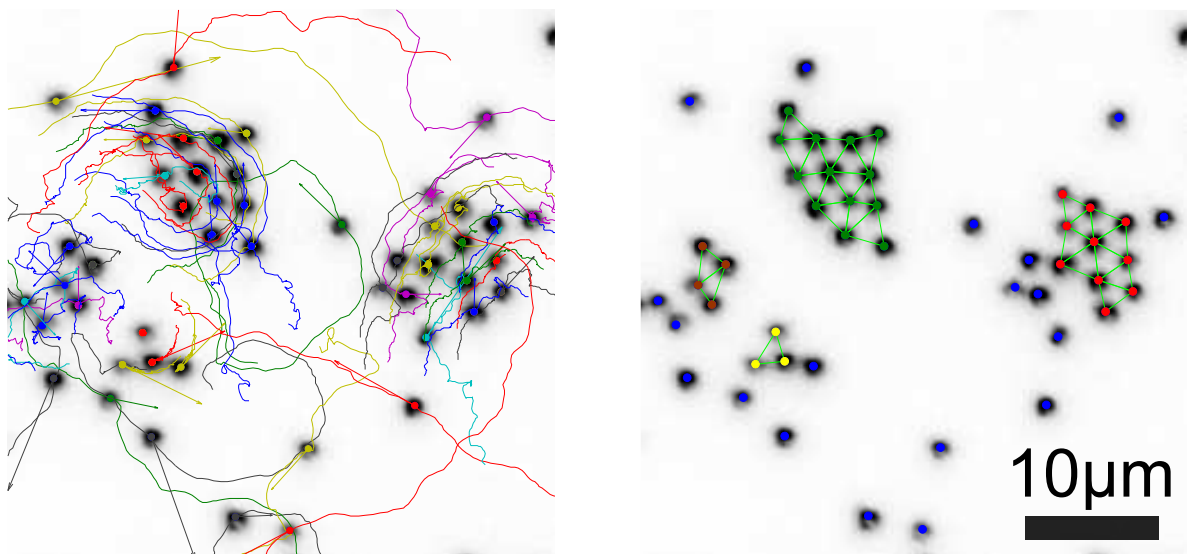


FIGURE 5 – Détection et reconstitution des trajectoires des colloïdes (gauche), et détection des clusters (droite). Voir le film n°3 des sup.mat.

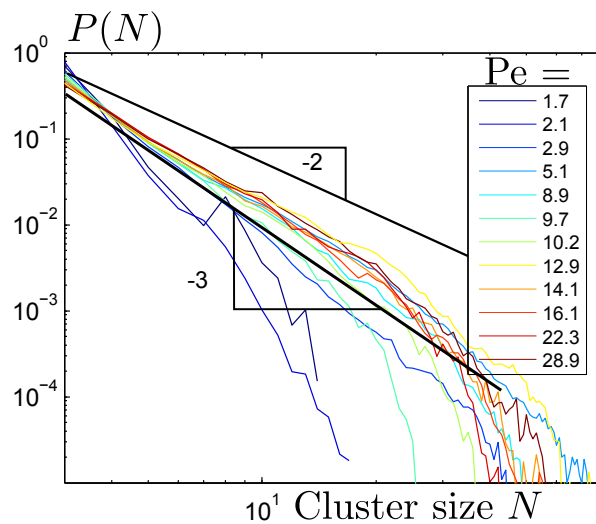


FIGURE 6 – Fonction densité de probabilité de la taille des clusters, pour 12 concentrations différentes en eau oxygénée, compatible avec une loi de puissance d'exposant -3.

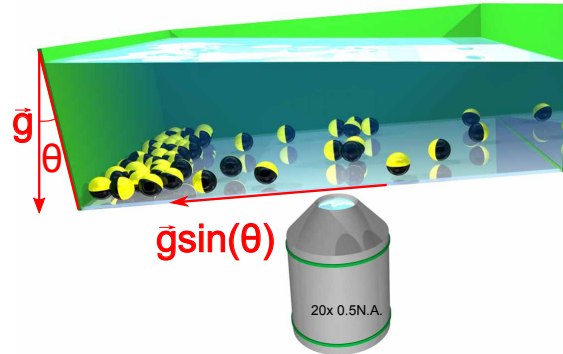


FIGURE 7 – Schéma de l'expérience de sédimentation. L'inclinaison de la cellule simule une gravité réduite.

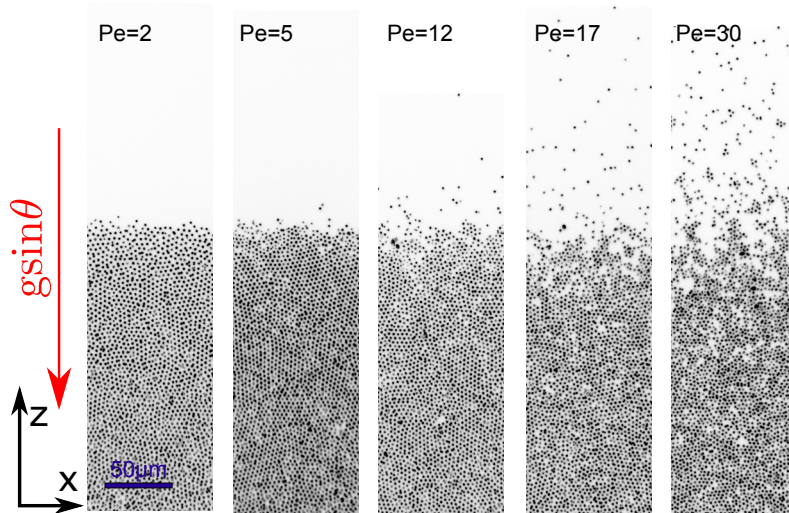


FIGURE 8 – Images du système en sédimentation pour 5 activités différentes. La phase gaz au sommet de la cellule est un gaz parfait, tandis que la phase dense est vitreuse dans le cas passif et devient un “verre actif” à plus haute activité. Voir le film n°9 des sup.mat.

La phase la plus dense a un comportement très intéressant ; l'activité semble s'opposer au "jamming"¹⁷, et la phase active est plus libre, et mobile, bien que plus dense. C'est un véritable liquide actif, montrant de l'ordre polaire, des fluctuations importantes de densité ainsi que de vitesse.

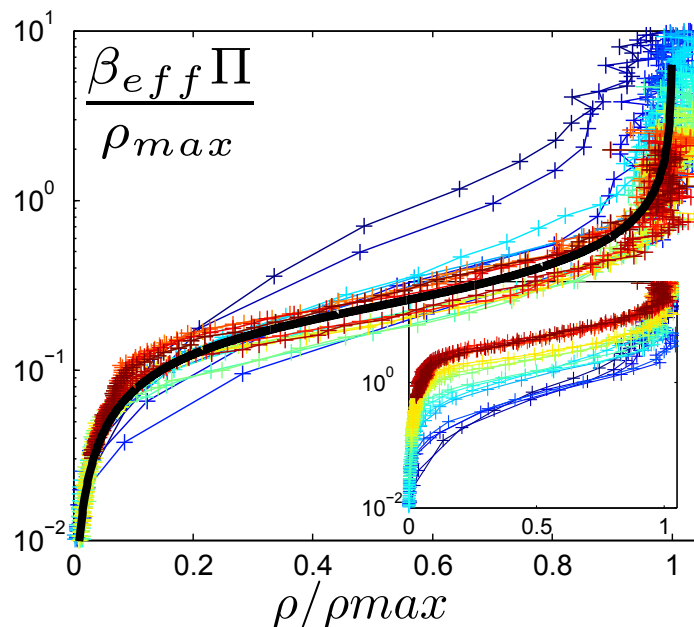


Figure 9: Équation d'état du système actif : les courbes reliant pression, température et densité pour 21 activités, et sans mise à l'échelle (insert)

On peut alors mesurer une équation d'état, qui semble bien coller au système :

$$\frac{\Pi}{k_B T_{eff} \rho_{max}} = \frac{\rho / \rho_{max}}{(1 + b \rho / \rho_{max}) \sqrt{1 - \rho / \rho_{max}}},$$

avec $b = 4$. Il semble surprenant qu'une équation d'état aussi simple, puisse rendre compte d'un phénomène si complexe, c'est le miracle habituel de la physique réductionniste.

¹⁷Ce terme désigne le blocage des particules par leurs voisins dans les systèmes granulaires désordonnés.

Contents

| | |
|--|-----------|
| Introduction | 3 |
| Résumé | 9 |
| 1 Collective behavior in active matter. | 25 |
| 1.1 Observations of collective effects | 26 |
| 1.1.1 Classification and characterization of collective effects | 27 |
| 1.1.2 Macroscopic aspects | 30 |
| 1.1.3 Soft active matter | 35 |
| 1.2 Theory of active matter | 38 |
| 1.2.1 Microscopic equations | 38 |
| 1.2.2 Hydrodynamic continuum model | 42 |
| 1.2.3 Conclusion | 43 |
| 1.3 Conclusion | 44 |
| 2 Gold-Platinum Active Colloids | 45 |
| 2.1 Synthesis of active particles | 46 |
| 2.1.1 Gold-platinum Janus Colloids | 46 |
| 2.1.2 Synthesis of the gold colloids. | 47 |
| 2.1.3 Deposition and platinum coating. | 49 |
| 2.1.4 Re-suspension and Sample preparation. | 50 |
| 2.1.5 Evolution of the Active colloids for the study of collective effects. | 51 |
| 2.2 Characterizing the interparticle interaction. | 52 |
| 2.3 Microscopy observations | 55 |
| 2.3.1 External darkfield microscopy. | 57 |
| 2.3.2 Janus Polarity. | 58 |
| 2.4 From movies to trajectories | 59 |
| 2.4.1 Particle detection | 59 |
| 2.4.2 Trajectories reconstruction. | 61 |
| 2.5 Differential dynamic microscopy. | 63 |
| 2.5.1 Principle | 63 |
| 2.5.2 Image analysis | 64 |

| | | |
|----------|--|------------|
| 2.6 | Acquisition | 66 |
| 2.6.1 | Hardware and software. | 67 |
| 2.6.2 | System development and evolution. | 71 |
| 2.7 | Conclusion | 71 |
| | Appendix A: Electrocatalytic microswimmers | 73 |
| 3 | Dynamics of the Cluster Phase | 81 |
| 3.1 | Weak interaction limit | 85 |
| 3.1.1 | Persistent random walk. | 86 |
| 3.1.2 | Experimental investigation. | 89 |
| 3.2 | Interaction between colloids | 92 |
| 3.2.1 | Steric interactions. | 93 |
| 3.2.2 | Hydrodynamics | 93 |
| 3.2.3 | Chemical | 95 |
| 3.3 | Static description of the clusters: | 97 |
| 3.3.1 | Activity measurement | 97 |
| 3.3.2 | Average cluster size. | 98 |
| 3.3.3 | Péclet Number measurement | 101 |
| 3.3.4 | Structure | 102 |
| 3.3.5 | Systematic detection of the clusters | 106 |
| 3.3.6 | Cluster size distributions. | 109 |
| 3.3.7 | Conclusion | 111 |
| 3.4 | Dynamic clusters | 112 |
| 3.4.1 | Measuring cluster dynamics | 112 |
| 3.4.2 | Velocities distribution | 114 |
| 3.4.3 | Modeling velocities | 115 |
| 3.4.4 | Other Dynamic | 118 |
| 3.5 | Other Experiments and Models | 118 |
| 3.5.1 | Experimental contributions. | 119 |
| 3.5.2 | Numerical simulations. | 120 |
| 3.6 | Conclusion | 121 |
| 4 | Sedimentation experiments | 123 |
| 4.1 | Sedimentation experiments | 124 |
| 4.2 | From sedimentation profiles to osmotic pressure | 126 |
| 4.3 | A thermal Gas phase. | 128 |
| 4.4 | The dense phase. | 130 |
| 4.4.1 | Structure | 133 |
| 4.4.2 | Conclusion | 135 |
| 4.5 | Measuring an equation of state for an active system? | 135 |
| 4.6 | Conclusion | 139 |
| | Conclusion | 141 |

| | |
|---------------------|------------|
| <i>CONTENTS</i> | 23 |
| Bibliography | 143 |

Chapter 1

Collective behavior in active matter.

Many systems, with very different interactions, exhibit collective effects, from herds of mammals to flights of birds, from social insects to bacterias. Collective behavior span very different physical causes, time and length scales. However, all these systems have in common to be composed of smaller interacting entities, which are dissipating energy either stored internally, or harvested in the environment, hence the name “active matter”.

In this thesis, we use a statistical physics approach. Schematically, statistical physics states that for large assemblies, the specific nature of interactions does not matter, and very generic conservation principles are derived. In the case of active matter, very few generic principles are known, and even the observables are not known. What macroscopic observables should we study in active matter? Which microscopic degrees of freedom are relevant? Microscopic, in this chapter will designate properties defined at the same length-scale as the individual. The microscopic density is, as usual, the particles’ positions; individual velocities, trajectories or orientations are also microscopic variables. More importantly, internal “hidden” variables, such as the amount of internally stored energy, or the sex of the animal, are also necessary for a complete description of the system, however hard to measure. We have to hope that a description that ignores these variables will still be able to predict collective behavior.

The microscopic behavior of the system is not our primary concern. What we want is a large-scale description of collective effects. The main question we ask is the following: *What are the most generic sufficient causes creating collective behavior?* While we know that activity and interactions are necessary, it is also clear that they are not sufficient to create collective effects; perhaps the specific nature of the activity and interactions, and their coupling has to be taken into account.

These questions have been addressed in previous works, although not completely answered. As the field of active matter is very active and still expanding, In this chapter, I will only present a brief snapshot of the state of the field at the beginning of my thesis¹. I will focus on experimental active systems, and will present the theoretical background required for a basic understanding of the subject. I will try as much as possible to motivate theoretical description by experimental observations. Although we will do experiments at the colloidal scale, I will present many results for macroscopic systems, to reinforce the similarities between length scales.

1.1 Observations of collective effects

In this part we analyze previous experiments on collective systems. As mentioned earlier, a wealth of very different systems have similar collective behavior, though they differ by their size, from micrometer-scale bacteria to meter-scale animals, by the physical nature of interparticle interactions, chemical, visual or auditive², mechanical, or, rarely, all at the same time³. The number of individuals also varies, from several scores of sheep to billions of bacteria. We will focus first on collective behavior for meter-scale systems and then on the colloidal scale.

As we will discuss, there is an important difference between these two length scales since the physical forces at play are very different. For colloidal systems, friction is extremely high, and there is no inertia; the thermal fluctuations also play a great role by randomizing particles' orientations and positions.

I will try to identify, for each system, the nature of interactions and the timescales in the system. For many biological systems, the longest time scales are defined by the decay of internally stored energy⁴, often over a few hours. We would like to describe collective behavior as stationary phenomenon, otherwise defining conserved quantities is going to be very hard. We try to find which observables are common among all experimental systems, and will focus only on a limited number of

¹Recent reviews by C.Marchetti *et al.*[11] and by T.Vicsek *et al.*[12], each citing more than 150 articles, albeit with major overlap, have been published in the past two years.

²I do not pretend that individuals interact through light or sound. This is rather a carrier for a social interaction, for example, in low density human crowds, human avoid each other as much as possible. There is no physical interaction, although people need to be able to see each other if they are to avoid a collision.

³Social insects come to mind. Ants for example have a very complex signaling network inside colonies, are forced to follow scent tracks, colonies are constrained by mechanical rules...

⁴For macroscopic natural systems, day/night cycles also play an important role, as many animals choose to go to sleep[13].

examples for better clarity.

1.1.1 Classification and characterization of collective effects

Systems at equilibrium are bound by symmetry laws to remain boring⁵, they must be homogenous⁶, and at rest, since thermodynamical equilibrium imposes mechanical equilibrium. However, for active out of equilibrium systems, spontaneous symmetry breaking is allowed, caused by the interplay between interparticle interaction and energy injection in the system through activity; the system can start to flow, can exhibit large density fluctuations, spatial and polar ordering, a variety of phenomenon called collective behavior⁷.

Several parameters are very important to characterize the different systems with collective effects. The first and most obvious is the nature of the collective effects, their spatial and temporal ordering. Other important parameter are the physical way energy is introduced in the system and the interparticle interactions that differ by their physical nature, and also by their symmetries. I will briefly comment on those different points.

Energy input: The activity necessary to the emergence of collective effects implies energy dissipation by individuals. The manner in which it is injected in the system can be very different. The energy can either be stored inside individuals (animals, bacterias) or harvested in the environment (vibrated granular, active colloids). This is important as for harvesting particles, it gives rise to new possibilities of interactions through the medium. If one particle consumes energy locally, the energy will not be available to the next particle that wants to harvest energy there. By not considering systems under external constraints, we consider systems in which the energy injection is performed at a single particle scale. the particles themselves are driving the system and providing all the energy for any collective effect.

Nature of the collective effects: Many names designate collective behavior, especially among macroscopic animals. Schooling, herding, flocking, swarming all refer to the particular type of animals exhibiting

⁵This is more a provocative thought than a factual comment.

⁶As a consequence of the Mermin-Wagner theorem[14].

⁷We do not consider as collective behavior spontaneous motion arising from external constraint, nor from boundary interactions. For example, *e. coli* rotates counter-clockwise when close to a wall, and so does an assembly of such bacteria. This does not constitute a collective effect.

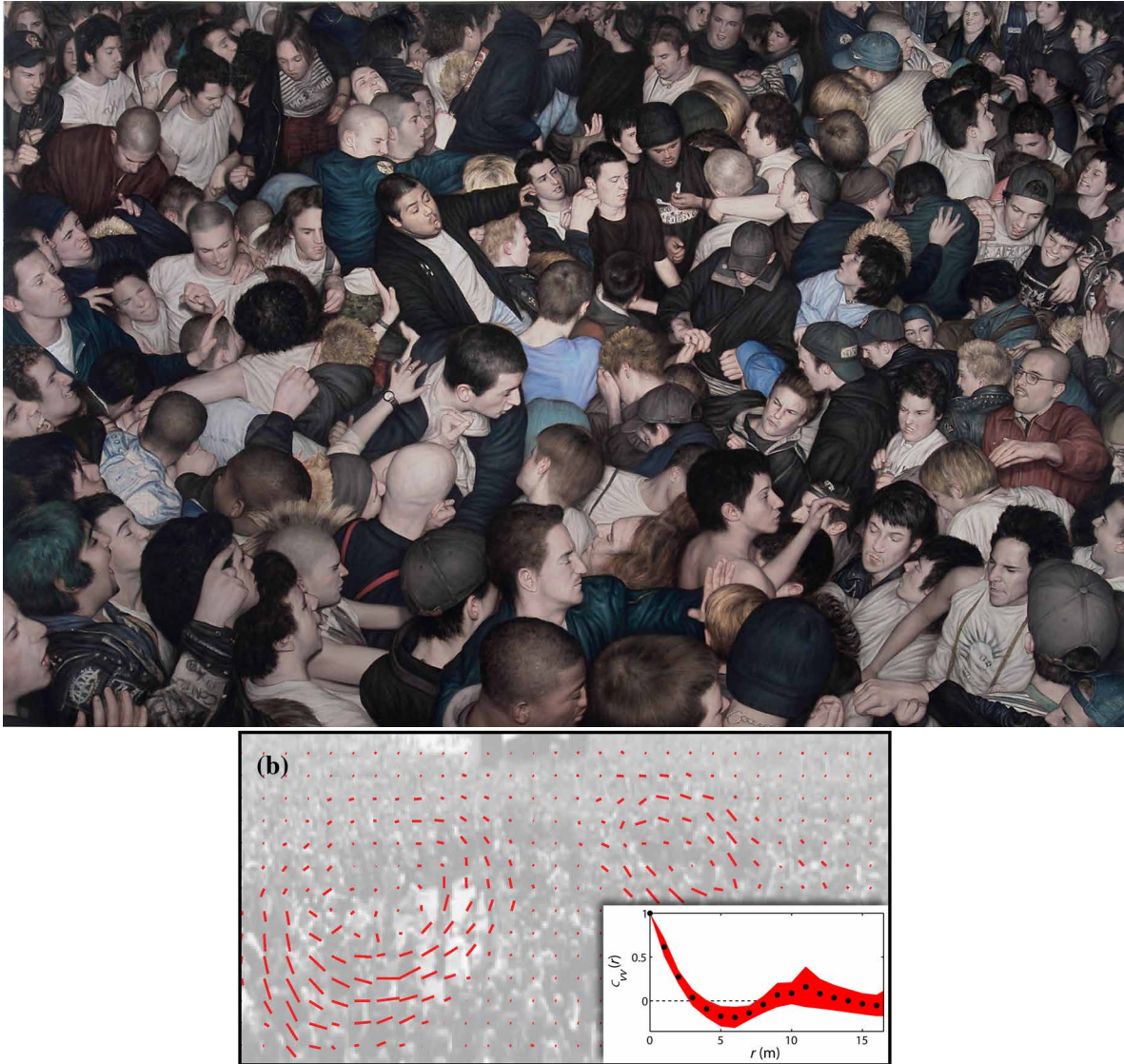


Figure 1.1: (top) Crowd of ~ 200 humans during a hard rock concert (Dan Witz). Although seemingly disordered, slow vortexes spontaneously emerge. As seen in (bottom) velocity field overlay over a human crowd, with velocity-velocity correlation function as a function of distance (inset), showing vortexes, which appear spontaneously when activity is high enough among the happy metal fans (from [15]). The interaction is mostly social and mechanical. Although many videos exist, filming is not easy, and the unruly crowd makes experiments not very reproducible. See this video. Typical duration ~ 1 h.

these collective behaviors: fish, social mammals, birds and bees, respectively. We do not want to focus on vocabulary but rather describe the different categories of collective effects. All the terms used refer to similar behavior, with all animals roughly going in the same direction. Other collective effects reveal spatial ordering, with the emergence of spatial structures. A first classification criterion is thus the nature of patterns that have been created: clusters, stripes, lines, mills, waves, etc. What is especially important is their symmetries. The collective effects can exhibit positional, polar, or nematic ordering. It is this diversity that we need to understand.

Physical nature of interactions: The physical nature of interparticle interactions is also a classification factor. They can be physical: through direct contact or distant forces, mediated by the medium, such as hydrodynamical interactions. Chemical interaction arise through diffusiophoresis or chemotaxis. Social interactions lead to internally decided trajectory changes, depending on properties of other perceived individuals, either through smell, sound, or vision. Physical and chemical interactions are much simpler to quantify than social and biological interactions. This gives a first hint as to why model physical systems are very useful for quantitative measurements.

Symmetries of the interactions: The physical nature is less important than the resulting symmetries of the interactions. Interactions can be isotropic or anisotropic; polar or apolar, and the range can vary, both in the time and space.

Depending on the interaction rules between particles, the resulting collective effects will be different. First important point: the absence of interactions implies an absence of collective effects. As in an ideal gas, the behavior of the assembly will be the average behavior of a single entity. Interactions that only take into account particles positions, can give rise to *positional* collective effects, such as spatial ordering or clustering⁸. Active colloids probably fall into this category⁹[17], as do some robotic systems, and sometimes bacterias[10, 18]. More complex interactions take into account particles orientations, but not directions, thus leading to *nematic* collective effects. Vibrated rods[19] or some cells[20] fall into this category. The most common and easily seen type of interaction are polar interactions, leading to *polar* collective effects, in which individuals

⁸Clustering also leads to local polar ordering, as most particles cannot interpenetrate, thus cannot have opposite direction when close to one another. This implies similar directions, and thus a local polar order. The possibility of a global or large scale polar order is a very tough question, whose answer is not yet fully clear[16, 11].

⁹read this thesis to know more!



Figure 1.2: School of $\sim 10^6$ big-eye scads (SteveD/Flickr/WikiMedia). All fish go in the same direction, which implies polar order, but without positional order. The shimmering pattern of fishes makes it hard for predators to attack individual fishes. The interaction is social and hydrodynamical in nature. Collective swimming is slightly more energy-efficient, due to energy saving by swimming in the updraft of the previous fish, similarly to the tour de France “peloton”. This type of motion stops when the fishes need to gather food, as they will spread out to eat plankton. Typical duration ~ 1 day to several weeks.

move or orient themselves with the same orientation and direction. Most biological examples fall in this category (see the figures in the next pages), schools of fish[21], or flocks of birds¹⁰[22]. Bacteria also experience polar interactions, through hydrodynamics[23, 11, 24, 25].

1.1.2 Macroscopic aspects

I will give a few examples of macroscopic collective effects; Although the experiments I have done are at a colloidal scale, the reader is probably already familiar with these, and it will serve as a bridge towards

¹⁰Of course, saying that the interaction between wildebeests, or starlings, is polar is a gross over-simplification, and nothing more than the first order (we have to hope it is first order) term to describe the actual, more complex social interaction between these animals.

the stranger effects that occur for colloidal systems. The advantage of macroscopic systems, is that individuals can be seen and tracked fairly easily. No complex acquisition system is required, at least for 2-D motion, such as herds and crowds. For schools of fish, their opacity prevents full tracking in the case of large schools. For birds, setups of stereographic pairs of camera, that have become common in the film industry are used to observe the three-dimensional trajectories of the animals.

In all biological macroscopic systems, the individuals are using internally stored energy to move¹¹. If we consider the system as the ensemble of individuals without the medium¹² in which they move, an important property is that neither individuals nor the group have a conserved momentum. Indeed the medium can dissipate momentum freely. A fish, for example, can stop moving without having to give its momentum to its neighbors, as it can dissipate it in the water.

The main limitation for the study of these systems is that it is hard to control biological elements. The social behavior can be very complicated, the boundary conditions very badly defined, as it is very hard to confine a flight of birds (see fig. 1.4) or a school of fishes (see fig. 1.2). For experimental studies, assemblies of animals are confined in small containers. For example, fish are confined to a 2D container [21, 26] in order to study their schooling, which is now limited to 2D schooling. Ants are very easily confined in small observation setups [27], without any dramatic change in environment. When animals become hungry or afraid, they can also change their behavior, sometimes in subtle ways.

Reproducibility can be hard in biological systems, which motivates the use of artificial systems such as robots, or vibrated granular rods or asymmetric disks [28, 29]. These two model systems of vibrated grains at the centimeter scale have been used to show the first examples of collective effects in active matter, with rather different observations between them. Narayan *et al.* [29] use assemblies of rods, which interact through hard core repulsion to give nematic ordering of the system. However, the system is out of equilibrium, and dissipating energy at the individual particle scale, but cannot really be called active in the sense that individual units do not move in a preferred direction, and are indeed apolar. Deseigne *et al.* [30, 28] use true self-propelled particles, and they observe polar ordering and giant number fluctuations. The interaction is polar due to solid friction and the boundaries of the system also play a role, by re-injecting particles towards the center, however, their role is not yet

¹¹Although for short time scales, motion without internal energy spending is possible, for example by converting potential energy for birds, or by being pushed by other individuals in a crowd.

¹²It can be water, air or simply the ground surface

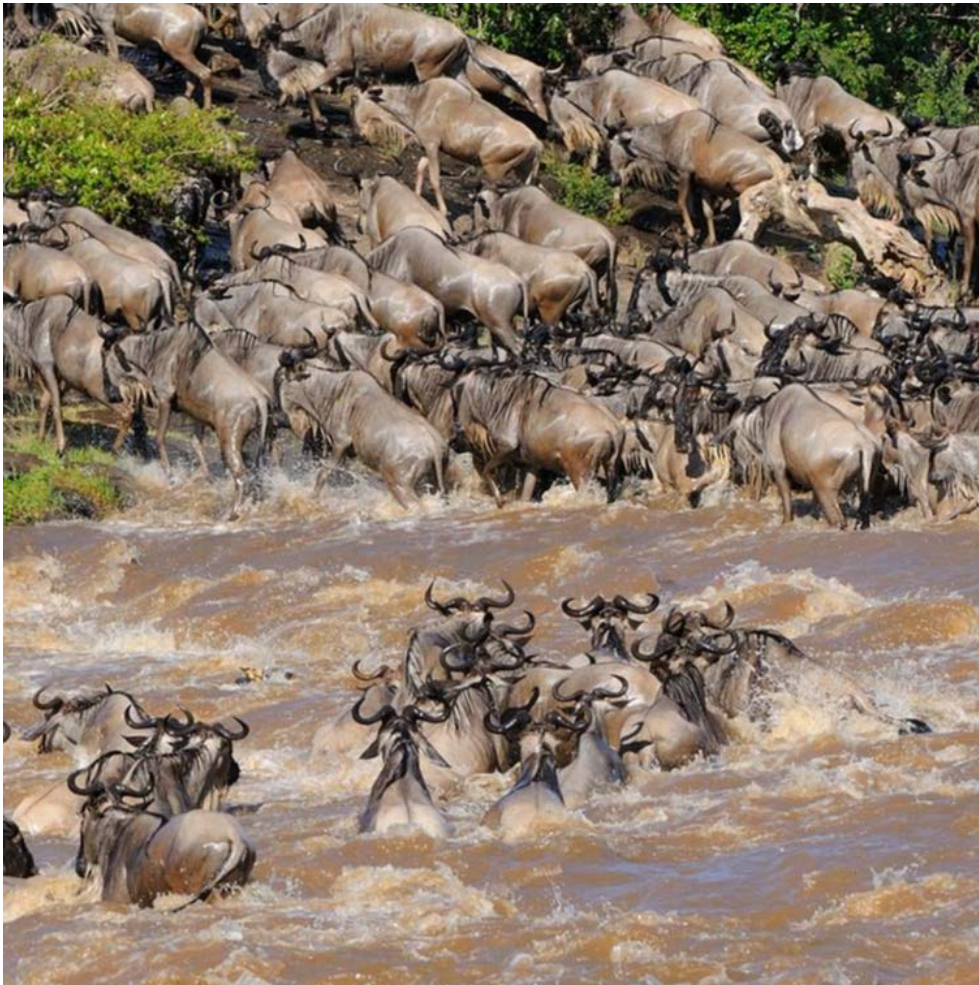


Figure 1.3: Herd of ~ 500 wildebeests (Gerard David). The wildebeests swim across the Mara river all at the same time to decrease exposition to predators. When moving on ground they exhibit polar ordering only, but when swimming, they form compact clusters. The interaction is mostly social and mechanical. See video1 & video2. Typical duration ~ 1 h.

fully understood.

For most large-scale biological systems, the interaction is polar: individuals tend to follow their neighbors, not by going towards them, which would be a positional interaction, but by aligning velocities with them. Aligning velocities implies

$$\mathbf{v}_j(t + dt) = \alpha \mathbf{v}_j(t) + (1 - \alpha) \langle \mathbf{v}_i(t) \rangle_{i \in \text{neighbors}},$$

with $\alpha \in \mathbb{R}$. Although defining which neighbors are taken into account can be done in many very different ways, most animals take into account in their neighborhood only animals they can see, hear or smell. Birds for example seem to consider the closest birds in every direction, and not simply the closest [22].

As density increases, the polar velocity of the active individuals decreases due to crowding effects. Indeed, most of the time, individuals cannot interpenetrate, thus have to stop instead of colliding. When density reaches a certain threshold, the jamming transition blocks the particles (see fig. 1.1 and 1.3). Humans in the classical music concerts are so densely packed that they almost stop moving, although long-range slow patterns can emerge [15][31][32]. Similarly for wildebeests, the high density of animals at the riverbank slows the animals, easing predator strikes. Traffic jams are another common example of “jamming” transition.

Other model systems include assemblies of robots [33] that are also easy to track¹³, since they often record their position through time by themselves. Artificial robots can have any kind of interaction coded into its software layer, which makes it similar to numerical simulations, a limitation is the computation time for very complex interactions. Flying robots (quad-copters) assemblies have been shown to cooperatively juggle with balls and sticks [38].

However different, all these systems have in common that activity and interparticle interactions are required to observe collective behavior. Our experiments occur at very different length scales, and the physical nature of interaction will be different, however, the collective behavior observed will have great similarities. We also note that active model systems can show collective behavior, and offer opportunities for quantitative measurements.

¹³It is not very clear to me whether robots assemblies are an actual experimental system, or rather a “numerical experiment” system. However, their usage is increasing and with the increased mobility of computing power, sure to develop [34]. Science fiction is also full of small microrobots or nanobots that self assemble to construct objects, and sometimes eat everything in rebellion against humanity [35, 36, 37].



Figure 1.4: Murmuration of $\sim 10^5$ starlings above Rome (Paolo Patrizi). With only social interaction, mesmerizing patterns emerge. There is clear local polar order, although the murmuration's center of mass stays almost fixed, which implies that the polar order disappears either for long range or for long times. See also these videos. Typical duration ~ 3 h.

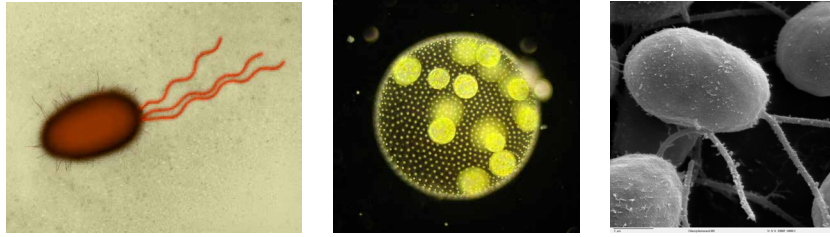


Figure 1.5: The cast: active particles at colloidal scale, from left to right: *escherichia coli*, a $5\mu\text{m}$ long (flagella included) bacteria, propelled by the rotation of its flagella (image: Dennis Kunkel Microscopy, Inc.); *Volvox carterii*, a 1mm algae that swims thanks to thousands small flagella covering its surface; *chlamydomonas reinhardtii*, a $2\mu\text{m}$ algae that swims with two flaying flagellas. (images: Wikimedia)

1.1.3 Soft active matter

At the colloidal scale the physical phenomena are very different. The thermal fluctuations are very important, and randomize particles orientations and positions; friction is huge, which means there is generally no conservation of momentum. However, as a side note, systems in which the total momentum is constant include notably systems made of actin filaments and micromotors in a bath of ATP that provides energy[39]. This is a medium of great biological importance, since it fills our cells, assures their rigidity and deformations. This category of active matter has a very rich collective behavior, including polar ordering; the interested reader can refer to [11]. We will leave this particular case aside, and focus on active systems without conservation of momentum. Indeed, all the experiments I made during this thesis are on swimming colloidal systems, and thus follow the low Reynolds constraints; and do not have conservation of momentum.

Most of the collective behaviors observed at this scale are on biological systems. They are (slightly) easier to control than their macroscopic counterparts, but harder to observe. Bacteria such as *escherichia coli*, or *bacillus subtilis*, algae such as *chlamydomonas reinhardtii*, or *Volvox carterii* (see fig. 1.5), share similar propulsion mechanisms [40, 41] (and see Annex A.3 and A.4) and lifestyles; cells such as pancreatic cells have no dedicated propulsion system, but growth and multiplication can create motion. All these actors convert internally stored energy into motion, and interact through chemical signals and hydrodynamic interactions[11, 24, 18, 42], while cells have mechanical interactions.

Collective behavior in assemblies of colloidal swimmers show very different qualitative behavior. Systematic flocking is much rarer, although there are some examples of very directed motion, such as traveling solitary



Figure 1.6: Fractal spatial patterns emerge in an assembly of *escherichia coli* bacterias (from [2]). The individuals are μm -scale and the structures $\sim 100\mu\text{m}$ long. The interaction purely mechanical in nature, and arises during the grow cycle of a 2D layer of bacterias. There are three bacterial families, differing only by their color. See a simulation video.

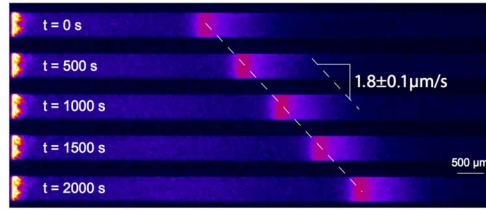


Figure 1.7: Solitary wave of *escherichia coli*, (from [43]) the shape of the pulse is constant, as is its velocity $v = 2\mu\text{m}\cdot\text{s}^{-1}$, two orders of magnitude below the swimming velocities of individual bacteria $v \sim 100\mu\text{m}\cdot\text{s}^{-1}$.

waves of bacteria[43] (see fig. 1.7). Most collective effects are disordered, because of the natural fluctuations of motion at colloidal scales. Individual swimmers often use run-and-tumble strategies to explore space; every second or so, they will change direction, simply by picking a new direction at random. This is called a tumble event. The rate at which they tumble, or the run duration, is affected by many external parameters, including concentration gradients, which allows bacterial chemotaxis. These individual fluctuations make long-range order more difficult to obtain, and destabilize positional structures.

The competition between this destabilizing noise and structuring interactions creates a rich palette of patterns, such as fractal patterns produced during the growth of a bi-dimensional layer of bacteria (see fig. 1.6). Another example are the convection patterns in bioconvection (see fig. 1.8), an experiment very similar to Rayleigh-Benard convection, although the driving force of the convection is the coupling between the collective consumption of oxygen, and the vertical upwards swimming triggered in cases of low oxygen concentration. In this experiment, a closer look at the convection cells reveals “turbulent” patterns (same figure, left panel), whose amplitude is $\sim 30\%$ of the swimming velocity.

Other active particles are artificial colloids, such as Janus colloids[44], or AgCl particles[45], which use the energy stored in the surrounding medium, through peroxide disproportionation, or light-triggered chemical reactions. The interactions are chemical and hydrodynamical in nature, thus much simpler than biological interactions, although these artificial swimmers have not yet been deeply analyzed. Observing and quantifying collective effects in these systems had not yet been performed at the beginning of my PhD, and was thus my main objective.

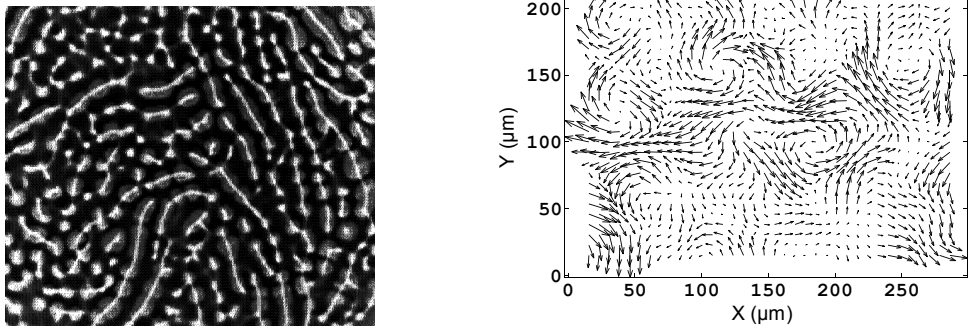


Figure 1.8: (left) Bioconvection patterns in suspensions of *bacillus subtilis* (from [1]), very similar in aspect to patterns from Rayleigh-Marangoni or Rayleigh-Benard convection. The bacteria tend to swim upwards owing to oxygen depletion caused by their presence. The interactions are chemical only in this case. (right) “turbulence” in assemblies of the same bacteria. Average velocity fields, measured through PIV, show large scales eddies. The scale arrow on the right represents $35\mu\text{m}\cdot\text{s}^{-1}$. At this small scale, the hydrodynamic part of the interaction is important to create polar order. See this video for an example of swarming in *e. coli*.

1.2 Theory of active matter: how to explain collective effects?

After a qualitative description of collective effects, we need a coherent framework to model these very different phenomenon. As mentioned earlier, several very different approaches exist, and we will present them schematically.

We first describe a “microscopic” model of active particles, and the way it is used for numerical experiments on active matter; then we show how this model can be coarse-grained into a hydrodynamic model.

1.2.1 Microscopic equations

Microscopic models are classified in the exact same way as experimental systems, by the nature of interactions, and the conservation of energy and momentum. These models are used in two ways. They can serve as microscopic models for a statistical physics or hydrodynamic modeling, or they can be used as is for numerical simulations. The first two models we present are minimal models that do not conserve energy or momentum,

1.2.1.1 Explicit polar interaction

The simplest model at the single particle level giving rise to collective behavior is probably the “standard Vicsek model”, proposed by Vicsek et al. [46, 12]. Momentum nor energy are conserved, and an explicit polar interaction is chosen. This model assumes that all particles are identical, described by their position \mathbf{r}_i , their velocity \mathbf{v}_i of amplitude v_0 , amplitude assumed to be constant for all particles. The velocity evolves through:

$$\mathbf{v}_i(t + dt) = v_0 \frac{\langle \mathbf{v}_j(t) \rangle_{j \in \text{Neighborhood}}}{\left| \langle \mathbf{v}_j(t) \rangle_{j \in \text{Neighborhood}} \right|} + \overline{\Delta T}_i \mathbf{v}_i(t),$$

the neighborhood is a circle of radius R , centered on particle i , and $\overline{\Delta T}_i$ is a random rotation matrix¹⁴, $\overline{\Delta T}_i = \begin{pmatrix} \cos \Delta\theta_i & -\sin \Delta\theta_i \\ \sin \Delta\theta_i & \cos \Delta\theta_i \end{pmatrix}$, where $\Delta\theta_i$ is a random angle taken with uniform probability on the $[-\eta/2, \eta/2]$ interval and η is the amplitude of the angular noise. The term $v_0 \frac{\langle \mathbf{v}_j(t) \rangle_{j \in \text{Neighborhood}}}{\left| \langle \mathbf{v}_j(t) \rangle_{j \in \text{Neighborhood}} \right|}$ is an alignment term, making each individual follow its neighbors. The position follows naturally:

$$\mathbf{r}_i(t + dt) = \mathbf{r}_i(t) + \mathbf{v}_i(t)dt.$$

The behavior of this system depends on the amplitude of the noise η , and on the number density ρ , basically the average number of particles inside each neighborhood. Obviously, if the noise is much higher than the alignment term, no collective effect can arise¹⁵.

This system is studied by molecular dynamic simulations, a numerical way of solving the coupled differential equations above. Large number of particles are simulated, up to 10^5 [47], using supercomputers¹⁶.

The variety of possible collective effects, depending on noise and density, is surprisingly rich, and includes clusters, swarms, and bands, structures with polar order, and different positional ordering. One of the key questions for this system is what is the nature of the transition from a disordered phase to a polar ordered phase (see fig. 1.9). The polar order parameter is $\varphi = \frac{1}{v_0} \langle \mathbf{v}_i \rangle$, the average¹⁷ reduced velocity of the system, reaching 1 for a fully aligned system, and zero if the system has no long

¹⁴Expressed here in 2D, its 3D expression is a bit more complicated, since one needs to consider two non-independent random distribution for the angles.

¹⁵In the limiting case $\eta = 2\pi$, no ordering at all is possible, since the direction of each particle is fully randomized at each time step.

¹⁶A typical run might take ~ 1 processor.month, solved in one day by ~ 30 processors.

¹⁷The average has to be on a large enough system to have any statistical meaning, which has consequences for the study of the phase transition[48, 49].

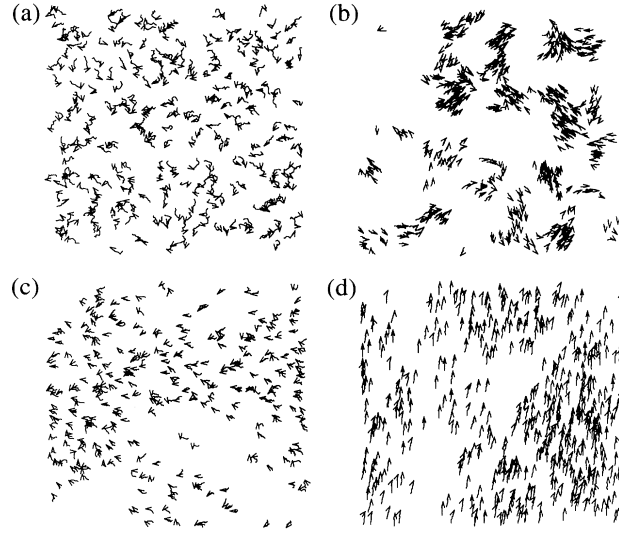


Figure 1.9: Collective effects ($N=300$) observed in the Standard Vicsek model, for different noise and densities. The arrows indicate particles velocities, and the small trailing curve their short-term trajectories. a) is the initial state, at medium density. b) low density, low noise leads to the formation of flocks. c) medium density, high noise disordered system, with small velocity correlation. d) high density and low noise, lead to a fully ordered system. (from [46])

range order. Vicsek *et al.* propose a second order (continuous) transition [46],

$$\varphi \sim (\rho - \rho_c)^\beta (\eta - \eta_c)^\delta,$$

where ρ_c and η_c are the critical density and noise, and β and δ their respective critical exponents. While Chate *et al.* [48, 49] advocate a first order (discontinuous) transition, other authors have proposed that the nature of the transition depends on the way noise is introduced in the system [50][51].

We have assumed an infinite size for the system, and finite-size scaling methods have been used to study the system behavior for various sizes [52], and found no significant difference.

Another difference is to use a nematic alignment instead of polar alignment. It leads to a larger variety of structures, with nematic ordering [53]. The advantage in this case of simulations is that they allow a much wider scope of parameters, when compared to experiments [54].

1.2.1.2 Apolar interaction

The simplest possible model [55, 16], without polar interactions, has the same update for positions, $\mathbf{r}_i(t + dt) = \mathbf{r}_i(t) + \mathbf{v}_i(t)dt$, a velocity that varies around a constant v_0 , and a repulsive force \mathbf{F}_i is added, as well as

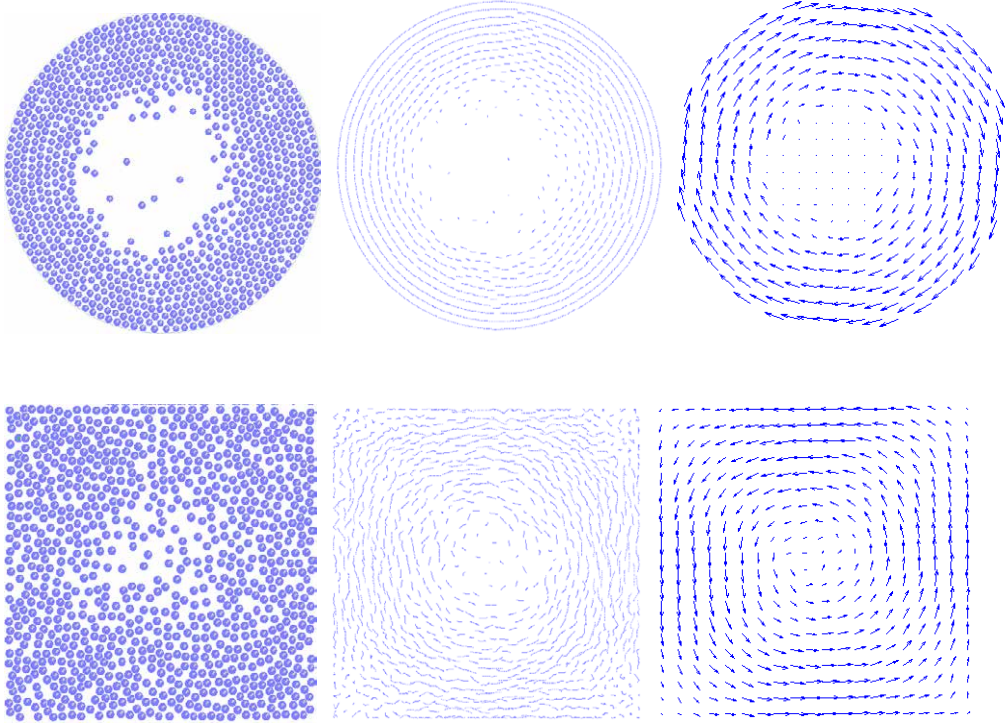


Figure 1.10: Collective effects ($N=900$) with apolar, inelastic interparticle interaction. The walls are reflective, i.e. they cause particles to move parallel to them. Positions (left); Short-term trajectories (middle); Averaged velocity field (right). The resulting state shows polar order, with the formation of a vortex, whose direction depends on the initial conditions. Square boundary conditions impose singularities at the corners; polar order; is maintained but not the spatial ordering present with the circular walls. (from [56]) See this video.

a random fluctuating force $\tilde{\mathbf{f}}_i$, typically white noise:

$$d_t \mathbf{v}_i = \mathbf{v}_i \left(\frac{v_0}{|\mathbf{v}_i|} - 1 \right) + \mathbf{F}_i + \tilde{\mathbf{f}}_i,$$

The repulsive force is $\mathbf{F}_i = \sum_{i \neq j} \mathbf{F}_{ij} + \mathbf{F}_{wall}$, where \mathbf{F}_{wall} is the force exerted by the wall on the particle, and the interparticle interaction is expressed as:

$$\mathbf{F}_{ij} = \begin{cases} (\mathbf{r}_i - \mathbf{r}_j) \left(\frac{r_0}{|\mathbf{r}_i - \mathbf{r}_j|} - 1 \right) & \text{if } |\mathbf{r}_i - \mathbf{r}_j| < r_0 \\ 0 & \text{if not,} \end{cases}$$

where r_0 is the size of a particle. While there is no result for large systems, small bounded systems shows emergence of polar order [16]¹⁸, with a

¹⁸The specific work by Derzsi and Viscek 2009, cited in [16] is unfortunately not accessible.

first order phase transition. Similar interactions, with an inelastic part, propose similar results (see fig. 1.10). This is surprising but the role of interfaces in the transition is not clear (see also experiments results by Deseigne *et al.* in [28][30]). Dissipative interaction could lead to effective polar effects [56], but for purely apolar forces another mechanism must be at play in order for large scale polar order to emerge. A possible explanation is the interplay between the local polar order that naturally arises, and possible emergent long-range interactions in the system, such as cooperativity effects near the jamming transition.

This type of apolar interaction can easily be expanded to attractive forces, and one can thus observe spatial ordering, and local polar order, with swarms, mills, and bands. These structures are only stable in the presence of noise, which is interesting.

1.2.1.3 Other theories

There are many other microscopic theories, and all are more complicated than the two we just presented, which are really minimal models giving rise to collective effects. Other models take into account new conservation laws, for example, they conserve energy, or momentum. While these models are more complex, they also have a simpler theoretical use if one wants to derive hydrodynamic equations for example. Limitations such as having an interparticle interaction that depends on a potential energy have deep signification, leading to new conserved quantities.

Another aspect we did not discuss is the interplay between high density behavior such as jamming [11, 57, 55], and activity. Activity has deep consequences, increasing [58, 59] the jamming density. These results are discussed along our experimental contributions in chapter 4.

1.2.2 Hydrodynamic continuum model

From these microscopic models, it is possible to derive hydrodynamic equations for the averaged quantities. We schematically describe the methods and physical assumptions used notably by Toner and Tu[60, 61, 11], focusing on the standard Viscek model, with polar alignment.

The microscopic density and polarity field are:

$$\begin{aligned}\rho(\mathbf{r}, t) &= \sum_i \delta(\mathbf{r} - \mathbf{r}_i(t)) \\ \mathbf{p}(\mathbf{r}, t) &= \frac{1}{\rho(\mathbf{r}, t)} \sum_i \frac{\mathbf{v}_i(t)}{|\mathbf{v}_i(t)|} \delta(\mathbf{r} - \mathbf{r}_i(t)).\end{aligned}$$

The number conservation is expressed as

$$\partial_t \rho(\mathbf{r}, t) = -\nabla \cdot (v_0 \rho \mathbf{p}),$$

with v_0 the particles' velocity. Separating the forces that derive from a potential from those that don't, the time evolution of the polarity is:

$$\partial_t \mathbf{p} + \lambda_1 (\mathbf{p} \cdot \nabla) \mathbf{p} = \frac{1}{\gamma} \frac{\delta F_p}{\delta \mathbf{p}} + \mathbf{f},$$

where λ_1 controls the advection of the polarity, and γ is a rotational velocity, expressing how hard it is for particles to turn. The last term \mathbf{f} , that holds all forces not deriving from a potential, is assumed to be a white Gaussian noise, independent of local density ρ or polarity \mathbf{p} .

With a suitable choice of potential, the dynamic equation writes:

$$\begin{aligned} \partial_t \mathbf{p} + \lambda_1 (\mathbf{p} \cdot \nabla) \mathbf{p} &= - \left[\alpha(\rho) + \beta |\mathbf{p}|^2 \right] \mathbf{p} + K \nabla^2 \mathbf{p} \\ &\quad - v_1 \nabla \frac{\rho}{\rho_0} + \frac{\lambda}{2} \nabla |\mathbf{p}|^2 - \lambda \mathbf{p} (\nabla \cdot \mathbf{p}) + \mathbf{f}, \end{aligned}$$

where ρ_0 , $\alpha(\rho)$, β , K , v_1 and λ describe the interaction potential. ρ_0 is the average density; α , and β produce a phase transition for the polarity with respect to density; K gives the importance of nematic ordering; v_1 and λ control splay in the system.

The traditional way of analyzing such hydrodynamics interaction is to do linear stability analysis around stable states, to see which modes are selected. The isotropic state can be unstable depending on the above parameters [62], a density dependent velocity leads to a density phase separation, a spinodal decomposition in dense zones and low density gas. With different parameters, density waves can propagate [63], similar to sound waves. This is a first example of the structures the model can lead to, but the ordered state can also be unstable, leading to more complex patterns, such as bands, polarization sound waves, and giant density fluctuations.

This method can be expanded to the case of nematic interactions, and describes other types of instabilities, that lead to nematic ordering. There is to my knowledge no hydrodynamic theory for positional interaction, that would lead to polar ordering.

1.2.3 Conclusion

Experiments show a great wealth of structured collective effects, in a myriad of different systems, with interactions varying widely, in physical nature and in symmetries. The theories are also very different, and the

minimal models proposed also create a great variety of collective effects. To constrain these models, and to help finding the parameters that are not necessary to get collective effects, well controlled experiments are necessary, which require model experimental systems. This is why we have developed a system of physical colloidal active swimmers, whose physical nature is detailed in the next chapter.

1.3 Conclusion

The experimental and theoretical studies set a context at the beginning of this PhD, which motivates our study of a model physical abiotic active system, at the colloidal scale, to bring a contribution to the study of the generic physical causes of collective behavior.

Our use of a colloidal scale system allows for hydrodynamics and chemical interactions. As a model system, we will be able to control activity, and see the evolutions of the collective effects with respect to activity. The simple observation of collective effects is by no means guaranteed, as we need to find or create an experimental system whose operating parameter, in terms of interactions and activity, fall in the region allowing collective behavior.

We will use a statistical physics approach, trying to link microscopic-scale observations, with macroscopic properties.

Long term questions. The fluid-mechanics approach to the description of collective effects, with the coarse-grained density and velocity field is very promising. The main question I would like to see answered is the following: *is it possible to derive hydrodynamics equations for the active system*, by using a simple microscopic model? If yes, *which terms appear that describe activity*, and how are quantities such as *viscosity linked to activity and interparticle interaction*?

Key ideas for this chapter

1. Collective effects are beautiful, and exciting to observe. Very different systems exhibit similar behavior.
2. A hydrodynamic theory can be built from microscopic principles. Collective effects require and are controlled by activity and interactions.
3. There is a need for experiments on model colloidal systems to constrain models, and to find which ingredients are essential to collective effect.

Chapter 2

Gold-Platinum Active Colloids

At the beginning of my PhD, experiments with active colloids had been performed in our group at low colloidal concentrations. These experiments [64] showed that at low concentration, the active system behaves as an ideal gas, with a temperature different from the room temperature, an *effective temperature* controlled by the motion of the colloids¹.

To be able to observe collective behavior in such an abiotic system, we need to be able to manufacture artificial swimmers, that can reach high swimmers concentration, in order to reach high interaction between swimmers. Starting from existing active colloids designs[65][66][64], it has taken a lot of experimental developments during my PhD, to manufacture swimmers that could swim at high concentrations. After a brief explanation of the physical origins of our particles' activity, the first section presents the development of our active colloids. This chapter is technical in nature, and presents mainly information aimed at reproducing the experiments we performed. The reader not interested in technical details can skip this part.

In order to get some information on the interaction between two of the swimmers I developed, which is needed to understand the collective effects that could arise, I present the microfluidic experiments use to get an indirect characterization of the interaction.

A last aspect of experimental developments done during this thesis is a dramatic change in acquisition systems. Analyzing low density ($\phi \sim 0.1\%$) assemblies of a score or so swimmers is very different in terms of acquisition material and software for post treatment than a dense ($\phi \sim 30\%$) assembly of *thousands* of swimmers. As swimmers get closer to each other, the amount of detection errors increases, and tracking algorithms require

¹Instead of $PV = Nk_B T$ the following relation holds true: $PV = nk_B T_{eff}$, where T_{eff} is the effective temperature and depends on the activity of the system.

much higher acquisition frequencies, which in turn requires the use of industrial cameras, fast data storage and transfer systems. The next three sections present details on the acquisition system, and how it was scaled.

2.1 Synthesis of active particles

The Janus colloids used at the beginning of my thesis were latex-platinum Janus, however, we have never been able to see collective effects with these. The main problem was that as we increased concentration, a step required to increase interparticle interactions, the amount of dioxygen released by the assembly of swimmers increased proportionally. This led to the apparition of bubbles in the system, which change drastically the dynamics of the system. The next obvious step to reduce oxygen generation is to have the colloids sediment in a 2D layer, which will reduce the total number of colloids in the sample. With a very small volumetric concentration, one can reach very high surface concentrations. This is easily done by increasing the thickness of the Platinum coating (at 20nm, the latex-platinum colloids are sedimented in a 2D layer $\sim 100\text{nm}$ thick). However, I could never observe active motion of the microswimmers close to a surface, as was observed for gold-platinum rods[67][68][65][69]. This led us to want to use gold-platinum colloids². Since the dissolving membranes used for the traditional synthesis proposed originally by T.Mallouk *et al.* were not sold anymore, we had to adapt it as is presented in what follows.

2.1.1 Gold-platinum Janus Colloids

Before presenting the colloid synthesis, I briefly sketch the physical origins of our Janus colloids' activity. The microswimmers we developed are $2\mu\text{m}$ in diameter gold spheres with one half coated in platinum. when immersed in a solution containing hydrogen peroxide at volumetric concentrations $[\text{H}_2\text{O}_2] \sim 10^{-4}$, they disproportionate the peroxide following:



As long as the concentration in O_2 remains below the saturation concentration, $[\text{O}]_{\text{sat}} = 3.10^{-4}\text{mol.L}^{-1}$, the dioxygen stays in solute form without creating bubbles. As peroxide is disproportionated, the colloid self-propel at constant velocities $v \sim 3\mu\text{m.s}^{-1}$.

Qualitatively, the chemical reaction (see fig. 2.1) imposes a difference of potential between the gold and the platinum faces, which causes an

²Isotropic swimmers would have been easier to produce for sure, but are yet only theoretical[70].

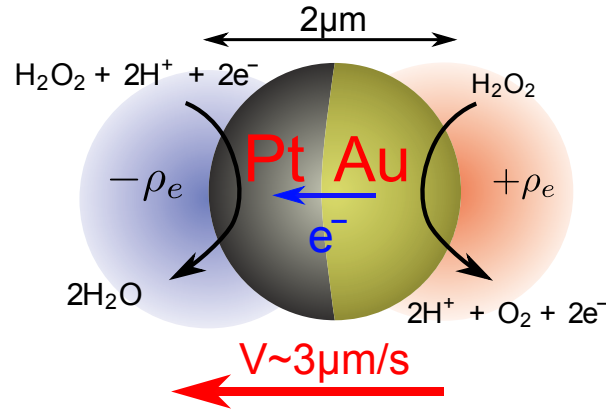


Figure 2.1: Schematic of the chemical reactions propelling the gold-platinum microswimmers. The microswimmer act as a battery in the peroxide bath, the gold electrode playing the role of the cathode, while the platinum, owing to its lower electronegativity, is the anode. Overall, the peroxide is disproportionated through $2\text{H}_2\text{O}_2 = 2\text{H}_2\text{O} + \text{O}_2$, while the exchanged electrons create a current through the colloid, which creates an electric field around the colloid, which in turns pumps electrophoretically the charged liquid in the electric double layer, which equate propulsion with velocities $v \sim 3\mu\text{m}\cdot\text{s}^{-1}$, with volumetric concentration in peroxide of only 10^{-4} .

electric current through the colloid, and the migration of the electric double layer at the surface of the colloid, owing to electrophoretic effects. This in turn propels the colloid (see details in annex A, and see sup. mat. movie 1). The colloid consumes peroxide in an homogeneous manner, and creates a gradient of concentration around itself. As we will see in sec. 2.2, the peroxide repels the colloids, and colloids move owing to diffusiophoresis in peroxide concentrations gradient, towards regions of low concentration in peroxide, that is, towards each other.

The synthesis of the microswimmers is presented in details in what follows. We first synthesize spherical gold colloids (see fig. 2.2), then these colloids are coated with a thin film of platinum on one half only, then resuspended, and introduced in the observation chamber.

2.1.2 Synthesis of the gold colloids.

Gold colloids are synthesized in the lab following methods adapted from Matijevic[71].

To prepare the gold solution, 380mg tetraaurochloric acid (Sigma) is added to 1g of a 37%w chloridric acid solution (Roth), and 1g of a 7%w gum Arabic solution (Sigma). To prepare the reducing solution, 500mg isoascorbic acid (Sigma) is added to 9.5g of a 7%w gum Arabic solution. For dilutions, we use de-ionized water (18.2M Ω). In a 10mL round-bottom

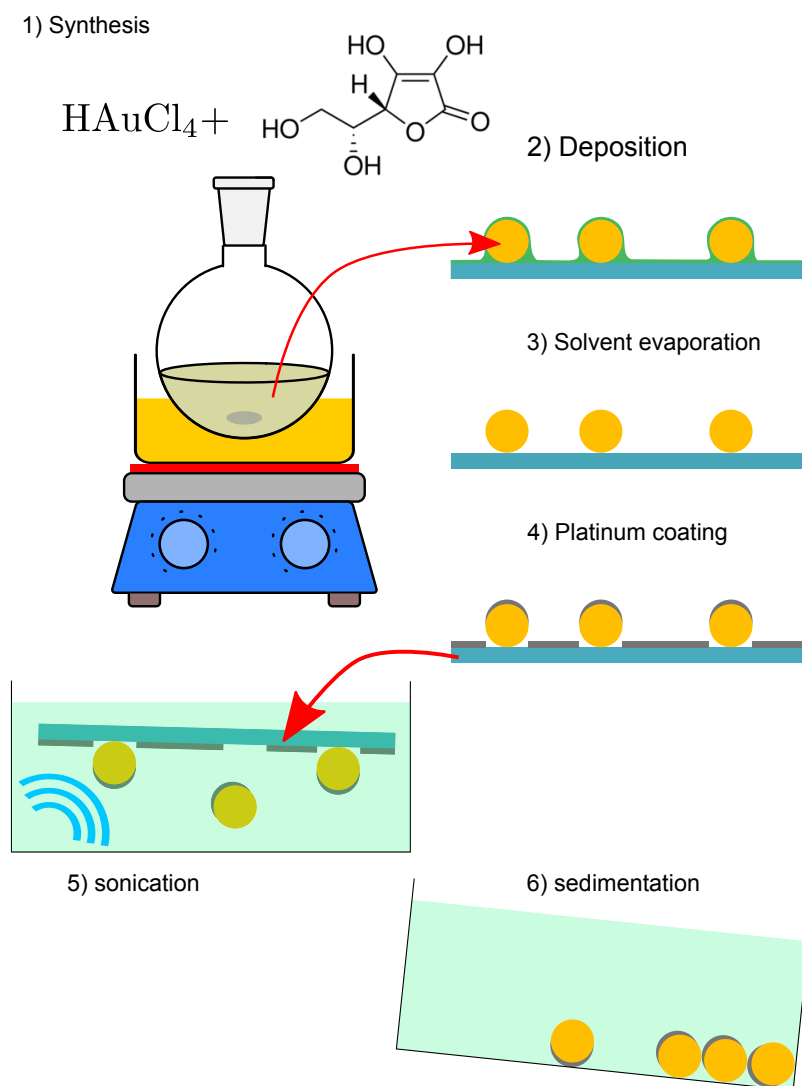


Figure 2.2: Janus Fabrication in six steps: 1) synthesis of the gold colloids 2) Deposition on a glass slide 3) Evaporation of the solvent used in step 2. 4) A thin film (20nm) of platinum is deposited on one half of the colloids. 5) The glass is sonicated to resuspend the Janus colloids, 6) They sediment at the bottom of a beaker, ready for use.

flask, under fast magnetic steering, 1mL of the gold solution is quickly added to 2mL of the isoascorbic acid solution. In 3s, the yellow color of Au^{3+} ions disappears. During the next 20s the solution turns dark brown. The solution is then heated in a water bath at 80°C for 1h. Colloids are washed three times with water, then the three times with acetone.

A synthesis of $\sim 100\text{mg}$ of colloids is more than enough to last for an entire thesis. The colloids have a 10% polydispersity, we measure an average size $2.2 \pm 0.2\mu\text{m}$, using scanning electron microscopy images, counting by hand ~ 200 colloids. Some very small colloids have diameters $d < 800\text{nm}$, while the larger ones, sometimes not very spherical, can have diameter up to $4\mu\text{m}$.

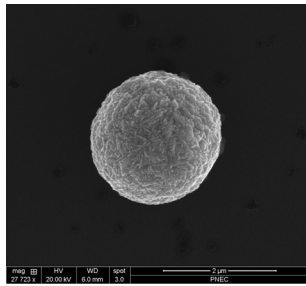


Figure 2.3: A home synthesized gold colloid observed by SEM, image R. Fulcran. The scale bar is $2\mu\text{m}$.

Limitations and evolutions. This method seems very random in its results, and probably needs better control than what we have in the lab: higher mixing velocities, accurate temperature controls, cleaner glassware. With the same initial concentrations I obtained very different resulting sizes. B. Abecassis, who had been a postdoc in the lab, has done the first batch of colloids at the ESPCI, and has come to help us start our synthesis.

2.1.3 Deposition and platinum coating.

The deposition of gold colloids on glass is adapted from processes previously developed in the group, with important changes, since the sticking properties of gold on glass are very different than those of latex, implying very different concentrations and deposition times.

The colloids are re-suspended in 10mL isopropanol (Sigma) at very low ($\sim 10^{-7}$) volumetric fraction. A thin film of the suspension ($200\mu\text{L}$ on a $52 \times 75\text{mm}^2$ glass slide) is deposited onto a glass substrate. The liquid is evaporated under a laminar flow cabinet leaving a monolayer of colloids at a very low surface concentration to avoid the formation of dimers or trimers of colloids, that are impossible to separate in the next steps [?, 66]. We measure less than 10% of dimers. 20nm of Pt is then deposited onto the colloids through ion beam epitaxy. This step is done in a clean room facility at the INL/INSA Lyon, by J.Gregoire.

The main limitation in this step is the quantity of colloids that we can create in one batch. The number of defective colloids is also quite high, with $\sim 10\%$ dimers and trimmers, that behave differently from individual

colloids.

2.1.4 Re-suspension and Sample preparation.

The glass slides holding the colloids are sonicated for approximately 30s in a 15cm diameter flat beaker containing $\sim 0.3\text{L}$ of de-ionized Water ($18.2\text{M}\Omega$). The sonication time is long enough so that most of the colloids are detached from the glass substrate, but the Platinum covering the rest of the glass remains stuck to the glass. To avoid the detachment of platinum from the glass, we stop the sonication as soon as we see cavitation on the glass, as small bits of platinum are easily leaving the glass when small bubbles appear. The beaker is then tilted with a 30° angle to let the Janus colloids sediment at the bottom. With a good choice of sedimentation angle, most of the small bits of platinum and glass that have been suspended by the sonication process will be differentially sedimented, since they stick more easily on the glass, and will not be mixed with the Janus colloids.

Once the colloids are sedimented, we place them in an observation chamber: a well from a 96-well plate with a flat clear imaging bottom (ref 353219 from BDbioscience catalog³) (this series has the flattest bottom, and a constant $170\mu\text{m}$ thickness for optical compensation).

The surface has received a chemical treatment, promoting cellular adhesion. This treatment is very important to obtain colloid motion, as these Janus colloids, do not swim on most surfaces, probably owing to surface chemistry effects⁴. After discussions with E.Clement and G.Mino, we tried several different treatments for glass, from chemical etching to plasma cleaning. By chance, we found that the TC+ treatment from BD biosciences is an extremely good surface treatment for our microswimmers, they swim on it 5 times faster than on plasma-cleaned glass. The precise nature of this treatment is kept secret by the manufacturer, but it includes at least one plasma cleaning. Maybe the nature of the polymer film (polystyrene) is also modified. They move five times as fast on this substrate when compared to standard glass.

The sedimentation length of the particles is $l_g = \frac{k_B T}{mg} \sim 10\text{nm}$, they can be stuck in a well if the height of local inhomogeneities is above

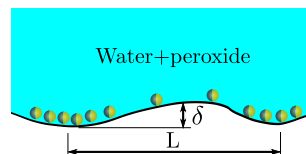


Figure 2.4: Schematics of the bottom of a cell. The characteristic depth δ of the inhomogeneities is of order 10nm . While their length L is of order 1mm .

³Since the acquisition of BD-Bioscience by Corning, this is probably ref #3904 from the Corning catalog.

⁴They do not move on SU-8, silicon, or silicium, and a little on glass, even when plasma-cleaned.

l_g . Even though the bottom of the plate is very flat, the typical depth of heterogeneities is $\sim 10\text{nm}$ and their length $\sim 1\text{mm}$ ⁵. The colloids naturally sediment to the lowest zones. To make an experiment at constant density, we simply find a zone that has an homogenous distribution of colloids over an area much greater than the observation area: $350 \times 350 \mu\text{m}^2$. To make a sedimentation experiment, we simply go to a zone that has a shallower bottom and that present a densely packed solid. A depth of 50nm should be enough.

If allowed to evaporate, the liquid in the cell convects, stirring the whole cell and moving the colloids at the bottom with velocities of order $\sim 1\mu\text{m.s}^{-1}$. Since this convection velocity is of the same order of magnitude as the propulsion velocities, it has to be avoided. We fill the Cells adjacent to the observation cell with water as well as the interstitial space between the cells, to get an atmosphere saturated with H_2O . The resulting convection velocities are rarely above $0.05\mu\text{m.s}^{-1}$.

2.1.5 Evolution of the Active colloids for the study of collective effects.

Observing collective effects requires a high concentration in microswimmers. Indeed, as swimmers get closer to each other, their interaction increases, potentially leading to collective behavior. The latex-platinum colloids previously developed in the lab [64] could not be studied at high concentrations, due to oxygen production leading to bubble formation. To avoid the production of oxygen, I have probed three main leads:

1. Use a two dimensional system. By increasing the mass of the colloids, they can sediment in a 2D layer. This decreases the amount of oxygen produced by as much as 10^5 . Indeed, the important parameter in the system, as far as the interparticle interactions are concerned, is the distance between swimmers. In 3D, $d = \rho^{-3}$, while in 2D, $d = \rho^{-2}$. since the production of peroxide is always proportional to ρ , the 2D case is much more favorable. In our case however, the chemistry of the interface prevented this trick with latex-platinum colloids. They simply do not swim on a glass surface, which led me to study gold-platinum colloids.
2. Another idea is to use oxygen scavengers: species that will consume the oxygen as it is produced, such a dimethyl sulfoxide (DMSO (CH_3)₂SO). However, we could not get active propulsion with DMSO

⁵ These values are orders of magnitude indirectly measured from the spatial distribution of colloids, and not accurate measurements from interferometry or AFM surface characterization.

in the system. Maybe the DMSO prevents the disproportionation of peroxide.

3. Use a different propulsion reaction, that does not produce a gas. We tried organic reactions, the Heck-Suzuki catalysis, Cannizzaro reaction, and the purely mineral dissolution of vaterite (CaCO_3) in acid. The organic reactions are failures, in the sense that no active motion is observed. It is hard to find a reaction that can produce as much energy as the disproportionation of peroxide ($3.10^2\text{kJ}\cdot\text{mol}^{-1}$). Moreover, the lack of proper chemical equipment implied it was hard to know if the chemical reaction had actually worked. The dissolution of vaterite has shown promising results, and might be used in the future.

The gold-platinum colloids we have developed, rely on a 2D approach, but also on the fact that gold-platinum colloids are ~ 1000 times more efficient, swimming ten times as fast with only 1% of the fuel⁶. Increasing the efficiency implies we can increase the swimmers concentration without worrying about oxygen bubbles. Another point is that with spherical Janus colloids, the steric interaction is simpler, when compared to rods that have a polar⁷ interaction. The spherical shape has one additional advantage in that the friction is smaller so the shape is more efficient

2.2 Characterizing the interparticle interaction.

A key element to predict the possible collective effects in our system would be to fully characterize the interaction between two swimmers. However, as we will see later (see sec. 3.2) a quantitative characterization is not easy. Here we present an indirect way to measure important characteristics of the interaction.

To characterize the chemical interaction between our colloids, during S. Guerraz master's internship, we used a microfluidic device specifically designed to study diffusiophoresis. Indeed, a active colloid consumes peroxide, and thus creates a gradient of peroxide around itself, we propose an experiment to see how a colloid behaves in the gradient created by its neighbors. Designed in 2008 by B. Abecassis *et al.*[72], the device (see fig. 2.5) is a $50\mu\text{m}$ high, $400\mu\text{m}$ wide, and 8cm long micro-channel with 3 inlets. The two inlets on the side are linked together to equalize the pressure. A

⁶This is not a thermodynamic efficiency, they probably consume the fuel much faster.

⁷It is at least nematic[11], not necessarily polar.

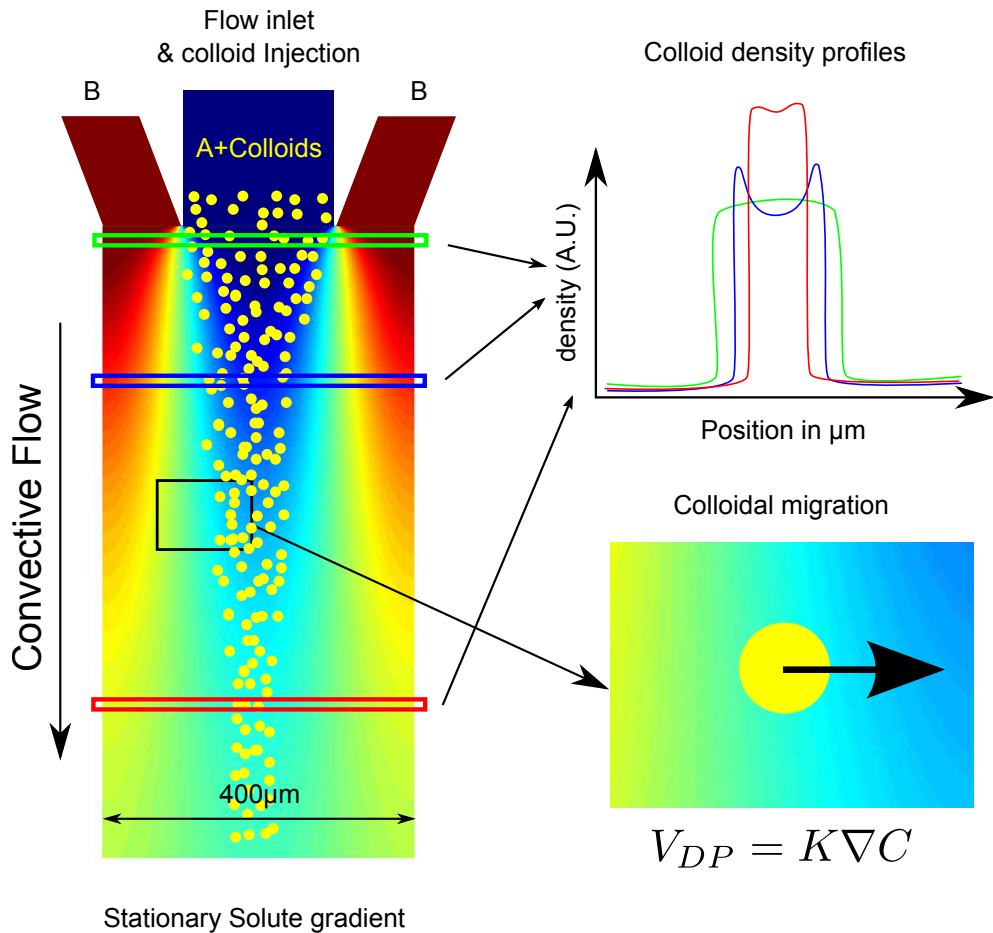


Figure 2.5: Sketch of the Ψ -shaped channel. The colloids suspended in solution A are injected in the center, while solution B is injected on both sides. The resulting concentration field, computed with a simple Euler algorithm, and represented as color hues, moves the colloids along its gradient owing to diffusiophoresis. The concentration profile in colloids is measured along the axis orthogonal to the flow. The time evolution of the density profile allows us to measure the colloids velocity, and thus the diffusiophoretic constant.

dual Syringe-pusher (KDSscientific, Harvard apparatus, or Nemesys) is used to inject fluids at controlled rates (usually $\sim 20\mu\text{L}\cdot\text{min}^{-1}$) inside the channel. In the center channel, the colloids (100nm GFP-labeled latex colloids) are injected in suspension in solution A (A can be a solution containing $0.1\text{mol}\cdot\text{L}^{-1}$ of peroxide). Solution B (e.g. deionized water) is injected on the sides. Depending on the nature of the injected solutions, a solute gradient is established in the channel. As diffusion equation are well-known, the precise shape of the concentration gradient can be obtained by numerical simulations; and also experimentally by using fluorescent markers such as fluorescein as a solute. The colloids will move inside this gradient of concentration C owing to diffusiophoretic effects [73, 74]:

$$\mathbf{v}_{DP} = \nabla KC.$$

For many species, even the sign of the diffusiophoretic constant K is unknown. The experiment consists in a measure of the time evolution of the colloidal density profile. From the time evolution of the colloidal density and solute concentration distributions, assuming an infinite Péclet⁸ number, we can invert the distribution evolution equation:

$$\begin{aligned} \partial_t \rho &= -\nabla \cdot \mathbf{v}_{DP} \rho, \\ &= -\mathbf{v}_{DP} \cdot \nabla \rho - \rho \nabla \cdot \mathbf{v}_{DP}, \\ &= -\mathbf{v}_{DP} \cdot \nabla \rho, \end{aligned}$$

with ρ the colloid density, and assuming an incompressible fluid. Since at infinite Péclet, the density variations are only in the direction orthogonal to the fluid flow,

$$\mathbf{v}_{DP} \cdot \nabla \rho = K (\partial_x C) (\partial_x \rho).$$

This allows us to measure K ,

$$K = \frac{\partial_t \rho}{(\partial_x C) (\partial_x \rho)}.$$

We perform this experiment for various molecular species, saccharose, hydrogen peroxide, alcohol, and salts. This experiment allows us to confirm that peroxide is a repellent species for the latex colloids⁹. Although

⁸Infinite Péclet $\text{Pe}=vR/D$, where v is the flow velocity, implies that the fluid is advected infinitely fast by the flow, and its motion does not modify the solute concentration profile. In our case the Péclet is $\sim 10^4$.

⁹A secondary property of these experiments is that they allow us to measure K in a very accurate manner, since we measure K for many different concentrations and gradients, that takes into account the fact that K is not a constant, but rather a function of the concentration in peroxide. The time evolution equation can be rewritten by taking into account the diffusion of the peroxide, and then inverted to

the colloids we studied are not made of gold (experiments with gold colloids were not possible due to their heavy weight), we can postulate that gold colloids will behave similarly, and migrate towards regions of low concentration in peroxide.

2.3 Microscopy observations

We simply ask of our observation system images whose quality is sufficient for an easy and reliable particle detection. As always, microscope observations are a compromise between resolution, at high magnification, and the size of the observation field. This has consequences on the observable dynamics of the colloids, as will be explained in the third chapter.

To make observations of colloids, the optical microscope is the perfect tool. The high resolution offered by standard microscopy allows an easy detection of the colloids. However, it is important to note that image quality is extremely important to avoid detection errors.

We use a leica DMI 4000B inverted microscope. For most experiments, in order to have good statistics and a large observation area, we use a 20x plan fluotar objective, with a numerical aperture of 0.5, and 1.6x a magnification lens inside the microscope. The overall magnification is 32.16x, measured with a microscope calibrator ruler (Nikon), meaning that the $5.5\mu\text{m}$ pixels of our camera gather light from a square of side $0.171\mu\text{m}$. Although the pixels are squares, the light sensitive area is rectangular, which reduces the resolution. Diffraction also reduces resolution, the theoretical minimum size the microscope should be able to resolve is

$$d = \frac{\lambda}{2\text{N.A.}} \sim 500\text{nm},$$

N.A. being the numerical aperture of the microscope. The actual resolution of the microscope is smaller than this limitation, owing to lens aberrations, to diffusion inside the sample. Our has a decreased sharpness because of these effects.

Another aspect of image quality is the contrast. As our colloids are opaque, the contrast in transmission mode is very good (we easily get a ratio between the colloids and the background of ~ 100). however the diffraction ring around each colloid means that the image of two colloids close to each other is blurred into one elongated colloid. The human eye

measure $K(C)$:

$$\partial_t \rho = -\nabla(K(C) \cdot C \cdot \nabla \rho).$$

However, while for ionic compounds the functional form of $K \sim 1/C$ can be found, it is harder for other components, especially since there is no theoretical predictions.

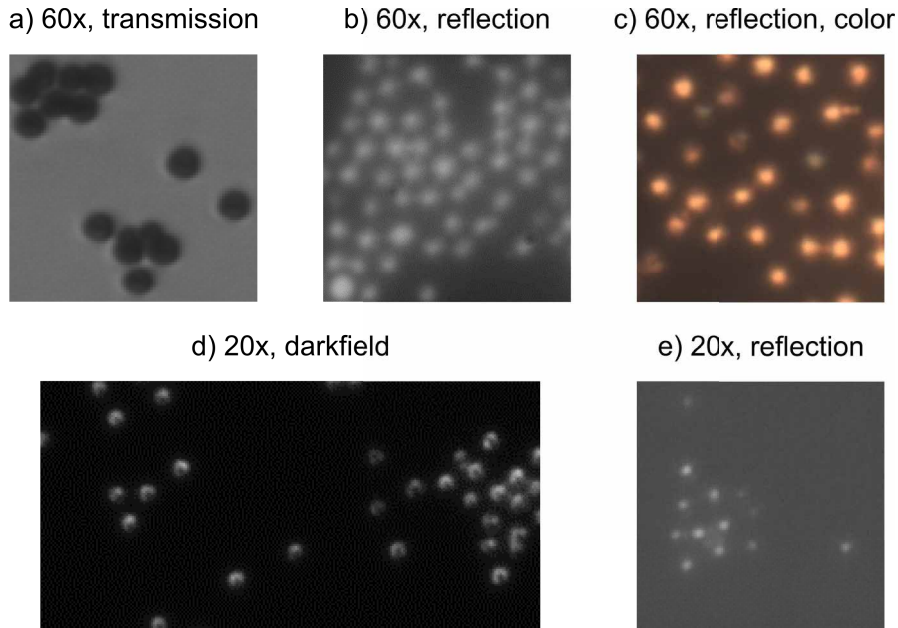


Figure 2.6: Typical best image quality for different observation methods, and several magnifications. All images are 20 μm high. a) transmission mode, 60x. This image has a very high contrast, however, diffraction and shadow effects make the colloids hard to identify, especially in the lower cluster. b) In reflection mode, with the same magnification, the contrast is decreased, but colloid detection is easy. c) In color mode, we can observe the platinum faces (blue) and the gold (yellow). However, at high magnification, the observation field is small as is the total number of colloids observed. To increase it, we must lower the magnification. d) external darkfield 20x. Very high contrast, good detectability. e) 20x, reflection, the contrast is quite low, but tracking is still possible although some errors are introduced. (compressed from a 12-bit image). The encoding for these images might not be pixel-accurate, however, the images have not been modified in any way and are as faithful as possible to what the camera saw.

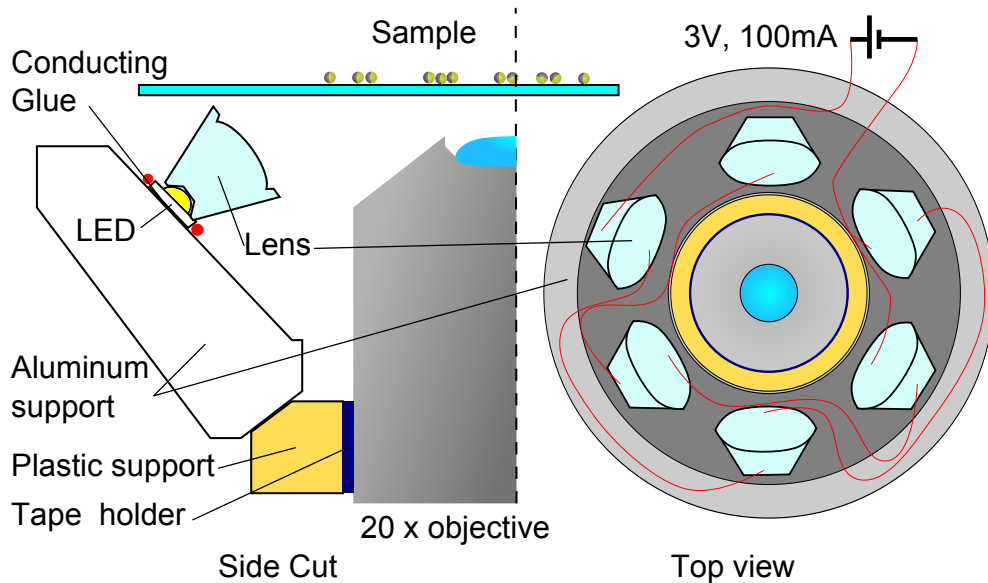


Figure 2.7: Schematic of our external darkfield microscopy lightning ring, and photo. The microscope objective is 2.7cm in diameter. The six 1W photodiodes are focused on the sample with small plastic lenses. The aluminum ring serves as a holder and radiator for the diodes, that are glued to it with thermal conducting glue.

has no problem detecting that the ovoid shape is in fact two colloids, but it is much harder for a computer algorithm. Even for the human brain, identifying colloids in an assembly of four or more blurred colloids is hard. The transmission mode is thus reserved for illustrative movies. In reflection mode, the light reflected by the colloids allows an easier detection of the center.

2.3.1 External darkfield microscopy.

In standard reflexion mode, the contrast is sub-optimal, which led to detection failures for the smallest, dimmest colloids.

To increase contrast in reflection mode, we developed at the end of my PhD, as part of F.Ginot master's internship, an external darkfield lightning ring. Similar in concept to standard lightning rings developed for photography, this ring (see fig.2.7) emulates a darkfield microscope by lightning the sample only with rays having a very high angle with respect to the optical axis. The light that is back-scattered inside the sample cannot enter the objective, leading to a dark background, and dramatically increasing contrast. Indeed, the colloids are ten times as bright as the background, which allows easy thresholding in the next step.

Limitations and evolutions : At the very beginning of the project, the use of green fluorescent latex colloids, allowed an easy imaging, with

very high contrast. The shift to gold colloids, decreased the contrast dramatically, when using standard reflection microscopy, because of back-scattered light. The background is only 10% darker than the colloids with the lowest brightness. Moreover, the background was not homogenous, and the darkest colloids were darker than the background, forcing us to use increased 12-bit image depth in our imaging, slowing acquisition¹⁰, and doubling file size¹¹. Even then, the intensity fluctuations of some colloids led their intensities below that of the background for one or two frames, leading to broken trajectories. This problem is fully solved using our darkfield lightning setup.

2.3.2 Janus Polarity.

To observe the emergence of nematic order in an assembly of Janus colloids, we need to measure their orientation. The gold half and the platinum half do not have the same color, due to the optical properties of the two different metals. Gold appears yellow under a white light, while a thin 20nm platinum layer is blue. To measure this difference in color, we use a color camera (Baumer HXG40c) (see sec.2.6 for details on the acquisition system) and a high aperture objective (63x water-immersion objective, Nikon, N.A.1.2). The color difference between gold and platinum is not very sharp, and requires color balance tuning to show it. Our darkfield ring does not yet work for the high-aperture objectives, we use the standard reflection mode, with low contrast.

To measure the orientation, we need two angles per colloid: θ its in-plane angle, and ϕ its declination, the angle with respect to the vertical. To measure these angles, we need to detect the gold and platinum parts for each colloid. This problem is a color segmentation problem, we have three colors to detect, one is the dark background, one is the yellow of the gold face, and the last the blue of the platinum-coated face. Each pixel in the image is a 3-component vector: RGB. Each of the parts we are trying to distinguish is a badly defined cluster in RGB-space. Segmenting colors means identifying three different clusters among all pixels. The easiest way to do this is by simple thresholding: the darkest areas belong to the background. We then use the Lab* color space to maximize the distance between blue and yellow. This gives acceptable results, but the variability between colloids, and the noise inside each colloid make it a non practical method for quantitative analysis.

¹⁰Besides the increase in bandwidth, that limits the maximal acquisition speed, increasing the bit depth to 12-bits quadruples the readout time of CMOS sensors.

¹¹Although 12-bit images should only be 50% heavier than their 8-bit counterpart, all standard image encoding schemes only allow 8 or 16 bit per channel, which wastes 4 bits.

Limitations and evolutions : Our being able to resolve the color difference between gold and platinum is quite recent. It is limited by the residual chromatic imperfections of the objective. Only the central 40% of the image is usable the exterior rim has blue halos on the side of the colloids facing away from the center, similar to a platinum coated face. Compared to the other monochrome camera used for most of the other experiments, The color detector is also less sensitive (by $\sim 60\%$), and the Bayer filtering (see sec. 2.6.1.4) decreases accuracy (by $\sim 50\%$). The images are not yet usable for standard analysis techniques. Other segmentation methods, such as principal component analysis¹² have been tried, to no avail. The next step is to develop a darkfield ring to enhance the contrast with high numerical aperture objectives. The colors can already be seen with the 20x objective. The use of smarter algorithms, for segmentation, either with vector support machines[75] or learning algorithms, is also planned.

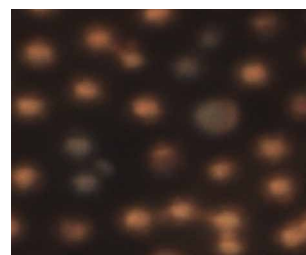


Figure 2.8: Color photography of Janus Colloids. Gold appears yellow, and platinum blue. The color saturation is enhanced to increase color separation. The image is 10 μm wide. Platinum half-caps can be seen.

2.4 From movies to trajectories

Most analysis we want to make are similar to what is done in molecular dynamics simulations. We want to measure dynamical properties, scattering functions, mean square displacements... However, we have to measure the positions and velocities of the particles before we can try this approach. Since the beginning of this project, several algorithms, developed almost 10 years ago have been at the heart of every analysis I have done. I will present first a simple detection algorithm, then the trajectory reconstruction algorithms all written by Crocker *et. al.*[76] that we use in their Matlab iteration from Grier and Weeks.

2.4.1 Particle detection

The particle detection step is by far the most time consuming. Very large sets of data have to be analyzed, a typical movie of 2000 frames weights 8GB. A day's worth of experiment easily weights over 200GB. These amounts of data rule out the use of computing clusters for the analysis,

¹²Changing colorspace to maximize the distance between colors is one possible change of color representation. Principal component analysis is the method that find the optimal color representation.

since the data transfer is often slower than doing the computation on a workstation. Data transfer on the ENS cluster is below 1MB/s, meaning two days to transfer one day of experiments. Not to mention that most clusters are pretty mean with HDD space...

We use a powerful workstation (4-cores, 64GB ram, 800GB of raid5 disk space, 6TB of slow HDDs). We read each image I as a matrix of doubles. The natural computing element in Matlab are doubles, required for most image filters or analysis. This leads to a real waste of ram by a factor 8. I_{xy} is the value of the pixel at position (x, y) in the image. After a Gaussian filtering to remove high spatial frequency noise in the image, we detect all local maxima above a threshold T . The nature of the filtering has great influence on the number of maxima detected in a single colloid. If the high frequency noise is high enough, several secondary maxima can be detected inside a single colloid. All these local maxima could be associated with colloid centers. A single colloid, especially large ones can have two local maxima inside the colloid image. For each pair of maxima, separated by a distance smaller than d , we remove the maximum of smaller value. If both maxima have the same value, we remove one at random. To achieve a better accuracy (the authors claim sub-pixel accuracy), we draw a circle \mathcal{V} of radius d around each maxima, and define the coordinates of the center of the colloid as the center of mass of all pixels in this circle :

$$\begin{aligned} X &= 1/\gamma \sum_{i \in \mathcal{V}} x_i I_{x_i y_i} \\ Y &= 1/\gamma \sum_{i \in \mathcal{V}} y_i I_{x_i y_i}, \end{aligned}$$

where $\gamma = \sum_{i \in \mathcal{V}} I_{x_i y_i}$. The algorithm originally used Gaussian averaging because of the theoretical shape of fluorescent colloids. However, our colloids are not fluorescent, and taking the barycenter, has no real effect, as can be seen in fig 2.9.

Since all images are independent, the code is easy to parallelize, and I obtain an almost threefold gain in computing time (Matlab uses 4 cores while the processor uses hyper-threading and has 8 available logical cores). The most time consuming step is the image loading, and the maxima detection. Overall, it takes about one second per image. At the end of this step, we have a matrix of all positions, containing for each time step the coordinates of each particle's center.

This detection method is extremely simple, and works reasonably well, at each time step, less than 0.1% of all particles are lost, and we are able to detect $\sim 10^4$ particles in a field of view, giving statistics comparable and even exceeding molecular dynamic simulations. For each

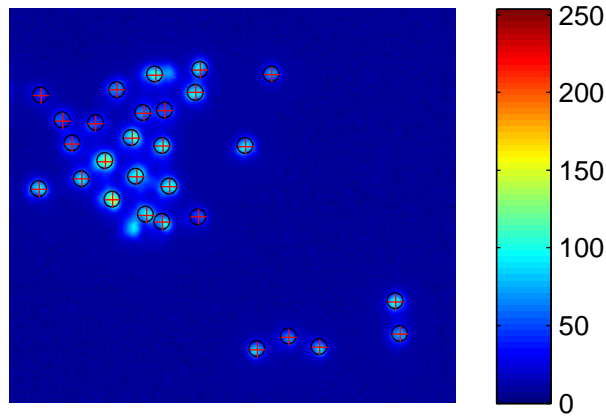


Figure 2.9: Detection of colloids, and trajectory reconstruction. Red + indicate the position of colloids, black circles, the position of local maxima above threshold T . The underlying image is an image without filtering, color coded to enhance visibility. Several detection errors can be seen. The image is $30\mu\text{m}$ wide .

movie, depending on lightning conditions and density, we tune T the threshold, D the minimum distance between colloids.

Limitations and evolutions. This detection technique gives an accuracy of about one pixel or $0.2\mu\text{m}$. Between each frame a particle will move very often by a single pixel. This limitation is very important when we will measure velocities, for even a fixed immobile particle could be erroneously associated with a displacement between two frames. Another limitation is that it does not work very well for low contrast images. Without the darkfield lightning ring, the contrast is not high enough to define a proper threshold for the first step. I developed a watershed segmentation algorithm, that has the advantage of a much better handling of secondary minima. However, since the contrast offered by darkfield microscopy is so high, we came back to this algorithm that was used for the first generation of polystyrene-platinum fluorescent Janus colloids.

2.4.2 Trajectories reconstruction.

Once we have the positions, measuring the velocities requires the reconstruction of the trajectories of the particles. The problem of reconstructing trajectories is central in many experiments, especially for all Brownian motion experiments. Very smart algorithms have been written[77] for 2D tracking in a 3D world, since losing particles is frequent. Also in turbulent regimes one can use the persistence of the trajectories to estimate a likely future position for a particle[78]. In our case, we focus on a simple

case: for an ensemble of N particles, with positions $\mathbf{r}_{i(t)}(t)$ ¹³, while we know only $\mathbf{r}_i(t)$. The trajectories are functions $i(t)$ that minimize at each time step:

$$S(t) = \sum_{i=1}^N \left(\left| \mathbf{r}_{i(t)}(t) - \mathbf{r}_{i(t+1)}(t+1) \right|^2 \right).$$

Evaluating this sum is extremely difficult. This problem is of the same factorial complexity class ($o(N!)$) as the traveling salesman problem. Since we have $\sim 10^4$ particles, $N!$ is way too large to allow the sum to be computed. Another problem is that particles may leave the observation area. Which means we operate at variable N . A last undesired effect is the loss of particles for one frame when the detection algorithm fails.

Using again the algorithms by Grier and Crocker[76], to seriously limit the computation time, we set a maximum allowed displacement δ . We will have to be careful to acquire images at sufficiently high velocities so that even the fastest particles move by less than δ . We transform the sum above in a very simple sum by taking $\delta < D$, where D is the minimum distance between two colloids. D is less than any colloid diameter. For our experimental system, we take $D = 1.2\mu\text{m}$, and $\delta = 1.0\mu\text{m}$. This allows us to measure velocities of up to $20\mu\text{m}\cdot\text{s}^{-1}$. We have verified that even for the highest peroxide concentrations, no colloid has a velocity higher than $15\mu\text{m}\cdot\text{s}^{-1}$.

Once these limitations are set, there can be at most one solution for all colloids that stay inside the observation field. The algorithm that compute trajectories is then limited to compute trajectories between a given colloid and all colloids on the next frame within a distance δ of the original position of the colloid, however, since $\delta < D$, there is no more than a single colloid in this region. This is a much simpler $o(N\log N)$ problem.

For particles that leave or enter the observation area, they enter at positions that do not belong to any neighborhood previously defined. They are simply labeled as new particles. This step is fast, taking only one minute to analyze 10^4 particles during 2000 time steps.

Limitations and evolutions. This algorithm can be made to work out of this very constraining regime if the average distance d between colloids is much larger than the maximum allowed displacement. This algorithm defines how the acquisition has to be done. With first camera used during this thesis, frame rates could not go above 10Hz, and it was very difficult to track dense assemblies, and the presence of clusters made it very long to run. This is what motivated the use of a new and faster camera (see sec.

¹³One has to be careful to note that at that point, the i^{th} particle at time t is not the same particle as the i^{th} particle at time $t + 1$. The objective of trajectory reconstruction is to find the proper indexing of the particles.

2.6). It is also very constraining with detection errors, in that whenever a colloid is lost on one frame, the trajectory stops. Several algorithms have a memory that allows reconstruction of trajectory with uncertain detection. However, these algorithms have to make assumptions on the trajectories that could bias the statistics of displacement, especially at low activity in the Brownian case. This is why they could not be used in our case.

2.5 Differential dynamic microscopy.

A recent method to study the dynamics of a system, inspired by dynamic light scattering techniques, is an indirect measurement of the intermediate scattering function $f(\mathbf{q}, \tau) = \frac{S(\mathbf{q}, \tau)}{S(\mathbf{q}, 0)}$, where $S(\mathbf{q}, \tau) = \langle \rho(\mathbf{q}, t) \cdot \rho^*(-\mathbf{q}, t + \tau) \rangle_t$, where ρ is the density. This method is extremely fast and does not require the user to be able to see the particles, and has been used with bacteria below the detection limit[79][80], or 100nm colloids[81][82, 83].

2.5.1 Principle

To compute the intermediate scattering function, from a high frequency movie of the experimental system, each frame being defined by an intensity matrix $I(\mathbf{r}, t)$, we first compute the differential image correlation function:

$$g(q, \tau) = \langle |I(\mathbf{q}, t) - I(\mathbf{q}, t + \tau)|^2 \rangle_{t, \theta},$$

the average is done over all time steps, and assuming isotropy of the system, an angular averaging is performed. From mathematical considerations on the link between the image intensity $I(\mathbf{r}, t)$ and the density in colloids $\rho(\mathbf{r}, t)$, it can be proven[79, 84, ?] that:

$$g(q, \tau) = A(q) (1 - f(q, \tau)) + B(q).$$

where A and B are two functions: A is related to the optical properties of the imaging system, but also to the structure of the sample; B is a measure of camera noise. To measure $f(q, \tau)$, information has to be added. The usual way is to provide a model of A , B , and f , with as many free parameters as necessary, and then to fit the measured g , with the predicted functions. Another way is to note that physically, for all q ,

$$\lim_{\tau \rightarrow 0} f(q, \tau) = 1 \text{ and } \lim_{\tau \rightarrow \infty} f(q, \tau) = 0,$$

which allows a measurement of A and B by measuring the limits of g .

However, this method is sensitive to noise on B and A , and requires certainty that we have reached a fully uncorrelated regime for the long time limit, and access to very short times ($\tau \ll q/v$, where v is the average velocity of the swimmers, see below) to measure the limit as τ goes to zero.

2.5.2 Image analysis

There are three major phenomenon that we would be able to observe, with dynamic differential microscopy: the translational passive Brownian motion; the active ballistic regime; and the long-term persistent random motion. However, we will see that they occur on very different time and wave-vector scales.

The first aspect we want to observe is the *active ballistic regime* this requires access to a large range of τ , in order to measure the small and high τ limits of $g(q, \tau)$. What we require is that for shortest τ_{min} times, there should be almost no loss of correlation ($f(q, \tau) \sim 1$), i.e. each colloids moves by a small amount when compared to pixel size. This translate into the condition: $v\tau_{min}q_{max} \ll 1$. For long times, we want full loss of correlation ($f(q, \tau) \sim 0$), thus $v\tau_{max}q_{min} \gg 1$. To be able to resolve *translational passive Brownian motion*, the colloid must move at least one pixel $l = 1/q_{max}$ owing to diffusion, $\tau = 1/Dq_{max}^2$, faster than owing to active motion, $\tau = 1/vq_{max}$. Thus $q_{max} > v/D \sim 50\mu\text{m}^{-1}$, which is very hard to attain, especially at high activity. Our current setup does not allow us to observe the passive Brownian regime. On the other hand, if we want to observe the *long-term persistent random motion*, we need observation times τ_{max} much larger than the rotational diffusion time $\tau_R \sim 10\text{s}$, and since we still need to be able to track the colloids, we also need $\tau_{min} < R/v \sim 0.1\text{s}$.

For our experimental system, $v \sim 10\mu\text{m}\cdot\text{s}^{-1}$, and we cannot observe these three phenomenon with the same experiment. We choose to focus on the active ballistic motion, and take: a square observation field $560\mu\text{m}$ across, and our pixels are $\sim 5\mu\text{m}$ (we use a 20x magnification objective), we have thus access to wave vectors q from $\sim 3\cdot 10^{-3}\mu\text{m}^{-1}$ to $\sim 0.2\mu\text{m}^{-1}$. We use an acquisition frequency $f = 200\text{Hz}$, we have access to time distances τ from¹⁴ $1/f$ to $10^4/f$.

We thus have access to $10^{-2} < qv\tau < 15$. While this is enough to observe the ballistic regime, this is not enough to observe passive Brownian motion, as $v/D \sim 20\mu\text{m}^{-1}$, while $q_{max} = 0.2\mu\text{m}^{-1}$. On the

¹⁴the long range limit is defined by the size of mass storage, and depends on the acquisition frequency: for slower acquisition rates, slower, more spacious hard disk drives can be used (see 2.6).

other hand, $\tau_{max} \sim 50s$, which is not large enough when compared to τ_R for acceptable observation of the persistent random motion. In our case, the different regimes are too far from each other in the q, τ plane for this observation method to allow a correct overlap. We had to choose to focus on only one zone, the active ballistic regime.

To measure the intermediate scattering function we have to compute:

$$g(q, \tau) = \langle |I(\mathbf{q}, t) - I(\mathbf{q}, t + \tau)|^2 \rangle_{t, \theta},$$

where $I(\mathbf{q}, t)$ is the Fourier transform of the image $I(\mathbf{r}, t)$, and θ denotes angular averaging. For each time difference τ , at each time step t we need to compute a difference and a product, then a time and angular average. To decrease the computing time, we simplify the computation by noting that:

$$\begin{aligned} |I(\mathbf{q}, t) - I(\mathbf{q}, t + \tau)|^2 &= (I(\mathbf{q}, t) - I(\mathbf{q}, t + \tau)) \\ &\quad \cdot (I(\mathbf{q}, t) - I(\mathbf{q}, t + \tau))^*, \\ &= |I(\mathbf{q}, t)|^2 + |I(\mathbf{q}, t + \tau)|^2 \\ &\quad - 2\text{Re}(I(\mathbf{q}, t) \cdot I^*(\mathbf{q}, t + \tau)). \end{aligned}$$

The first two terms in the sum average out, then,

$$g(q, \tau) = 2 \langle |I(\mathbf{q}, t)|^2 \rangle_{t, \theta} - 2 \langle \text{Re}(I(\mathbf{q}, t) \cdot I^*(\mathbf{q}, t + \tau)) \rangle_{t, \theta}.$$

Computing $\langle |I(\mathbf{q}, t)|^2 \rangle_{t, \theta} = I(q)$ is a very fast and simple operation. Computing $\langle \text{Re}(I(\mathbf{q}, t) \cdot I^*(\mathbf{q}, t + \tau)) \rangle_{t, \theta}$, is simpler, since for each time difference, we only have one product to compute. This simplification divides running time by a factor of two.

To compute $g(q, \tau)$, all images are loaded in memory¹⁵ into a 3D $I(x, y, t)$ matrix, then Fourier-transformed into a complex matrix $I(q_x, q_y, t)$. We compute its time and angular average $I(q)$. Then, a parallel loop runs for each τ , computing for each time step the product $I(\mathbf{q}, t) \cdot I^*(\mathbf{q}, t + \tau)$, discarding its imaginary part. Then the average is done over time steps t , and over angular orientations. As mentioned before, we have only measured $g(q, \tau)$, and not our function of interest $f(q, \tau)$. We need a model of colloidal swimming to extract $f(q, \tau)$ from $g(q, \tau)$. This will be discussed in sec. 3.1.2.2.

¹⁵This algorithm requires at least 48GB of ram to compute $g(q, \tau)$ on a 4GB movie. This is linked to the fact that Matlab uses double precision digits for its FFT algorithms.

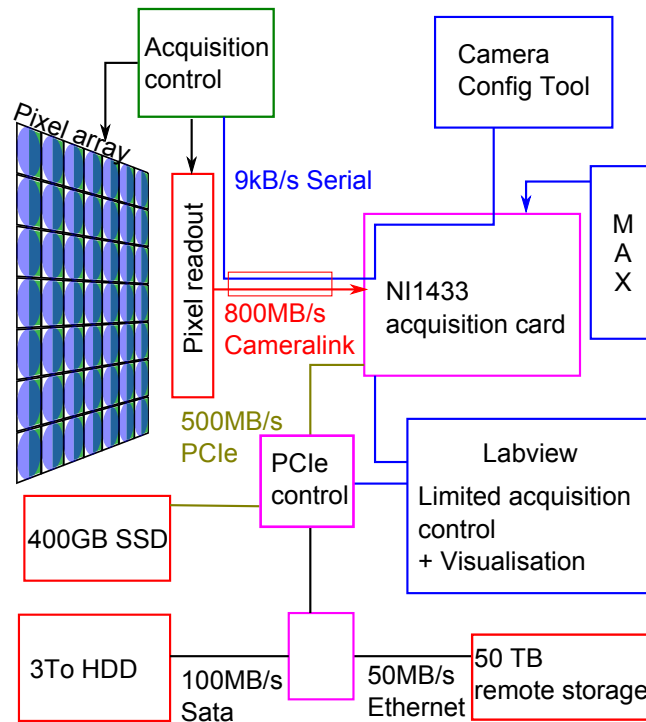


Figure 2.10: Acquisition system schematics. Software elements are in blue, storage in red, transfer elements in purple. One-way communication indicated by arrows. Software: “Max” controls the NI1433 acquisition card, the “Camera config. tool” controls the camera controller setting frequency, exposure time, and communication parameters, and “Labview” allows visualization, and limited acquisition control. The maximum allowed bandwidth are noted for each physical connection.

2.6 Acquisition

This part presents how the acquisition is performed, from the hardware specifications to the software tweaks that have been performed, and the developments I have made during my PhD. It is technical, as it assumes basic knowledge of recent computer hardware interfaces, and can be skipped for a first reading. It is intended for readers interested in creating a high-speed acquisition system. Sec. 2.6.2, presents the evolution of the acquisition system during the last three years.

A schematic of the acquisition system with the different bottlenecks is presented in fig 2.10.

When recording movies we need to obey specific constraints; listed from the strongest to weakest for our system.

- Mass storage bandwidth ($\sim 500\text{MB/s}$)
- Mass storage space ($\sim 400\text{GB}$)
- Camera-computer interface bandwidth ($\sim 800\text{MB}\cdot\text{s}^{-1}$)

- Image readout time (4ms)
- Image exposure (from 10 μ s to 40ms depending on lightning conditions)

It is important to keep in mind that the weakest link in this constraint chain will set the overall properties of the acquisition. To get continuous operation for long durations, it is important to operate below any bottleneck, to avoid the loss of even a single image. This section shows how complicated hardware-software interface can get.

2.6.1 Hardware and software.

We use a Baumer HXC40 camera. The camera is chosen for its high definition (2048 \times 2048 5.5 μ m pixel size), high sensitivity, and extremely high transfer rate (800MB/s means 180 frames per seconds (fps) at full resolution). To achieve this high streaming rate, the camera cheats the standard camera-link interface. The amount of data produced by the camera is 4Mo per image, meaning 80MB/s at 20fps (the maximal allowed bandwidth, selected by the SSD, is 500MB/s). In one hour of experiment, we create \sim 300GB of data. This stream is transferred through a cameralink cable to an acquisition card(NI-1433, PCIe frame grabber, National instruments) on our computer. The frame grabber has 512MB of on-board RAM, but not readily accessible from the software layer.

To record the images, we use a Dell workstation with 12Go RAM, 6TB HDD, a PCIe SSD (OCZ revodrive 3, 400GB), and a PCIe NI1433 acquisition card for camera-link cameras. The acquisition card is not directly compatible with the specific model of camera we use, which makes it harder to interface, as explained below.

The system has to control acquisition parameters : frequency, exposure, bit depth, number of images to acquire, and optionally regions of interest, or sub-binning of the image.

We use four different software to control the camera. The first is the control software distributed by Baumer, that controls communication parameters for the data source, frequency, exposure, bit depth and sub-binning. Then the camera file generator, distributed by National Instruments (NI) allows the writing of custom drivers to read information sent by the camera. For each set of communication parameter, a new driver has to be written. Max, the general purpose peripheral controller from NI, allows the control of which driver is used and has to be used when the image size changes. Lastly Labview allows basic control such as

the directory to which the images are recorded, the number of recorded images, and can crop the images if necessary¹⁶.

The really annoying part of this is that although interdependent on each other there is no communication allowed between these pieces of software. Labview cannot be used to send commands to the camera, nor to tell Max which driver to choose, which prevents a clean and simple design for the acquisition system.

Lastly, we use a color camera (Baumer HGX40c) that has the same properties as the monochrome camera, with an added Bayer filter in front of the sensor, that filters colors. The camera is interfaced through a simple dual Ethernet connection to a 4-channel PCIe gigabyte switch inside the computer. Its usage is much simpler. However it is less sensitive by $\sim 60\%$ and less accurate by $\sim 50\%$, due to Bayer filtering. And acquisition speeds are limited to 30Hz.

2.6.1.1 Communication parameters.

The camera is controlled by serial commands sent through a virtualized serial port inside the cameralink cable. Since the frame grabber is not fully compatible with the camera, Labview cannot be used to send commands to the camera¹⁷. The camera uses standard serial commands¹⁸ to modify most of its parameters. The camera-manufacturer control software, is the only software that can send data to the camera.

The camera sends a stream of bits containing the image to the frame grabber, and the communication parameters allow the translation of this binary stream into an image. All communication parameters have to be set to the same values on the camera and on the frame grabber by their respective controllers: the camera-manufacturer control software and Max. These communication parameters are:

- Number of taps: the cameralink interface is a parallel interface composed of up to 10 communication channels. The number of channels used defines which part of the image is sent to which channel. In our case, the image is sliced vertically into up to 10 channels.
- Image size: the exact size of the image has to be provided to reconstruct the image on arrival. Should the sender and receiver

¹⁶Cropping the images after they have been transmitted is done to save disc space and to reach higher frame rates, when disc writing speed is limiting. It is best to use region of interest definitions directly from the camera, but this requires restarting Max to change communication parameters.

¹⁷Even though incompatible, it should be able to send binary commands, but I never managed to get the camera to respond to any of the most basic commands.

¹⁸wf0004040000fa20 is the command that sets the exposure time to 8ms.

values differ, the image at time t will spill onto the next time step. By default equal to 2048×2048

- Bit depth : the size in bits of each pixel : 8 or 16, although only the first 10 or 12 bits hold data anyways, the rest is padded with zeros. Defaults to 8.

For each set of communication parameters, a communication driver has to be written using the “camera file generator” from NI. Once this driver is loaded with Max, the user sends commands to the camera using the camera-manufacturer control software. Some commands have to be sent as hexadecimal codes. Then, Labview is started to control the acquisition.

2.6.1.2 Acquisition control.

Once Labview is started, the user can see the images coming from the camera. The user should now control, through the camera-manufacturer control software, exposure time to get the best contrast, and acquisition frequency according to which timescales of the system he wishes to study.

Special care has to be taken to reach very high frequencies : the camera has to be allowed to transmit the content of every pixel at time step t while the next exposure is being done. The pixel frequency should also be set to its maximum, 48MHz, to lower the readout time. The pixel frequency is the refresh rate of the pixel, increasing it improves sensitivity and lowers readout time, at the expense of an increase in power consumption, that implies higher sensor temperature ($\sim 60^\circ\text{C}$, which meant we had to install a passive cooling system) and higher noise. Lastly, the user should check that the bandwidth of the SSD ($\sim 300\text{MB}\cdot\text{s}^{-1}$) is not saturated, and that the planned number of frames is small enough to fit on the 400GB SSD.

2.6.1.3 Image recording.

We typically record ~ 2000 images at 20Hz (resulting bandwidth: $80\text{MB}\cdot\text{s}^{-1}$). This frequency allows tracking of individual particles while acquiring for more than one minute and makes it possible to study the behavior of the clusters. The images are directly sent to the SSD. The SSD has to be emptied every day (sometimes more than once a day) and we use standard hard disk drives, and a network attached storage¹⁹ for long term storage.

For DDM experiments, we record 10^4 , 1024×1024 images at 200Hz (resulting bandwidth $200\text{MB}\cdot\text{s}^{-1}$). To avoid losing frames and slowing the operating system, we disable the displaying of frames, that taxes the

¹⁹Whose bandwidth was below $10\text{MB}\cdot\text{s}^{-1}$ until the very end of the thesis, when it reached an acceptable $50\text{MB}\cdot\text{s}^{-1}$.

graphic card. Taxing the graphic card is a problem, since the card is controlled by the same PCIe controller that also controls the SSD and the frame grabber. They all have the same bandwidth, set by the PCIe controller bandwidth (Intel X58). With a constructor rated $0.5\text{GB}\cdot\text{s}^{-1}$, per PCIe channel (up to six channels), the controller should be more than enough to hold $3\times 200\text{MB}\cdot\text{s}^{-1}$, but it is practically incapable of doing so. Any data going into the graphics card lowers the bandwidth of both the SSD and the frame grabber.

We have no low level control of priorities for resource acquisition, but the operating system seems to be doing an okay job, since at low frequencies Matlab and an acquisition can run at the same time without losing frames.

2.6.1.4 Color Camera.

In order to detect swimmers orientation, we need to be able to detect the colors of the colloids: the light blue of the platinum and the yellow of the gold. The color camera is simpler to use although less sensitive (by 60%) and less accurate (by 50%). This loss of sensitivity and accuracy is caused by the color filters, set in front of each pixel, that sets the pixel color. These filters are arranged in a Bayer matrix; half the pixels are green, 25% blue and 25% red.

We use a color camera (Baumer HGX40c). The camera is interfaced through a simple dual Ethernet connection to a 4-channel PCIe gigabyte switch (Intel 82574L) inside the computer. The http protocol used by the camera allows extremely easy communication, At each frame, the camera sends additional data containing all the image properties, and the user can send information to modify any of the camera properties. The Labview code is very simple and allows fine tuning of all camera settings. However, Max is not yet compatible with Ethernet link aggregation, which slows down by half the Bandwidth of the camera to $120\text{MB}\cdot\text{s}^{-1}$ (30fps at 4Mpx), instead of the full theoretical $240\text{MB}\cdot\text{s}^{-1}$. These acquisition rates are correct, but not high enough for demanding applications²⁰ which justifies all the effort put into interfacing the fast cameralink camera.

The two cameras can be set to acquire at the same time, however, the acquisition is not yet done with an external source of trigger, the only reliable way of synchronizing the two cameras.

²⁰DDM are and particle image velocimetry with bacteria, are currently done in the lab.

2.6.2 System development and evolution.

First colloid observations were done with a 1.3Mpx firewire camera (Hamamatsu ORCA-ER), which had a maximum frame rate of 10Hz. For the fast swimmers we developed, it was much too slow²¹, and the observation area was only $200 \times 150 \mu\text{m}^2$, which allows the simultaneous tracking of only $\sim 1.10^3$ colloids. Colloids would go across the observation area without changing direction, which prevents the study of the persistent Brownian motion. To improve on these flaws, I changed the acquisition chain, imposing that the camera had to be able to follow $\sim 4.10^3$ colloids moving at $20 \mu\text{m} \cdot \text{s}^{-1}$. Our colloids measuring $2.2 \mu\text{m}$ in diameter, this led to an acquisition speed of 20Hz. Because of the low contrast we had at the time, 12-bit images were necessary, and a 20Hz acquisition frequency led to a very high bandwidth requirement of $160 \text{MB} \cdot \text{s}^{-1}$. A raid-5 assembly of 4 fast hard drives (15000rpm velociraptors, Western Digital), controlled by a PCIe raid controller (DSI 9620), led to writing speeds of $\sim 180 \text{MB} \cdot \text{s}^{-1}$. A fifty second (1000 frames) movie taking 8GB, the RAM could not be used as a buffer. The development of other experiments, with bacteria, or the differential dynamic microscopy, demanded increases in writing bandwidth, which led to the acquisition of a PCIe SSD, that, although rated for $500 \text{MB} \cdot \text{s}^{-1}$ writing speeds, only achieves $330 \text{MB} \cdot \text{s}^{-1}$, in standard operating conditions.

2.7 Conclusion

We have developed an effective colloidal-scale active system, with tunable activity and relatively simple interactions, all physical in origin, whether hydrodynamical, or chemical in nature. We also have developed a reliable detection and tracking for very large assemblies of $\sim 10^4$ particles; and implemented other analysis methods with differential dynamic microscopy.

The Next step. The important point that is missing is a characterization of interparticle interaction, that would allow us to precisely quantify which aspects of the interaction are preponderant (see sec. 3.2).

Minor points that could have great impact are to increase the accuracy of particle tracking, that is currently of a tenth of a particle diameter, and that limits our short term resolution of the particle's motion. Very long-term tracking is also a possibility, that requires the development of a new storage system, and new analysis algorithms, as well as better control of the swimmers activity. Another experimental development that will

²¹The maximum displacement between two frames v_{max}/f was often above the minimum nearest neighbor distance, which prevents efficient tracking.

have great impact on our experiment is the ability to detect polarization, that is to detect the platinum half from the gold half. As we saw in the previous chapter, direct detection of the polarization is required to quantify the polar ordering in the system.

The development of new active colloids to vary the nature of interactions, is also a very promising, although competitive endeavor.

Key ideas for this chapter

1. We developed the synthesis of an effective colloidal-scale active system, made of gold-platinum Janus colloids, with simpler interactions than bacterias, and tunable activity.
2. We developed microscope observation, and fast acquisition setup, as well as fast and reliable particle detection, tracking, and analysis, for large ($\sim 10^4$ particles) assemblies.

Appendix A : Electrocatalytic microswimmers.

This section details the physical phenomenon upon which our gold-platinum active colloids rely. Reading the first subsection should be enough to understand the basic physics of the motion, and the rest can be skipped at first, until one needs to understand the details of the swimming mechanisms.

The microswimmers we developed are 2 μm in diameter gold spheres with one half coated in platinum. when immersed in a solution containing hydrogen peroxide at volumetric concentrations $[\text{H}_2\text{O}_2] \sim 10^{-4}$, they disproportionate the peroxide following:



As long as the concentration in O_2 remains below the saturation concentration, $[\text{O}]_{sat} = 3.10^{-4}\text{mol.L}^{-1}$, the dioxygen stays in solute form without creating bubbles, that appear if the concentration crosses that threshold. As the nucleation of those bubbles takes time, it is believed that there are no nanosized bubbles in the system, although no experiment can rule this out yet. As peroxide is disproportionated, the colloid self-propel at constant velocities $v \sim 3\mu\text{m.s}^{-1}$.

Qualitatively, the chemical reaction (see fig. 2.11) imposes a difference of potential between the gold and the platinum faces, which causes an electric current through the colloid, and the migration of the electric double layer at the surface of the colloid, owing to electrophoretic effects. This in turn propels the colloid.

The physical mechanisms underlying this propulsion are the electrochemistry of the platinum and gold faces, the electrostatic equilibrium of charged species, the diffusion of all solute species, and hydrodynamics. In this section, we shortly investigate these four phenomena, and explain how they give rise to propulsion. Sen *et al.* [65][85] originally proposed a mechanism based on the surface tension change, i.e. a Marangoni-effect self propulsion, and nanobubbles [86], and a thermal viscous ratchet [87] have also been proposed as a propulsion mechanism. The mechanism

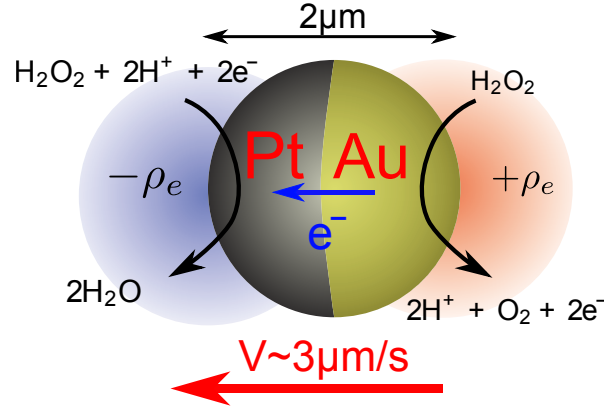


Figure 2.11: Schematic of the chemical reactions propelling the gold-platinum microswimmers. The microswimmer act as a battery in the peroxide bath, the gold electrode playing the role of the cathode, while the platinum, owing to its lower electronegativity, is the anode. Overall, the peroxide is disproportionated through $2\text{H}_2\text{O}_2 = 2\text{H}_2\text{O} + \text{O}_2$, while the exchanged electrons create a current through the colloid, which creates an electric field around the colloid, which in turns pumps electrophoretically the charged liquid in the electric double layer, which equate propulsion with velocities $v \sim 3\mu\text{m}\cdot\text{s}^{-1}$, with volumetric concentration in peroxide of only 10^{-4} .

presented below [88] is believed [84], to be a correct explanation, however, it does not take into account the fact that colloids swim on a solid surface and not in the bulk. The presence of this surface needs to be investigated, for its hydrodynamic interaction, but also for the chemical or electrostatic interaction with other swimmers.

A.1 Electrostatic equilibrium

By assuming a quasi static equilibrium, only one of Maxwell's equation applies:

$$\nabla \cdot \mathbf{E} = \frac{\rho_e}{\varepsilon_0 \varepsilon_r}.$$

Since we assume \mathbf{B} constant, $\nabla \times \mathbf{E} = \mathbf{0}$, and we introduce the electrostatic potential Ψ : $\varepsilon \nabla^2 \Psi = \rho_e$, where $\varepsilon = \varepsilon_0 \varepsilon_r$, and is assumed to be constant. The charge density

$$\rho_e = F \sum_i z_i C_i,$$

where F is the Faraday constant, z_i the number of charges born by species i , and C_i its concentration. The sum is made over solute species: HO^- , H^+ , O^2 , H_2O_2 .

The general equation governing the motion of ions is a modified

Fick equation, that takes into account advection by the fluid velocity field \mathbf{u} , and electromigration, the migration of ionic species under the influence of an electric field. The concentration flux density caused by electromigration is simply: $\mathbf{j}_i = \mu_i C_i z_i F \mathbf{E}$, with μ_i the mobility of species i . The contribution of chemical reactions is given by a source term S_i . We assume that the diffusiophoresis is negligible. All these ingredients lead to:

$$\frac{\partial C_i}{\partial t} + \mathbf{u} \cdot \nabla C_i = S_i + \nabla \cdot (D_i \nabla C_i + \mu_i z_i F C_i \nabla \Psi),$$

where D_i is the diffusivity of species i . Since the peroxide is metastable in water, chemical reactions are possible only on the catalytic surface of the colloids. In the bulk of the fluid, no chemical reactions occur, thus $S_i = 0$.

The simplest boundary conditions are $\Psi_{rod} = 0$, if we assume an uncharged colloid. However, we have to keep in mind that the chemical reactions at the surface of the colloid will create an effective potential at its surface. This hypothesis is quite weak, but taking into account surface charges does not change our conclusions. We also assume that the potential vanishes at infinity: $\lim_{r \rightarrow \infty} \Psi = 0$.

A.2 Electrochemistry at the electrodes.

Hydrogen peroxide is unstable in water, the disproportionation reaction $2\text{H}_2\text{O}_2 = 2\text{H}_2\text{O} + \text{O}_2$, has a $\Delta_r H^0 = 212 \text{kJ} \cdot \text{mol}^{-1}$, an energy density comparable to usual fossil fuel (propane or butane). All the energy necessary for propulsion must come from this disproportionation reaction, to swim at $10 \mu\text{m} \cdot \text{s}^{-1}$, at least 1fW is required, depending on the swimming strategy. However, this reaction is kinetically very slow, and peroxide solution take month to disproportionate. To increase the reaction velocity catalysis is often used.

A single metal Catalysis is possible [89][64][66], but less effective than the two-metal alternative [85],[68]. The disproportionation of peroxide consists of two simultaneous reactions, an oxidation :

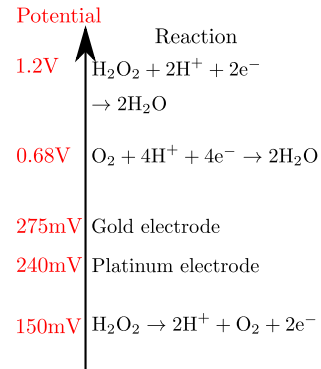
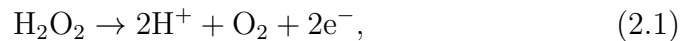
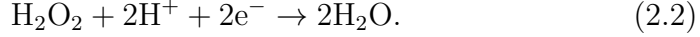


Figure 2.12: Schematic of the electrode potentials

and a reduction :



For single-metal Janus swimmers, both reactions occur at the same electrode. For bimetallic swimmers, composed of a gold half and a platinum half, the electrical properties of each electrode, decide that the gold electrode is the cathode (reduction), while the platinum half is the anode (oxidation). Platinum is less electronegative than gold (2.28 and 2.54 respectively on the Pauling scale [90]), and although both reactions can occur at any electrode, the gold electrode will favor reduction, and the platinum, oxidation.

The two electrodes are connected, charge conservation imposes that the electrons that enter at the anode exit at the cathode. For the current density, this implies $j_{anode} = -j_{cathode} = j_0$. Moreover, at the anode, the current density is linked to the density in hydrogen peroxide through [88]:

$$\mathbf{n} \cdot \left(-D_{\text{H}_2\text{O}_2} \nabla C_{\text{H}_2\text{O}_2} + C_{\text{H}_2\text{O}_2} \mathbf{u} \right) = -\frac{j_0}{2},$$

where \mathbf{n} is the unit vector normal to the surface, the peroxide diffusion coefficient, the concentration in peroxide, the velocity of the fluid. At the cathode,

$$\mathbf{n} \cdot \left(-D_{\text{H}_2\text{O}_2} \nabla C_{\text{H}_2\text{O}_2} + C_{\text{H}_2\text{O}_2} \mathbf{u} \right) = -\frac{j_0}{2}.$$

These two equations are simply a reformulation of Fick's law for diffusion : $\frac{dC}{dt} = D\nabla^2 C + S$, S being a source term accounting for chemical reactions. The first term is the advected concentration: $\frac{dC}{dt} = \frac{\partial C}{\partial t} + \mathbf{u} \cdot \nabla C$. The flux of peroxide through the interface is zero, the flux due to diffusion and the flux due to advection are compensated by the destruction of peroxide. The current density j_0 gives the rate of destruction of peroxide. Similarly, we can write the boundary conditions for all chemical species.

$$\begin{cases} \mathbf{n} \cdot \left(-D_{\text{O}_2} \nabla C_{\text{O}_2} + C_{\text{O}_2} \mathbf{u} \right) = j_0 & \text{at the anode} \\ \mathbf{n} \cdot \left(-D_{\text{O}_2} \nabla C_{\text{O}_2} + C_{\text{O}_2} \mathbf{u} \right) = 0 & \text{at the cathode} \end{cases}.$$

And

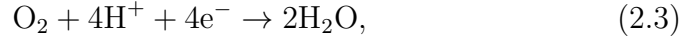
$$\begin{cases} \mathbf{n} \cdot \left(-D_{\text{H}^+} \nabla C_{\text{H}^+} + C_{\text{H}^+} \mathbf{u} \right) = j_0 & \text{at the anode} \\ \mathbf{n} \cdot \left(-D_{\text{H}^+} \nabla C_{\text{H}^+} + C_{\text{H}^+} \mathbf{u} \right) = -j_0 & \text{at the cathode} \end{cases}.$$

By assuming elementary reaction kinetics, we obtain:

$$\begin{aligned} j_0 &= k_1 C_{\text{H}_2\text{O}_2}, \\ j_0 &= k_2 C_{\text{H}_2\text{O}_2} C_{\text{H}^+}^2, \end{aligned}$$

where k_1 and k_2 are kinetic constants.

More detailed studies[85] have suggested a slightly different picture. The mixed potential, that is the potential of the electrode versus a Ag/AgCl electrode in an open circuit, under the action of several redox couples, of the gold electrode, $275 \pm 6\text{mV}$, is above that of the Platinum electrode ($240 \pm 10\text{mV}$). The potential of the reactions 2.1 and 2.2, versus the Ag/AgCl electrode are 150mV and 1.2V respectively. A different reduction reaction is proposed :



whose potential is only 0.68V , much closer to the potential of the gold electrode. While using this reaction changes all the subsequent equations, it does not modify the key conclusions.

A.3 Low Reynolds hydrodynamics.

The flow of solvent around the colloid is caused by the volumetric electric force on the charged fluid:

$$\mathbf{f} = \rho_e \nabla \Psi.$$

The flow equation is the stokes equation:

$$0 = \nabla p + \rho_e \nabla \Psi - \eta \nabla^2 \mathbf{u}, \quad (2.4)$$

where p is the hydrodynamic pressure, and η the dynamic viscosity. The incompressibility of the flow imposes $\nabla \cdot \mathbf{u} = 0$. In the reference frame of the swimmer, the boundary conditions are simply a no-slip condition on the swimmer $\mathbf{u} = 0$, and a no-stress condition at infinity:

$$-p\delta_{ij} + \eta [\partial_i u_j + \partial_j u_i] = 0.$$

All the effect of ions is limited to a small layer of typical length $\lambda_D = \sqrt{\frac{\epsilon RT}{2F^2 C_{\text{H}^+}}} \ll 200\text{nm}$.

A.4 Generalities for low Reynolds swimming

Independent of the swimming mechanism, the flow field must obey a few very generic laws[42][91][84][92], that all stem from the Stokes equation, with the incompressibility. In the stationary regime, and in the absence of electric effects, the Stokes equation is:

$$-\nabla p + \eta \nabla^2 \mathbf{u} = 0. \quad (2.5)$$

Unlike (2.4) which is non-linear because of the coupling between electric and velocity fields, this equation is linear, thus for forces small enough to stay in the low Reynolds domain, the relationship between force \mathbf{F} and velocity \mathbf{u} is also linear, as for torque \mathbf{M} and rotation rate $\mathbf{\Omega}$:

$$\begin{pmatrix} \mathbf{F} \\ \mathbf{M} \end{pmatrix} = \begin{pmatrix} A & 0 \\ 0 & C \end{pmatrix} \begin{pmatrix} \mathbf{u} \\ \mathbf{\Omega} \end{pmatrix}.$$

The absence of cross-coupling is due to the symmetry of the spherical swimmer, and more precisely to its absence of chirality; A and C are diagonal because the swimmer is spherical, and

$$\begin{aligned} A_{ij} &= 6\pi\eta R \delta_{ij}, \\ B_{ij} &= 8\pi\eta R^3 \delta_{ij}. \end{aligned}$$

. The Solutions of (2.5) can be expressed as linear combinations of the Stokeslet unit solution[93][42][94]: the flow response to a point force

$$\mathbf{f} = \mathbf{f}_0 \delta(\mathbf{r} - \mathbf{r}_0)$$

is

$$\mathbf{u}(\mathbf{r}) = G(\mathbf{r} - \mathbf{r}_0) \cdot \mathbf{f}_0,$$

where G is the Oseen tensor:

$$G_{ij}(\mathbf{r}) = \frac{1}{8\pi\eta} \left(\frac{\delta_{ij}}{|\mathbf{r}|} + \frac{r_i r_j}{|\mathbf{r}|^3} \right).$$

And $p(\mathbf{r}) = H(\mathbf{r} - \mathbf{r}_0) \cdot \mathbf{f}_0$, with $H_i(\mathbf{r}) = \frac{r_i}{4\pi|\mathbf{r}|^3}$.

For a self propelled particle there is *no external force acting on the particle*. Contrary to a particle that is sedimenting under the action of gravity, if we imagine a large, isolated sphere of solvent containing the swimmer, the sphere being isolated prevents the swimmer from being under the influence of an external force²². Yet, a swimmer in an isolated

²²Of course we are here completely neglecting the inertia of the swimmer, the corresponding force is 10 orders of magnitude below what is required for swimming.

sphere can swim, albeit without exerting a net force on the fluid. We thus impose that our solution is a sum of Stokeslet with a zero net force: $\sum_i \mathbf{f}_0^i = 0$. This leads to force dipoles and quadrupoles, and higher orders, by considering a Stokeslet at position $\mathbf{r}_0 + \xi$: [93]

$$\mathbf{u}(\mathbf{r} + \xi) = \mathbf{u}(\mathbf{r}) + (\xi \cdot \nabla)\mathbf{u}(\mathbf{r}) + \frac{1}{2}(\xi \cdot \nabla)^2\mathbf{u}(\mathbf{r}) + \dots,$$

the successive terms in the development giving the monopole, dipole and quadrupole contributions, in a very similar manner to the decomposition done in electrostatics [95]. Then the dipolar velocity field is, for a force dipole of force \mathbf{f}_0 , and dipole strength β , situated at the origin:

$$\begin{aligned} \mathbf{u}_D(\mathbf{r}; \mathbf{f}_0, \beta) &= (\beta \cdot \nabla)\mathbf{u}(\mathbf{r}) \\ &= \frac{(\beta \times \mathbf{f}_0) \times \mathbf{r}}{|\mathbf{r}|^3} - \left[\frac{(\beta \cdot \mathbf{f}_0) \mathbf{r}}{|\mathbf{r}|^3} - 3 \frac{(\beta \cdot \mathbf{r})(\mathbf{f}_0 \cdot \mathbf{r}) \mathbf{r}}{|\mathbf{r}|^5} \right]. \end{aligned}$$

For a quadrupolar velocity field, two constant vectors β and γ are necessary to describe the flow:

$$\mathbf{u}_D(\mathbf{r}; \mathbf{f}_0, \beta, \gamma) = (\gamma \cdot \nabla)(\beta \cdot \nabla)\mathbf{u}(\mathbf{r}).$$

Since $(\gamma \cdot \nabla) = \sum_k \gamma_k \partial_{r_k}$, with all these vectorial and scalar products, it becomes a real mess to compute (see [96] and [97]).

A.5 Resulting propulsion.

Since we have all boundary conditions, for the solvent velocity, for the concentrations, and for the electric potential, all these equations form a well posed problem, that can be solved numerically. For a negatively charged colloid, the resulting flow propels the particle platinum face forward, and all the effect of the electric field occurs in a small layer at the surface of the colloid. Indeed, the volume whose ionic charge is not balanced is limited to a small layer of typical length $\lambda_D = \sqrt{\frac{\epsilon RT}{2F^2 C_{H^+}}} \ll 200\text{nm}$. The fact that the effect of ions is limited to a small layer at the surface of the colloid validates another, more qualitative analysis of the swimmer's propulsion, that predicts the velocity by considering only the effective slip at the surface of the colloid [98]. The precise nature of the flow has consequences for the hydrodynamic interaction between colloids, but has to be computed numerically.

Chapter 3

Dynamics of the Cluster Phase

The development of gold-platinum Janus microswimmers described in the previous chapter allowed us to study a high-concentration assembly of active colloids, while avoiding the formation of bubbles. For the first time, collective effects, at colloidal scale in a purely abiotic system were observed. During the course of my PhD, the study of active colloids has been very active, and experiments have been performed by other groups, also observing collective effects; those experiments are discussed in section 3.5.

This chapter describes in details the behavior of an assembly of the gold-platinum active colloids I developed. When we add peroxide in an assembly of those Janus colloids, they become active, and start to move with a constant velocity $v \sim 2 - 10 \mu\text{m.s}^{-1}$. At low densities¹ ($\phi < 1\%$), the interaction between colloids is negligible (see sec. 4.3), and the colloids move as individual swimmers, as if they were alone, with a persistent Brownian motion, which is described in the first section.

At higher densities ($\phi > 2\%$) the main, most striking feature of our assembly of active Janus microswimmers, is the formation of clusters, that form what we call a *dynamic cluster phase*. These clusters are dense, highly ordered assemblies comprising from 3 to $\sim 10^2$ microswimmers, separated by a low density disordered gas of microswimmers (see fig. 3.1). This chapter analyzes qualitatively and quantitatively this dynamic clustering.

In a first section, we focus on the individual behavior of isolated colloids. Then, we will study the clusters. After a description of the algorithms I developed to define clusters, we will focus on their static

¹ ϕ is the area density, the dimensionless number giving the ratio of the area occupied by the swimmer versus total area. It is linked to the number density ρ by: $\phi = \rho\pi R^2$, where R is the particles' radius.

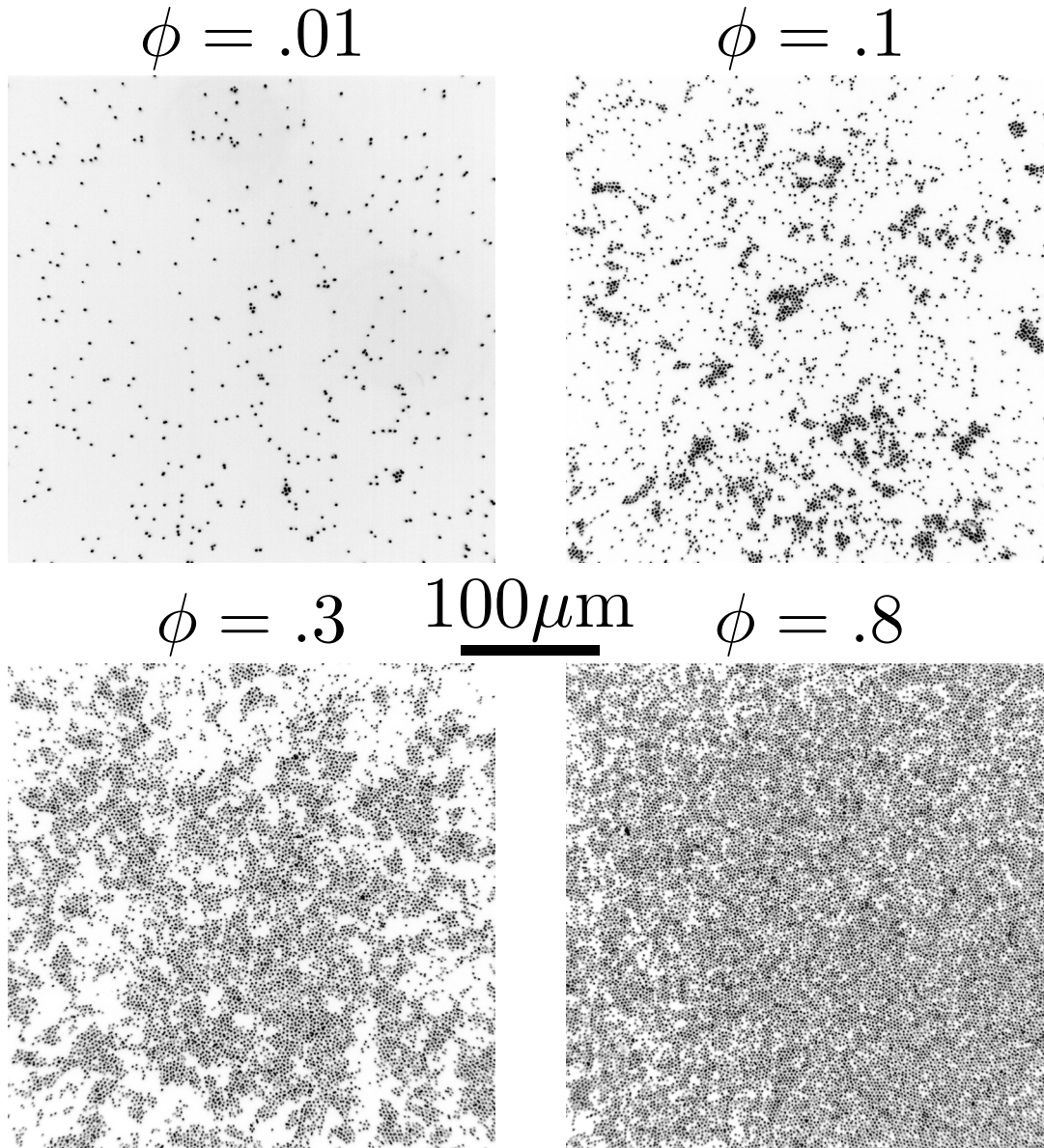


Figure 3.1: Assemblies of swimmers at different densities: a gas with almost no clusters at $\phi = 1\%$, cluster phase at $\phi = 10\%$, large, well structured clusters can be seen. At $\phi = 30\%$, the clusters are almost percolating and start to block each other. At $\phi = 0.8$, motion is almost blocked, although colloids can move in the defects of the glass structure. Films see Sup. mat. movie 5-7.

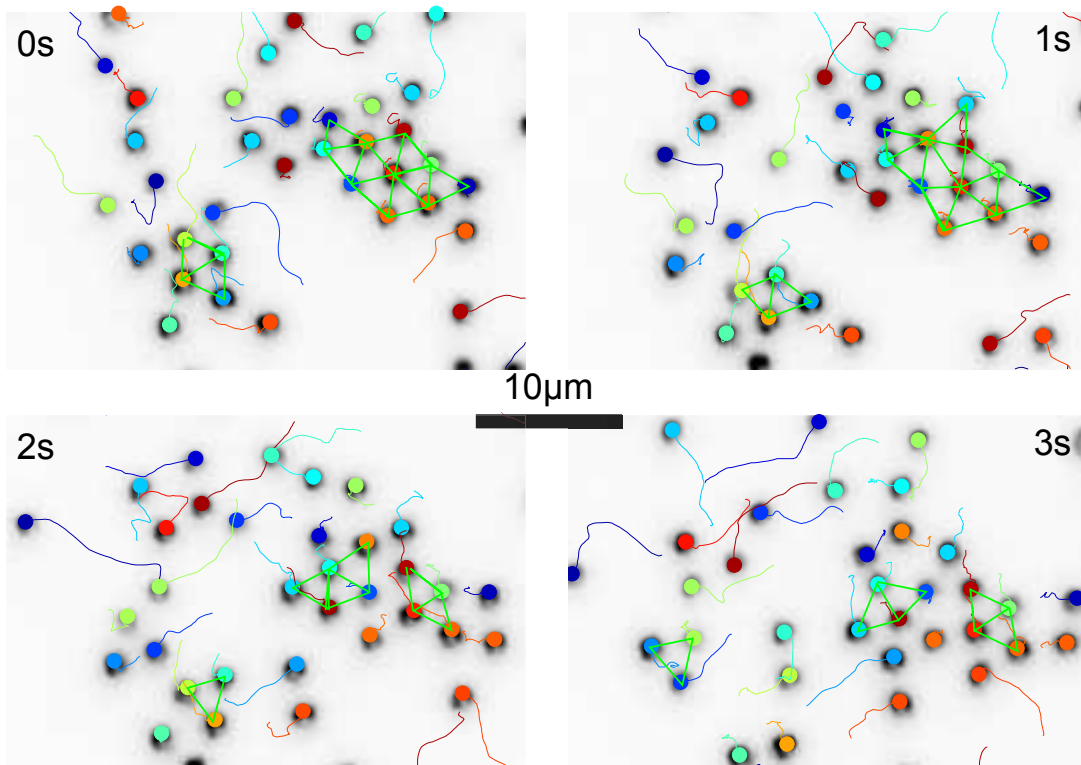


Figure 3.2: Two clusters exchanging particles. Each image is one second apart, the scale bar is $10\mu\text{m}$ wide. Each colloid has a unique color, and the trail behind the colloid plots its positions over the previous two seconds. Colloids join and leave the big cluster on the left part, it rearranges itself, while some colloids in the gas phase pass by without apparent interaction. See movie 3 & 4 in sup. mat.

properties: size and structure. The dynamic aspect of the clusters, that is their persistent motion, merging and separation in smaller clusters is analyzed quantitatively in the next section.

The goal of this part is twofold: we want to better understand the causes of the formation of clusters, and we want quantitative measurements that can be compared to other experiments, but also to theoretical and numerical studies.

Qualitative description of the clusters

Before characterizing the system, I'll give a quick qualitative description of the system. The system is composed of active particles, intrinsically out of equilibrium because of the dissipation of energy by each colloid ($\sim 2 \cdot 10^{-18} \text{W}$). This energy propels the colloids at constant velocity² $v \sim 2 - 10 \mu\text{m} \cdot \text{s}^{-1}$, but the rotational Brownian motion results in a diffusion of the direction of the velocity over $\tau_R \sim 10 \text{s}$, that results in turn in an effective diffusive motion [66] (see sec. 3.1.1). At very short times $t < 1 \text{s}$, the motion is ballistic with velocity v , while at longer time scales, it becomes diffusive, with diffusion coefficient $D_{eff} \sim v^2 \tau_R$. When in a low density assembly, they behave as an ideal gas³, the interparticle interaction being negligible. Their behavior is equilibrium-like and Einstein relations are respected, albeit with an effective temperature T_{eff} instead of the actual room temperature[64]. This effective temperature is of order 10^4K in our system.

However, when the concentration increases – and this is a new and original result – we observed for the first time in abiotic systems the formation of dynamic clusters⁴. The interaction between colloids leads to large departure from equilibrium behavior, as is proven by the presence of clusters, that are a very large violation of the Mermin-Wagner[14] theorem, that states that equilibrium implies an homogenous density. These clusters are motile assembly of colloids that are in equilibrium with the surrounding gas phase, constantly exchanging particles with the gas. They are much more ordered than the surrounding gas, and look like almost crystalline assemblies, but they still have defects, and break apart over $\sim 100 \text{s}$. The clusters formed are also very mobile, rotating with rotational velocity $\Omega \sim 0.1 \text{turn} \cdot \text{s}^{-1}$, and translating at velocities

²At very short time scales, $\tau_b < 1 \mu\text{s}$, the colloids have a ballistic motion. In the following chapter, this is neglected, although it could have interesting impact for the interparticle interaction[99].

³which has already been characterized experimentally in the group[64].

⁴To be fully honest, [45] had observed and published colloidal collective effects in abiotic systems, before us, however without certainty as to the stationary nature or to the nature of interactions.

$$v \sim 1\mu\text{m}\cdot\text{s}^{-1}.$$

| Timescale | | order of magnitude |
|---|---------------------------------------|--------------------|
| Ballistic motion at molecular scale | $\tau_b = \frac{m}{6\pi\eta R}$ | 1 μ s |
| Ballistic motion due to active propulsion | $\tau_a = R/v$ | 1s |
| Brownian diffusion time | $\tau_B = R^2/D$ | 5s |
| Brownian rotational diffusion | $\tau_R = \frac{4\pi\eta R^3}{k_B T}$ | 10s |
| Swimmers collision time | $\tau_c = \frac{\pi R}{4\phi v}$ | 10s ⁵ |
| Cluster collision time | τ_{Cc} | ~ 30 s |
| Cluster division time | τ_D | ~ 100 s |

Table 3.1: Important time scales in the system. Typical values: $m \sim 3\cdot 10^{-13}$ kg is the mass of a colloid, $v \sim 10\mu\text{m}\cdot\text{s}^{-1}$ the propulsion velocity, $R \sim 1\mu\text{m}$ the colloid radius, $\eta \sim 10^{-6}$ Pa.s the fluid's viscosity, $D \sim 0.2\mu\text{m}^2\cdot\text{s}^{-1}$ the Brownian diffusion coefficient for passive colloids, and $\phi \sim 0.1$ the area density. The cluster collision and division time are measured roughly from experiments, they depend on the cluster density, and their velocity, and have no theoretical expected value yet.

The clusters are exchanging colloids at their periphery with the surrounding medium (see fig. 3.2). Some colloids join a cluster for only a brief instant, less than one second, and then leave the cluster, especially when the colloid and the cluster have anti-parallel motion. Other colloids stay for much longer times. Of course colloids from the cluster are also detaching to go into the gas phase. The colloids in the center of a cluster can never leave it, but all clusters sometimes break apart in smaller clusters, meaning colloids in the center now become peripheral colloids, that can leave the clusters spontaneously. The last and rarer type of event that modifies clusters is the collision. When two clusters collide, they tend to form a larger cluster, however, this cluster is often not very stable and rearranges, and sometimes divides after the collision.

3.1 Weak interaction limit

Before focusing on collective behavior, we need to understand how an isolated colloid behaves, when it does not interact with other colloids. This is the case either when there is only one colloid in the system, or when the density is low enough, so that the interparticle distance is high (see movie 1 in sup. mat.). This section is mostly bibliographical in

| Displacement Δr | cause | times |
|----------------------------|---------------------------|------------------------------------|
| $\sqrt{\frac{k_B T}{m}} t$ | Molecular ballistic | $t \ll 1\text{ns}$ |
| \sqrt{Dt} | Brownian diffusion | $1\text{ns} \ll t \ll 0.2\text{s}$ |
| vt | Active ballistic | $0.2\text{s} \ll t \ll 10\text{s}$ |
| $\sqrt{v^2 \tau_R t}$ | Persistent random walk | $10\text{s} \ll t$ |

Table 3.2: Typical displacement and time scales in the motion of an isolated Janus microswimmer.

nature. We first describe the motion of an isolated swimmer: a persistent random walk, ballistic at short time scales and Brownian for long times. This isolated swimmer behavior is important and needs to be precisely known, to be able to measure swimmers velocities (see sec. 3.3.1). Then we present our experimental results on the behavior of an assembly of individual swimmers, studied through differential dynamic microscopy (see sec. 3.1.2.2), that probes the ballistic regime of the colloids.

3.1.1 Persistent random walk.

The microswimmers have a constant velocity, but the change in orientation of this velocity gives rise to a persistent Brownian motion, that has been under much scrutiny, both theoretical and experimental [66, 64]. The typical displacement and the time scale associated are summed up in table 3.2. In our analysis we do not consider the molecular ballistic motion, since the associated time scale is smaller by a factor 10^5 than the next smallest time scale in the system. The fact that Brownian diffusion is the dominant cause of displacement at short time scales has important consequences for the velocity measurement (see sec. 3.3.1).

3.1.1.1 Fluctuating forces

An isolated microswimmer, of radius R moves at a constant velocity $|\mathbf{v}|$, owing to propulsion effects, but the thermal fluctuations in the solvent change its spatial orientation \mathbf{u} . Since, owing to the propulsion mechanism of the Janus, \mathbf{u} is also the unit vector giving the orientation of the velocity \mathbf{v} , this rotational diffusion implies a diffusion of the direction of motion of the colloid. The swimmer follows a set of Langevin dynamic equations:

$$\frac{dr_i}{dt} = v_i + \frac{1}{6\pi\eta R}\delta F_i, \quad (3.1)$$

$$\Omega_i = \frac{1}{8\pi\eta R^3}\delta M_i, \quad (3.2)$$

where v_i is the i^{th} component of the velocity \mathbf{v} , $\Omega = \frac{5}{2}v \frac{\mathbf{r} \times \mathbf{u}}{\mathbf{r} \cdot \mathbf{r}}$, \mathbf{r} being the particle position, is the swimmer rotation velocity, and δF and δM are fluctuating forces and momentum respectively, Gaussian noises of power spectrum $\langle \delta F(0)\delta F(t) \rangle \propto kT\delta(t)$. See sec. 2.7 for details. Since (3.1) is linear, we can separate the effects of propulsion from the effects of fluctuations in the solvent. The fluctuations of the solvent will still affect the velocity $\mathbf{v} = v\mathbf{u}$. It is important to note, that being at small Reynolds number, the effect of propulsion is completely independent of the fluctuations of the solvent. For the solvent, at least at small scales, the fluctuation-dissipation theorem holds, and the temperature is well defined.

Separating the diffusive from the active motion: $r_i = r_i^c + r_i^d$, and

$$\begin{aligned} d_t r_i^c &= v_i, \\ d_t r_i^d &= \frac{1}{6\pi\eta R}\delta F_i. \end{aligned} \quad (3.3)$$

Equation (3.3) is the equation for Brownian motion, and yields:

$$\left\langle \left(r_i^d(t) \right)^2 \right\rangle = \frac{k_B T}{3\pi\eta R} t.$$

The direction of propulsion vector diffuses following:

$$\left\langle \phi_i^2 \right\rangle = \frac{k_B T}{4\pi\eta R^3} t,$$

where ϕ_i represents the two angles defining the vector \mathbf{r} in spherical coordinates:

$$\mathbf{r} = \begin{pmatrix} r \sin \theta \cos \psi \\ r \sin \theta \sin \psi \\ r \cos \theta \end{pmatrix},$$

And $D_R = 1/\tau_R = \frac{k_B T}{4\pi\eta R^3}$, is the rotational diffusion coefficient.

3.1.1.2 Random dynamics

To understand how \mathbf{v} evolves in time, and the consequences on the mean square displacement $\langle |\mathbf{r}(t)|^2 \rangle$, we note that the probability density

function $P(\mathbf{u}, t)$ for the orientation of the vector \mathbf{u} follows a diffusion equation[84][100]:

$$\begin{aligned}\tau_R \partial_t P(\mathbf{u}, t) &= \Delta P(\mathbf{u}, t) \\ &= \left(\frac{1}{\sin \theta} \partial_\theta (\sin \theta \partial_\theta) + \frac{1}{\sin^2 \theta} \partial_\psi^2 \right) P(\mathbf{u}, t).\end{aligned}$$

The general solution for this partial differential equation are spherical harmonics:

$$P(\mathbf{u}, t) = \sum_{l=0}^{\infty} \sum_{m=-l}^l C_{lm} Y_l^m(\mathbf{u}) \exp\left(-l(l+1) \frac{t}{\tau_R}\right),$$

where C_{lm} depends on the initial condition. For $P(\mathbf{u}, 0) = 1/4\pi$, that is a homogeneously distributed orientations,

$$P(\mathbf{u}, t) = 1/4\pi \int d\mathbf{u}_0 \sum_{l=0}^{\infty} \sum_{m=-l}^l Y_l^m(\mathbf{u}_0) Y_l^m(\mathbf{u}) \exp\left(-l(l+1) \frac{t}{\tau_R}\right),$$

The direction of the colloid loses its correlation exponentially. This change in direction modifies the mean square displacement, assuming an initial position at the origin:

$$\begin{aligned}\langle |\mathbf{r}^c(t)|^2 \rangle &= \int_0^t da \int_0^t db \langle \mathbf{v}(a) \cdot \mathbf{v}(b) \rangle \\ &= v^2 \int_0^t ds (t-s) \langle \mathbf{u}(s) \cdot \mathbf{u}(0) \rangle.\end{aligned}\quad (3.4)$$

Where

$$\begin{aligned}\langle \mathbf{u}(t) \cdot \mathbf{u}(0) \rangle &= \int d\mathbf{u} 1/4\pi \int d\mathbf{u}_0 \mathbf{u} \cdot \mathbf{u}_0 \\ &\quad \sum_{l=0}^{\infty} \sum_{m=-l}^l Y_l^m(\mathbf{u}_0) Y_l^m(\mathbf{u}) \exp\left(-l(l+1) \frac{t}{\tau_R}\right).\end{aligned}$$

In this sum, only the $m = 0$ terms are nonzero, and only the $l = 1$ term is nonzero. We thus obtain the much simpler:

$$\begin{aligned}\langle \mathbf{u}(t) \cdot \mathbf{u}(0) \rangle &= \int d\mathbf{u} 1/4\pi \int d\mathbf{u}_0 \mathbf{u} \cdot \mathbf{u}_0 Y_1^0(\mathbf{u}_0) Y_1^0(\mathbf{u}) \exp\left(-2 \frac{t}{\tau_R}\right) \\ &= \exp\left(-2 \frac{t}{\tau_R}\right).\end{aligned}\quad (3.5)$$

Reinjecting this in eq. (3.4), we obtain:

$$\langle |\mathbf{r}^c(t)|^2 \rangle = \frac{1}{2} v^2 \tau_R \left[\frac{2t}{\tau_R} + \exp\left(-2 \frac{t}{\tau_R}\right) - 1 \right].$$

However, since we only look at the 2D diffusion, we must multiply this result by $2/3$, since all spatial directions are independent. We finally obtain, adding the Brownian component,

$$\boxed{\langle |\mathbf{r}(t)|^2 \rangle = 4Dt + \frac{1}{3}v^2\tau_R^2 \left[\frac{2t}{\tau_R} + \exp\left(-2\frac{t}{\tau_R}\right) - 1 \right]}. \quad (3.6)$$

To conclude, at short time scales $t < \frac{D}{v^2} \sim 2.10^{-3}\text{s}$, the motion is purely Brownian, then becomes ballistic, then a persistent Brownian motion.

3.1.2 Experimental investigation.

To characterize the motion of a dilute assembly, we would like to fully characterize the mean square displacement, and see if it is compatible with the theoretical expectation we just derived.

3.1.2.1 Direct measurement of the dynamics.

There are two ways of verifying this theoretical prediction: either by measuring $\langle |\mathbf{r}(t)|^2 \rangle$, and checking if it follows eq. 3.6, or, if one has access to the orientation \mathbf{u} of the colloid, a direct measurement of $\langle \mathbf{u}(t) \cdot \mathbf{u}(0) \rangle$ can be made, which will verify that the colloid follows rotational Brownian motion, described by eq. 3.5.

Measurement of $\langle |\mathbf{r}(t)|^2 \rangle$ Our high velocity swimmers are too fast, thus is very hard to follow them for very long times. In a $350 \times 350 \mu\text{m}^2$ field of observation, swimmers going at $v = 10 \mu\text{m} \cdot \text{s}^{-1}$ will only stay in the ROI for $t = \frac{l_0^2}{v^2\tau_R} \sim 28\text{s}$. We would need an observation time large when compared to $\tau_R \sim 10\text{s}$. Moreover τ_R is experimentally a weak fitting parameter for eq. (3.6), in the sense that changing it by a factor 100 does not change the function much.

However, quantitative experimental verifications of these results have already been made, with other particles, in references: [66] and [64].

Measurement of $\langle \mathbf{u}(t) \cdot \mathbf{u}(0) \rangle$ Direct measurement of $\langle \mathbf{u}(t) \cdot \mathbf{u}(0) \rangle$ can be made for rods, or particles whose orientation is measurable. In our case, this is not possible yet, but might become in the future if our attempts at measuring colloid orientations through color detection succeed.

In experiments with gold-platinum rods, the orientation can be accessed directly, and the correlation function $\langle \mathbf{u}(t) \cdot \mathbf{u}(0) \rangle$ can be measured easily. Its exponential form has been verified [87], however, the decorrelation time τ_R seems to increase with the swimmer velocity v , perhaps

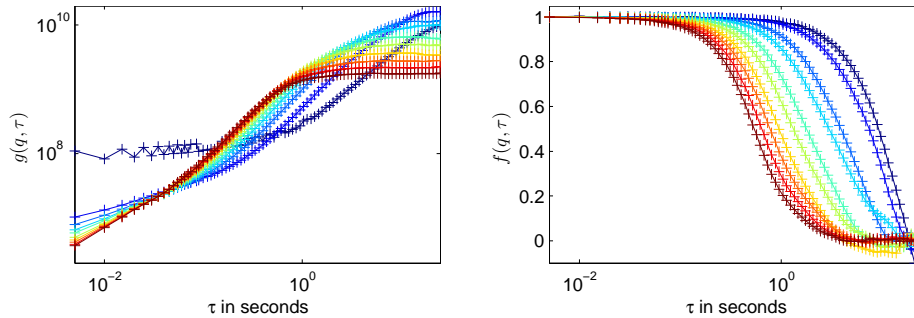


Figure 3.3: $g(q, \tau)$ (left) and $f(q, \tau)$ (right) as a function of τ , for q from $1.2 \cdot 10^{-2} \mu\text{m}^{-1}$ (blue) to $1.7 \cdot 10^{-1} \mu\text{m}^{-1}$ (red). The negative values for high q come from a bad estimate of $A(q)$. (see text)

through a coupling with the interface [101], or due to the specific mechanisms for swimming.

3.1.2.2 Dynamic differential microscopy

Since we cannot access the individual dynamics of swimmers, we try to probe it through a global measurement: the intermediate scattering function $f(q, \tau)$ (see sec. 2.5), measured by dynamic differential microscopy on a low area density $\phi \sim 1 \cdot 10^{-2}$ assembly of swimmers.

We compute (see 2.5)

$$g(q, \tau) = \left\langle |I(\mathbf{q}, t + \tau) - I(\mathbf{q}, t)|^2 \right\rangle_{t, \theta}.$$

From the measured $g(q, \tau)$, we compute the intermediate scattering function (see fig. 3.3):

$$f(q, \tau) = 1 - \frac{g(q, \tau) - B(q)}{A(q)}.$$

Assuming that $f(q, \tau)$ reaches its limits⁶, $B(q) = g(q, \tau_{min})$ and $A(q) = g(q, \tau_{max}) - g(q, 0)$. The shape of $g(q, \tau)$ makes it hard to decide whether it reaches its limit at short times. For longer times it works much better, although not for the smallest q .

We acquire 5000 frames at 200Hz. To increase acquisition speed, we use 1Mpx images, whose resolution is smaller than the images we use for particle tracking⁷. To measure the lowest possible wave vector, we film a $560 \times 560 \mu\text{m}^2$ observation field. Pixels are larger too, measuring $0.5 \times 0.5 \mu\text{m}^2$. The lowest possible value of q available, is $3 \cdot 10^{-3} \mu\text{m}^{-1}$, but there is not enough data points at the lowest values to compute a reliable

⁶From the definition of $f(q, \tau)$, for all $q, \lim_{\tau \rightarrow 0} f(q, \tau) = 1$. The existence of diffusive processes imposes $\lim_{\tau \rightarrow \infty} f(q, \tau) = 0$

⁷Pixels are $0.5 \mu\text{m}$ across instead of 171nm .

average, thus, the effective range of q available is from $1.2 \cdot 10^{-2} \mu\text{m}^{-1}$ to $1.7 \cdot 10^{-1} \mu\text{m}^{-1}$; and time shifts τ from $5 \cdot 10^{-3} \text{s}$ to 5s . We can see that the curve corresponding to the lowest value of q is noisy because of a lack of statistics⁸ (fig. 3.3, dark blue curve):.

The averaging over all times is very long ($\sim 5 \text{ks}$) and all images need to be loaded in RAM, which limits the amount of images we can effectively analyze. Since we need to record the Fourier transforms of these images, 5000 frames weight 40GB (each point in the matrices holds a complex single).

For time shifts τ , $\tau_a \ll \tau \ll \tau_B$, the colloids have a purely ballistic motion; Assuming a constant a velocity distribution $P(v)$, with uniformly randomly distributed orientations, it yields [79]

$$f(q, \tau) = \exp(-Dq^2\tau) \cdot \int_0^\infty P(v) \text{sinc}(qv\tau) dv,$$

Where D is the passive diffusion coefficient. The first term models the diffusive Brownian motion, while the second term models the ballistic motion. We have to note that since $1.2 \cdot 10^{-2} \mu\text{m}^{-1} < q < 0.17 \mu\text{m}^{-1}$, and $5 \cdot 10^{-3} \text{s} < \tau < 5 \text{s}$, with $D = 0.2 \mu\text{m}^2 \cdot \text{s}^{-1}$; then,

$$1.2 \cdot 10^{-7} < Dq^2\tau < 0.03 \ll 1.$$

We can thus neglect the effects of Brownian motion, in the accessible range⁹ of q and τ , and approximate: $\exp(-Dq^2\tau) \sim 1$. The intermediate scattering function becomes

$$f(q, \tau) = \int_0^\infty P(v) \text{sinc}(qv\tau) dv.$$

This implies that $f(q, \tau)$ is a function of $q\tau$ only. To verify this, we plot $f(q, \tau)$, for several q , as a function of $q\tau$ (see fig. 3.4). The collapse is acceptable, especially at low q , but there is still a clear splay of scattering functions for different q . This difference for high $q\tau$ might be due to the fact that for $\tau \sim \tau_R$, the rotational Brownian motion plays a role and the motion strays from a purely ballistic form into a diffusive active motion.

These preliminary results look promising, the next step is to analyze the longer-term behavior. We have not yet introduced the rotational

⁸The number of data points between values q_1 and q_2 is $\sim \pi q_2(q_2 - q_1)$, because of the azimuthal averaging, which implies that lowest values of q have low statistics.

⁹Similarly to our limitations on the measurement of velocities, we would need a better spatial resolution to be able to observe Brownian motion. Here we could see Brownian motion for $Dq^2\tau \geq 1$ and $Dq^2\tau \gg q^2v^2\tau^2$, which implies $q_{max} \gg \frac{v}{D} \sim 50 \mu\text{m}^{-1}$, for $v = 10 \mu\text{m} \cdot \text{s}^{-1}$, which in turns would require pixel much smaller than 20nm pixels, to be compared to the $0.5 \mu\text{m}$ we use.

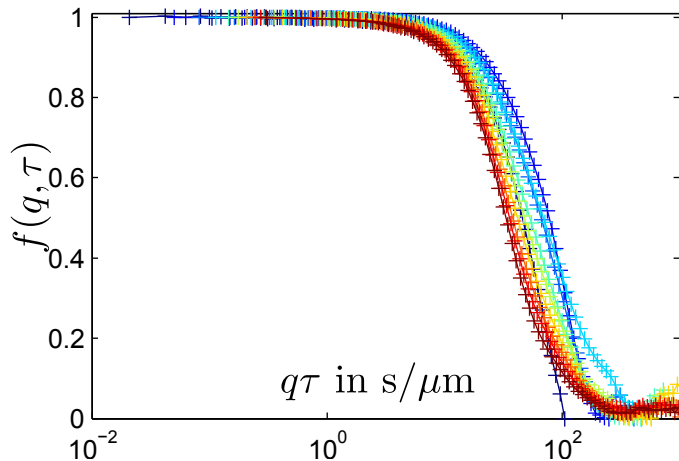


Figure 3.4: $f(q, \tau)$ as a function of $q\tau$, for q from $1.2 \cdot 10^{-2} \mu\text{m}^{-1}$ (blue) to $1.7 \cdot 10^{-1} \mu\text{m}^{-1}$ (red). The collapse is acceptable, but there is still a clear difference between scattering functions for different q .

Brownian motion, which modifies the long term trajectories of the colloids by changing ballistic behavior into a persistent random motion. By probing times longer than τ_R , we should be able to resolve the transition from purely ballistic to active diffusion. The theoretical predictions proposed by K. Martens *et al.* [102] are ready to be tested, once we measure long-term correlations.

Another interesting possibility is the study of the intermediate scattering function for a dense assembly of swimmers. This however requires experimental developments, notably to be able to record and analyze correlations for very long times¹⁰; as well as theoretical predictions of the behavior of dense assemblies.

3.2 Interaction between colloids

To understand the formation of clusters, we have to take into account the interaction between particles. We present all possible sources of interaction between our gold-platinum Janus, that have been suggested in the literature. The simplest part of the interaction is that colloids are solid and they cannot interpenetrate each other. Then, the hydrodynamic interaction between swimmers is detailed. The last part of the interaction is phoretic in nature, and comes from an effect similar to that which propels our active colloids. The goal of our experiments, presented in further sections, will be to find out which of these effects are key to the

¹⁰The cluster collision and separation times are around 100s, implying we need to record times much larger than 100s. At 200MB/s, our setup is currently limited to 400GB, or 2000s, which seems reasonable; however, unless we propose a smart algorithm, we will never be able to analyze that much information...

formation and dynamics of our clusters.

3.2.1 Steric interactions.

The simplest interaction between the colloids is a steric interaction. The colloids are made of gold, and thus incompressible. Although gold is one of the softest metals, the order of magnitude of forces in the system is the pico-Newton, and the bulk modulus of gold ($K = -V \frac{\partial P}{\partial V}$) being of order $K = 180\text{GPa}$, the change in size is of order $\sim 2 \cdot 10^{-16}\text{m}$, thus completely negligible. The colloids thus cannot interpenetrate, which has an important effect on their 2D arrangements.

The maximum area density ϕ , the ratio of the area occupied by the colloids divided by the overall area, for a 2D packing of monodisperse hard spheres is 0.908. However, the computation is non-trivial for random packings (RCP at 0.82 [103, 104]), and even harder once one adds polydispersity [105]. From our experiments, maximum densities are around 0.8. This limiting maximum density has an important effect on the shape and structure of the clusters.

For the passive case, the packing of hard disks in two dimensions is well studied, and the equation of state that is proposed is a variation of the Carnahan-Starling equation of state for hard spheres [106, 107, 108, 109]:

$$\beta\Pi = \frac{\rho}{(1 - \rho/\rho_{max})^2},$$

where ρ is the number density, ρ_{max} the maximum density in the solid, and Π the osmotic pressure, and $\beta = 1/k_B T$. A study of the existence of an equation of state in the active case is presented in chapter 4.

The electrostatic interactions between colloids also plays a role, but probably only in the passive case. Indeed, metallic colloids might be charged negatively [88], so they repel each other. However, as peroxide is introduced, its dissociation increases the amount of ions, thus screening the electrostatic interaction. The introduction of peroxide could also drastically change the surface charge of the colloids.

3.2.2 Hydrodynamics

Since we have not yet been able to observe the hydrodynamic field around our microswimmers directly, we must rely on indirect observations, and theoretical predictions to understand how the hydrodynamic interaction act on our colloids.

Measuring the displacement field around the colloid. We have not yet been able to measure the hydrodynamic field around our active

colloids. The first problem is that they are small, and their velocities are not high enough. The easiest method to measure the hydrodynamic field is by use of passive tracer colloids, of size $l \ll R$, that are simply advected by the hydrodynamic field around the active particle. The velocity field is then measured through particle image velocimetry, or by particle tracking velocimetry. This technique has been used experimentally to measure the hydrodynamic fields around *chlamydomonas* [40, 110]. To be efficient if we want a spatial resolution of order l , we would need, to be able to neglect Brownian motion when compared to advection over the length l . Thus swimming velocities of $v \gg 5\mu\text{m.s}^{-1}$, assuming $l \sim R/10$; for *chlamydomonas*, swimming velocities are of order $100\mu\text{m.s}^{-1}$, with peaks at $500\mu\text{m.s}^{-1}$. It would also be better to be able to work with colloids, that although active, is maintained in a fixed position, for example by an AFM tip, and displaced the fluid around them instead of moving, like micropumps [65, 111]. Approaches with optical tweezers have been tried, but the laser increases bubble formation dramatically.

The effect of the hydrodynamic field. The hydrodynamic interaction is the interaction of a colloid with the hydrodynamic displacement field created by its neighbors (see appendix A). The hydrodynamic interaction is dissipative in nature. In the absence of ordering in the system, it tends to reduce the velocity of active particles. However, the interactions can also promote ordering in the system, in which case the velocities of the colloids can be increased.

In the general case of swimming particles, many theoretical studies have focused on the impact of these interactions, for many different swimmers types, and they predict that, depending on the type of fluid flows, and more precisely on their symmetries, very different behaviors can arise. Pusher particles, such as bacteria, behave differently from puller swimmers, such as algae. Basically, pusher have polar interactions, while they are apolar in the case of pullers. In the case of an assembly of puller particles, the perturbations due to swimming have no effect, while they grow exponentially with time for pusher swimmers [25, 112, 23]. This leads to very different dynamics, and different collective effects in the two cases. For pusher, we can expect low Reynolds turbulence [113, 114], while symmetry prevents its appearance for puller particles. Of course, this has a major impact on mixing, as turbulence, and especially large scale motion is much more effective than diffusion processes. For our Janus particles, it is interesting to study mixing as a way to probe the symmetries of the hydrodynamic interaction. There is not yet any theoretical prediction for quadrupolar swimmers.

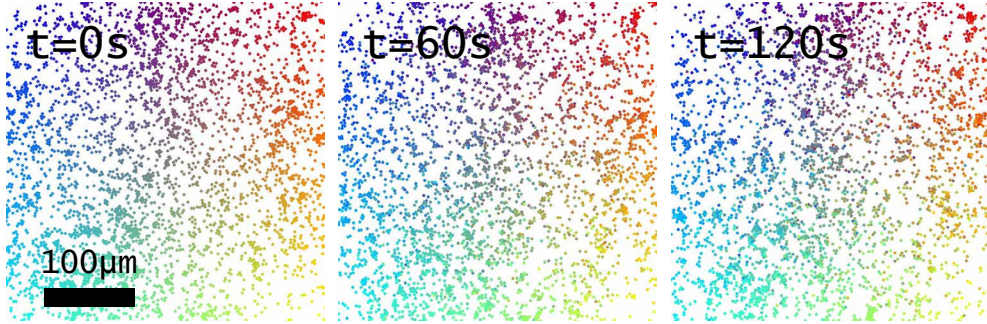


Figure 3.5: Experimental pictures illustrating the mixing in an assembly of Janus particles. Snapshots, at $t = 0$, 1min and 3min. The colloids color are chosen in function of the colloid position at $t = 0$. The scale bar is $100\mu\text{m}$. Very small mixing as for puller assemblies: no large scale eddies or turbulence. $\phi = 0.10$, $\text{Pe}=10$, $[\text{H}_2\text{O}_2]=5.2 \cdot 10^{-4}$. See sup. mat. movie 2.

A first experimental look In figure 3.5, we represent experimental snapshots of our system, for three different time steps, separated by 1min. The swimmers color is chosen by the position of the colloid at time $t = 0$. Thus, looking at the color repartition tells us that no large scale mixing is occurring in the system after 3 minutes. The mixing is enhanced by activity, only in so far as our active colloids have a much higher effective diffusion coefficient, but it is still diffusive mixing, as opposed to convective mixing.

3.2.3 Chemical

Phoretic effects are causing the self-propulsion of our Janus colloids. They also have an effect for the interparticle interactions.

The colloids act as microscopic batteries in water, and consume hydrogen peroxide fuel in the medium (see [65, 88]). Thus, they act as monopole drains for the peroxide concentration, and are thus surrounded by a homogenous gradient at long distance:

$$\nabla C \propto \frac{\alpha_C}{r^3} \mathbf{r}.$$

where α_C is the consumption rate of peroxide by a single colloid. In this gradient, the colloids move owing to diffusiophoresis [74], with velocity

$$v = K \nabla C,$$

where K is the diffusiophoretic constant, depending on the colloid nature, on the solute concentration C , and on the nature of the solute. From the time evolution of the distributions, assuming an infinite Péclet num-

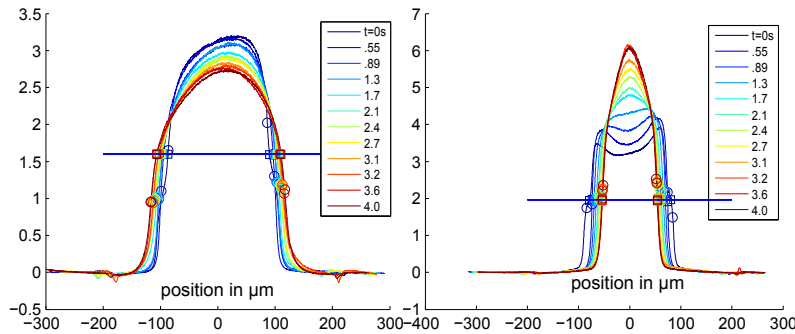


Figure 3.6: Widening (left) and focus (right) for Ψ -channel experiments. For the widening, the central channel contains colloid and 5% peroxide, while the side channels have DI water; for the focus, the central channel has water and colloids, while the side channels have 5% peroxide. The density profiles are shown as a function of spatial coordinate across the channel length, for different time steps. The blue curve is the initial condition, and the red one the final stationary distribution. With a 5% volumetric concentration in peroxide the widening and focus allow a precise measurement of the diffusiophoretic constant K that relates the solute gradient to the diffusiophoretic velocity: $\mathbf{v}_{DP} = K\nabla C$.

ber, we can invert the distribution evolution equation, to measure the diffusiophoretic constant:

$$\begin{aligned} \partial_t \rho &= -\nabla \cdot \mathbf{v}_{DP} \rho, \\ &= -\mathbf{v}_{DP} \cdot \nabla \rho - \rho \nabla \cdot \mathbf{v}_{DP}, \\ &= -\mathbf{v}_{DP} \cdot \nabla \rho, \end{aligned}$$

with ρ the colloid density, and assuming an incompressible fluid.

To quantify the interaction between colloids, we use 100nm latex colloids in a Ψ -shaped micro-channel [72] (see sec. 2.2). The most notable effect is that colloids are repelled by H_2O_2 ¹¹. We show in fig. 3.6 this behavior for a 5% gradient in peroxide. We plot the density profiles as a function of position across the channel axis, for different times. When peroxide is mixed with the colloids, we observe a widening of the colloid distribution, while when peroxide is on the side channels, the gradient is reversed, and we observe a focus of the colloid distribution.

The key result, is that for latex colloids, our microfluidics experiments show that the hydrogen peroxide is a chemorepellent. From this observation, and the fact that our clusters seem to be cohesive, we can postulate that hydrogen peroxide is a chemorepellent also for gold-platinum Janus colloids.

¹¹Repelling behavior is expected for most molecular species[74].

3.3 Static description of the clusters:

We have analyzed qualitatively the properties of the clusters, and know which interactions to expect. It is now time to quantify the properties of the clusters, with respect to the distance of the system from equilibrium. Indeed, while at equilibrium, we do not expect any clusters, we want to see how the clusters change as activity increases.

Before measuring clusters properties, we first focus on our measurement of activity.

The first and simplest properties of clusters measured is their average size. We will see that even such a simple measurement can give interesting hints as to the mechanism causing the formation of clusters. These very promising results led us to investigate the cluster sizes in more detail: the experimental development performed during this thesis allow us to gather very high statistics, by tracking up to 10^4 colloids. This allows us to measure the structure of colloids with a very good accuracy. And also analyze their size distribution in details. These methods will also be used in the next chapter.

3.3.1 Activity measurement

I describe in details how the velocity of colloids is measured. It might seem paradoxical that the first item in a section entitled Static description should deal with velocity measurements. However, the most obvious intensive parameter to describe the activity of the dynamic cluster phase is the velocity of the particles. It is the most obvious departure from equilibrium behavior, as peroxide is introduced in the system. We will use colloids velocities as a measure of activity in the system. And activity is the main control parameter used to gauge cluster properties.

We first measure the velocity of every colloid. Every trajectory computed previously (see sec. 2.4.2) is now smoothed through Gaussian averaging to remove Brownian motion. Then, the velocity of each colloid is computed at every time step. Computing velocities from trajectories is quite difficult. between two time steps divided by Δt , the displacement due to the Brownian motion and the 2D convective persistent walk is (see eq 3.6)

$$\Delta r^2 = 4D\Delta t + \frac{v^2\tau_r^2}{2} \left[\frac{2\Delta t}{\tau_r} + e^{-2\Delta t/\tau_r} - 1 \right],$$

where $\tau_r \sim 10$ s is the rotational diffusion time. To compute the velocity, one approach is to use the whole $\Delta r^2(\Delta t)$ curve and extract the velocity v from a fit. However, the rotational diffusion time depends non-trivially on the velocity v . Another problem is that the actual displacement

function converges very slowly towards the theoretical distribution. The usual way to avoid this problem is to compute an average over many trajectories, which is not possible in our case, since we want to measure individual velocities. We resort to a much cruder approach: define the individual velocity $v_i = \frac{\Delta r}{\Delta t}$. For times $\Delta t \ll \tau_r$, $v_i = \sqrt{\frac{4D}{\Delta t} + v^2}$. Because Brownian motion has a big impact on small displacements, we are limited in our choice of Δt by Brownian motion and rotational diffusion. If we choose $\Delta t \sim \tau_r$, the velocity decreases because of orientation diffusion, the first order correction being: $v_i = v \left(1 - \frac{2\Delta t}{3\tau_r} + o\left(\frac{\Delta t^2}{\tau_r^2}\right)\right)$. We thus have to strike a balance and take $\frac{4D}{v^2} \ll \Delta t \ll \tau_r$. Since $\tau_r \sim 10\text{s}$ and $\frac{4D}{v^2}$ can become large for small velocities, this balance is hard to strike. We choose $\Delta t = 3\text{s}$, and we have to accept that the measured velocity is an approximation at best, whose quality decreases when velocity decreases. The minimum velocity we can measure is $0.5\mu\text{m}\cdot\text{s}^{-1}$, and the error on velocity around 20%. In denser phases, the estimated diffusion coefficient decreases, because of local jamming. Measuring low velocities in the clusters is much more favorable.

It may seem strange that it's so hard to measure such a simple property as an instantaneous velocity. However, it is mainly a problem of scale. We have chosen to focus on the ballistic regime, but this excludes the short-time, short-range passive diffusion, and also the long-term, long-range active diffusion. To be able to resolve the passive Brownian motion, we need small pixels of size $l \ll \sqrt{\frac{4D^2}{v^2}} \sim 180\text{nm}$, which is approximately our pixel size. Thus we are not able to see precisely the Brownian to ballistic transition, but we could, using a higher magnification. On the other hand, to be able to resolve the active diffusive motion, we need an observation field of size L much larger than $v\tau_R \sim 100\mu\text{m}$, while we currently have $L = 350\mu\text{m}$. Thus, we are not able to watch the ballistic to active diffusion transition, although we could with a smaller magnification objective. To conclude, we are not able to observe all dynamical regimes at the same time, and our choice of observation scale is, as always, a compromise, and we decided to focus on the active ballistic regime.

3.3.2 Average cluster size.

Perhaps the simplest of measurable cluster properties is their average size. We will see how it leads us to propose that clusters are caused mainly by the chemical interaction between colloids.

3.3.2.1 Measuring the average size

The average size of the clusters is presented on figure 3.7, a). Here, the clusters were counted by hand, printing several images on a A4 paper

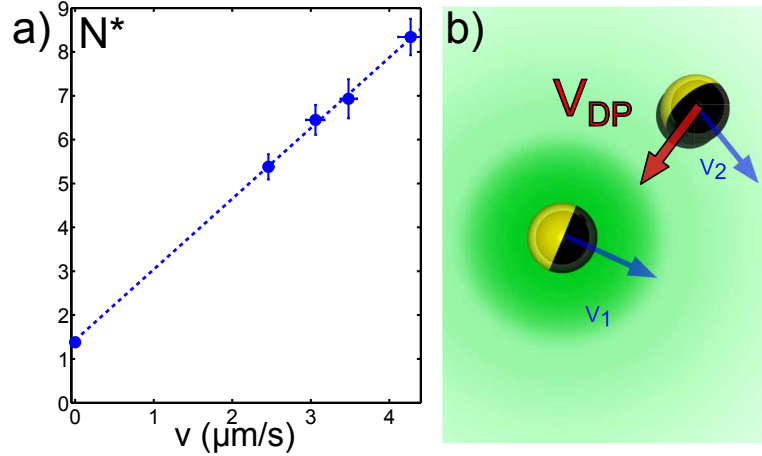


Figure 3.7: a) Average size N^* of clusters at $\phi = 5 \cdot 10^{-2}$, and various activities. The non-zero value of N^* at $v = 0$ is due to preexisting doublets and triplets. The linear fit shows very good agreement with our theoretical expectation (see Eq. 3.7). b) Schematics of the interaction between two swimmers. The green color intensity represents the peroxide depletion due to the first swimmer. The red arrow represents the diffusiophoretic velocity of the second swimmer in the concentration field created by the first.

sheets for each velocity, and counting cluster sizes by simply circling the clusters. For each velocity, about 500 colloids were counted, which is enough to measure an average size, but not to measure a size distribution, as is done in sec. 3.3.6. The same system was used during the whole experiment¹², a colloid assembly at area density $\phi = 5\%$, and between each increase in peroxide, we waited for 10 minutes for the system to reach a stationary state. We observe a linear increase of the cluster size with the velocity of free colloids. Obviously, at very high activities, the average cluster size should plateau at some value (it cannot increase beyond the system size), and this transition should be interesting to investigate. However, we do not see it at the range of velocities we can probe.

3.3.2.2 The Keller-Segel Model

We propose a model to account for the evolution of the average size of clusters with respect to the activity. We show that since our colloids are subject to chemical interactions (see sec. 3.2.3), they can sense concentration gradients, as do bacteria also with a very different physical mechanism. The role of chemical sensing has already been studied in the context of patterns and clusters formation of bacteria [115, 116, 117]. In a

¹²However, the acquisition rate, and detection accuracy with the present setup are not enough to use the quantification scheme proposed in sec. 3.3.6.

pioneering work, Keller and Segel (KS) proposed a mean field description, taking into account the diffusion of bacteria, the production and diffusion of a chemoattractant [116], and a drift induced by chemical sensing (a bacterial velocity $\mathbf{v} \propto \nabla c_{\text{chemoattractant}}$). In our context, a direct mathematical analogy may be drawn. The chemotactic drift is played here by diffusiophoresis, the motion of particles induced by solute gradients [74, ?] (see sec. 3.2.3). Indeed, due to the propulsion mechanism, each microswimmer creates a solute concentration gradient ∇C in peroxide around it and induces a corresponding diffusiophoretic drift of the other colloids: $\mathbf{v}_{DP} = K\nabla c$ [118, 88], with K a negative constant, as peroxide is expected to be a chemorepellent (see sec. 3.2.3). Such a mechanism, sketched in fig. 3.7, b), allows us to rationalize the various observations of dynamic attraction quoted above for active colloids under self-generated chemical gradients. The spatiotemporal dynamics of the active particle population can then be described at a mean-field level in terms of a (here, 2D) particle density ρ and peroxide concentration field c , using a KS description:

$$\begin{cases} \partial_t \rho &= D_\rho \nabla^2 \rho + K \nabla(\rho \nabla c) \\ \partial_t c &= D_c \nabla^2 c - \alpha \rho, \end{cases}$$

with $D_\rho = v^2 \tau_R$ the effective diffusion coefficient of the swimmers, D_c , the diffusion coefficient of peroxide, and α the consumption rate of peroxide.

An interesting feature of the KS equations is that they exhibit singular solutions, leading to a ‘‘chemotactic collapse’’ of the structure into a single or many dense aggregates [116]. This phenomenon introduces a threshold ‘‘Chandrasekhar’’ number, N_c , above which the bacteria population clusterizes, while below it remains homogeneous. The expression for N_c is (in 2D): $N_c = 4 \frac{D_\rho D_c}{K \alpha}$. Furthermore, as discussed in [116], $N^* = N_c$ is also expected to fix the typical size of a cluster.

Here, in order to connect this size to the experimentally measured velocity v of the swimmer, we first note that v is itself a function of these parameters. Indeed, the motion is driven by the chemical reaction at the surface of the colloids and following [88, 98], one expects typically $v \sim K^\alpha / R D_c$, so that $\alpha K \sim v R D_c$ [64]. Since $D_\rho = v^2 \tau_R$, this yields

$$N^* \sim \frac{v \tau_R}{R} \sim \text{Pe} \quad (3.7)$$

where $\text{Pe} = vR/D_0$ is a Péclet number characterizing the swimmer (D_0 the bare diffusion coefficient), and comparing the advection to the diffusion. This prediction is in good agreement with the experimental result in Fig. 3.7, $N^*(v) \propto v$, with furthermore a predicted prefactor given by an inverse velocity $\tau_R/a \sim 1 \mu\text{m}^{-1} \cdot \text{s}$, also in agreement with the experiments.

This KS chemotactic scenario points to the basic ingredients for the chemically powered swimmer particles and proposes a consistent and predictive explanation for clustering.

3.3.2.3 Limits of the model

The real mathematical description may be more complex as nonlinear mechanisms, such as a possible dependency of D_ρ on concentration ρ or with chemical concentration c (e.g., a decrease of D_ρ with a decrease in c , linked to a decrease in Janus velocity as the fuel concentration decreases), were not considered here but would anyway act as second order corrections which do not modify the basic instability. Such refinements would require further mathematical developments, as studied by Murray [18]. The concentrations considered are still low, and we expect that as colloidal concentration increases, these limitations might become more important. Indeed, we do not observe the relaxation toward a single cluster, predicted by the KS model. This implies that another mechanism is at play here, that tends to destabilize large clusters. Although not definitive, the long term behavior of the clusters will be studied quickly below. Comparisons to recent experiments and numerical simulation are performed in sec. 3.5.

Another limitation, is that as a coarse-grained and mean-field description, the KS model cannot describe the detailed kinetics of the aggregate formation and distribution nor its structure, which remain to be studied theoretically and experimentally in more detail. This is why I developed a high throughput acquisition system, capable of gathering high statistics on the clusters (see sec. 3.3.5).

3.3.3 Péclet Number measurement

As we just mentioned, the Péclet number $Pe = \frac{Rv}{D}$, where D is the diffusion coefficient of the Janus colloids in the absence of activity, seems a very good candidate for a more universal way of measuring activity¹³. The Péclet number has indeed been shown to be linked to the effective temperature in low density assemblies [64]. In sedimentation experiments we have verified that an effective temperature can indeed be defined for our system at low densities. In the cluster phase, we cannot easily define an effective temperature, and we simply measure the average velocity of our microswimmers. However the presence of clusters implies an heterogeneous density, and velocities are heterogeneous as well since clusters move slowly compared to individual colloids. Since the low density medium that surrounds the colloids can be thought of as a gas, we will

¹³Simply measuring the velocity of the particles is not very universal, and the Péclet number allows comparisons with very different experimental systems.

only measure the velocity of particles in low density zones. Counting clusters when measuring activity would decrease the average velocity of the swimmers but also change the measured activity when density is modified. Our definition of Péclet, based on a measurement only in low density areas, creates a density independence.

We define *free microswimmers* as colloids without any neighbor closer than $6\mu\text{m}$. We measure the Péclet number as:

$$\text{Pe} = \frac{R}{D} \langle |\mathbf{v}_i(t)| \rangle_{i,t},$$

the mean is calculated over time and over every free microswimmer, and $D = \frac{k_B T}{6\pi\eta R} = 0.21 \pm 0.05\mu\text{m}^2\text{s}^{-1}$ is the thermal Brownian diffusion coefficient, the error comes from the polydispersity, and the error on room temperature ($21 \pm 1^\circ\text{C}$)¹⁴. The typical Péclet number measured are between 4 and 40, with 2% error coming from the velocity dispersion. However, due to Brownian motion, the measured Péclet number for the passive case is around 4. The size polydispersity also creates a systematic error of $\sim 20\%$.

The Péclet Number we measure will be used to characterize the activity afterward. Higher Péclet means higher microswimmers velocities, higher dissipation, and a system that is further from equilibrium.

3.3.4 Structure

Now we have looked at very basic properties of the clusters¹⁵, another static property widely used to characterize structures, in ordered or disordered phases, is the structure factor. It is a standard tool in colloidal physics and more generally in the physics of liquids, that describes the structure of a liquid [8, 119, 14]. Its peaks correspond to wave-vectors at which it is more likely to find a neighbor. For a solid, the peaks are sharp delta-functions, while a liquid has broader peaks, that get broader as order decreases. This is a similar approach to what has been done in a dilute system, with the use of DDM, that measured a dynamic structure factor. The normalized static structure factor $S(q)$ is defined as the density-density correlations:

$$S(q) = \frac{1}{N} \langle \rho(\mathbf{q}) \rho^*(-\mathbf{q}) \rangle_\theta,$$

¹⁴It might be surprising, but the viscosity of water depends a lot on temperature.

¹⁵The term “cluster phase” designates the clusters and the low density phase around them, while the term “cluster” designates dense, cohesive and ordered assemblies of colloids, which undergo solid motion (see sec. 3.4).

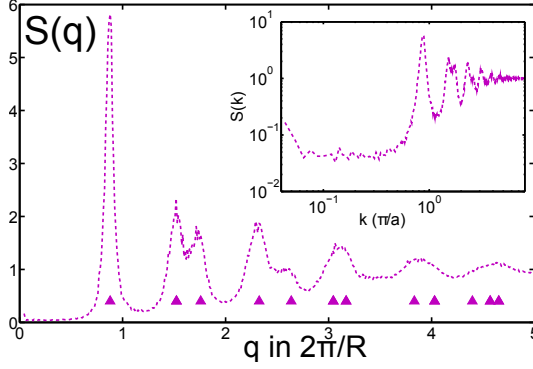


Figure 3.8: A typical structure factor for a dense assembly of swimmers in the passive case ($\phi \sim 0.7$), the wave vector is in units of $\frac{2\pi}{R}$, and the structure is disordered, as can be seen by the decay of the structure factor. The inset presents the same data on a log-log scale. The purple triangle represent the expected position of the peaks for a compact crystal.

where $\rho(\mathbf{q}) = \sum_{i=1}^N \exp(-j\mathbf{q} \cdot \mathbf{r}_i)$, and \mathbf{r}_i the position of colloid i , and N the total number of colloids. The average is over all orientations of the vector \mathbf{q} . To avoid complex number computations, and decrease the memory, and computation load, we simplify, by assuming the isotropy of the system, and we compute instead:

$$S(q) = \frac{1}{N} \left\langle \sum_{i=1}^N \cos^2 \mathbf{q} \cdot \mathbf{r}_i + \sin^2 \mathbf{q} \cdot \mathbf{r}_i \right\rangle_{\theta,t}.$$

The time average is an average over several time steps, which are taken as far as possible from each other so that they are uncorrelated. It is necessary for low-density systems, in which the number of particles per frame is low. We take about 10^{5-6} particles. We also do not count the lines $q_x = 0$ and $q_y = 0$, for they lead to artifacts due to finite size effects [79]. To study the low q behavior, we use our standard low magnification setup ($\sim 30x$ magnification). It is important here to be able to measure as many colloids as possible, since the minimum wave vector accessible is $q_{min} \sim 2\pi/R\sqrt{N}$, where N is the total number of colloids, and R the colloid radius. However, the error on position is of order one pixel, or 171nm^{16} . This leads to noise at high q , that manifests by broadening the peaks; so to study the high q behavior, we use high magnification objectives ($60x$ total magnification), which decreases statistics by a factor 4, while at the same time doubling accuracy.

We show in fig. 3.9 the static structure factor $S(q)$, for different activities and densities, as a function of wave vector in units of $\frac{2\pi}{R}$. To understand the structure of the cluster phase, we must first focus on the

¹⁶We use $\sim 30x$ magnification, and the physical size of camera pixel is $5.5\mu\text{m}$.

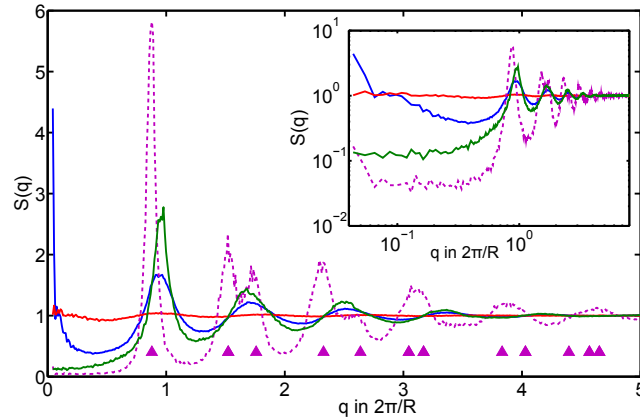


Figure 3.9: Static structure factor for different densities, as a function of wave vector in units of $\frac{2\pi}{R}$. The curves are in order red, blue, and green, with densities $\phi = 3\%$ (a gas), 0.3 (the cluster phase), and 0.8 (a dense phase) respectively, and Péclet ~ 15 . The purple dashed line is here to remind us what the passive solid looks like. The first striking result is that structuration increases with density: the denser the system, the higher the structuration. An important feature is the presence of a divergence at low q , only for the cluster phase, that implies a high compressibility.

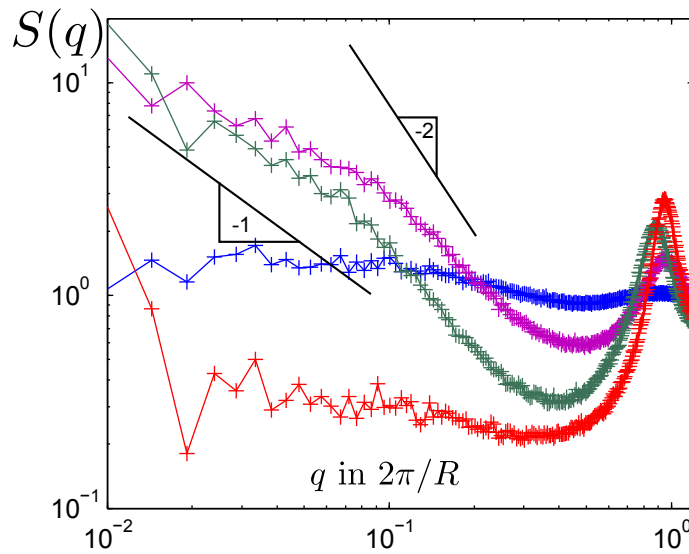


Figure 3.10: Low q behavior. We compare a gas (blue), a dense phase (red), and two cluster phases (green and purple) at different densities. Large statistics allow us to probe the low q region, where the difference between these phases can be seen easily. While the gas remains almost constant ~ 1 , the solid goes to zero, and the two cluster phases show a clear divergence, with exponent -1 . The two black lines are guides with slopes -1 and -2 .

dense phase. The passive solid is the phase with the highest structuration, showing clean, well defined peaks at the values expected for a crystalline structure. However, owing to polydispersity, the structure disappears for long distances. This can be seen by the decay in height and broadening of the peaks as q increases¹⁷. As activity increases, the structuration in the dense phase decreases, peaks become broader, and might also decrease faster, although this is harder to measure. A second effect is that density increases with activity, as can be seen by the shift of the first peak towards high q .

The structure factor of the low density gas phase (red curve in fig 3.9) is simply a constant, which tells us that it behaves (at least statically) as an ideal gas: the position of colloids are fully uncorrelated. A very slight structuration can be seen, as a small oscillation of the structure factor. This is due to the presence of residual clusters, the few clusters that are not due to activity but to the physical links created during the manufacturing process of the Janus colloids.

Since our main interest in this section is the structure of the clusters, it might seem strange to go into so much details about the gas and the dense phase. We observe that the structure factor of a cluster phase seems to be simply a “weighted average” of the structure factors of the gas and the solid phases. We propose a very simple explanation for this: clusters have the same geometric arrangement as the dense phase, and the low density phase in-between is an ideal gas. The higher the density, the sharper and higher the peaks in the cluster phase structure factor, as more and more of the sample has the properties of the solid phase.

To conclude from the point of view of the structure, we can see the clusters as pieces of highly ordered solid suspended in a low density disordered phase. However, as is shown later, the quantitative study of cluster sizes will reveal that the clusters are not in a different phase as the gas. This is one phase, whose structure is highly heterogeneous.

Low q behavior. An other important feature is the presence of a divergence at low q (see fig. 3.10), that implies a high isothermal compressibility [14] $\chi_T \equiv -\frac{1}{\phi} \left. \frac{\partial \phi}{\partial p} \right|_{T,N}$. The compressibility of the cluster phase being higher than the dense phase is obvious: there is more “free room” in the cluster phase than in the dense phase. However, it is harder to understand why the compressibility is higher than in the gas phase, which suggests critical behavior. Maybe the spatial density inhomogeneities increase the compressibility, in similar fashion to second order transitions. Here the activity would play the role of critical order parameter. The

¹⁷a toy model form of $S(q) = 1 + \sin(qd) \cdot \exp(-q\lambda)$, where d is the characteristic wavelength of the crystal and λ the characteristic size of crystal grains.

divergence of $S(q)$ as $q \rightarrow 0$ is compatible with a q^{-1} divergence, unlike the q^{-2} predicted by square gradient theory for second order phase transition [119, 8], the Orstein-Zernike form:

$$S(k) = \frac{1}{\frac{\chi_T^{id}}{\chi_T} + d^2 q^2},$$

where $\chi_T^{id} = \rho k_B T$ is the compressibility of the ideal gas at the same density as the system, and d a characteristic correlation length in the system. The existence of the divergence as $q \rightarrow 0$ is a proof that the compressibility vanishes. To qualitatively understand this phenomenon, we can postulate that the energy barrier between clusters and the gas phase is extremely small, so any increase in density would simply add particles to the clusters, without a resulting increase in pressure. The clusters are attractive and due to the chemical interaction between particles, and they are not contained by the osmotic pressure of the colloids themselves. This is easily seen in movies, as the amount of impacts on a cluster is definitely not sufficient to account for their cohesion (see fig. 3.2 and sup. mat. movie 6 & 7).

Another effect that is to be noted is that, as activity increases, the effective radius of the colloid decreases, as shown by the shift of the first peak, of the structure factor. This could be due to a screening of the electrostatic interaction between colloids by the propulsion reaction products, especially since ions are produced.

3.3.5 Systematic detection of the clusters

We have measured the average size of the clusters, and characterized their structure. These very promising results led us to want to measure even more precisely the clusters shape and size distribution, so we need a systematic characterization of clusters, a way to count thousands of clusters efficiently. We also need to be able to take into account the dynamic nature of the clusters: we do not want a definition based solely on proximity, as is done in many numerical and experimental situations.

We define clusters as assemblies of colloids that undergo solid motion. We do not use merely a proximity threshold definition, such as “clusters are assemblies of colloids whose nearest neighbor is at a distance closer than l_c ”, for we would miss the dynamical aspect of our colloids, we want to be able to measure meaningful dynamic properties, such as translation velocity, rotation velocity. The mere proximity is not enough, and we can see that some colloids are in contact with clusters, in that they are very close, but they are sliding on the side of a cluster. Our definition allows a capture of cluster breaking in a very accurate manner. If a

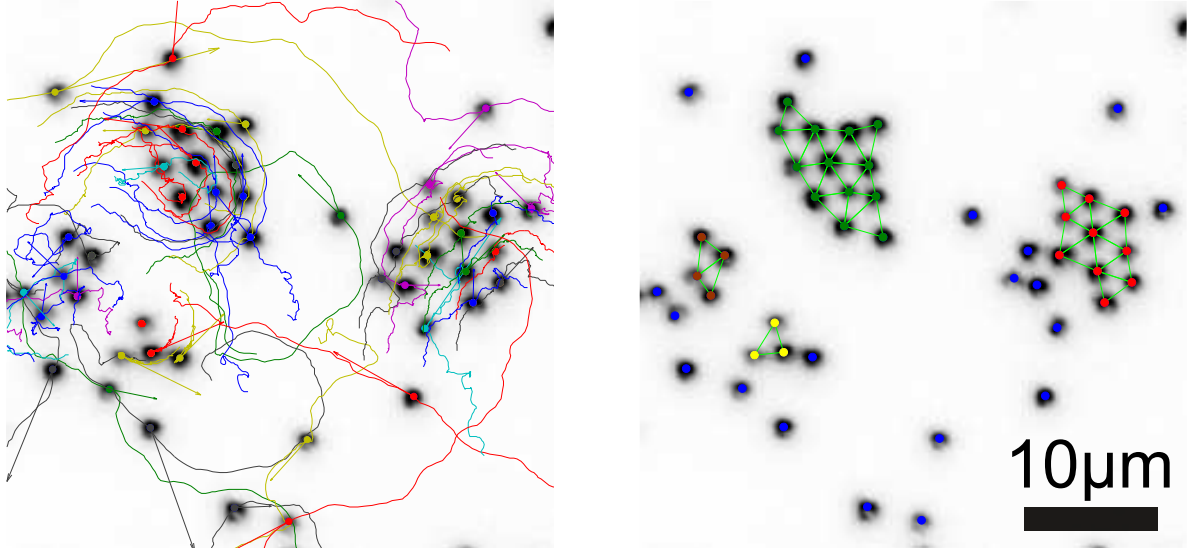


Figure 3.11: Trajectories, and velocities for an assembly of colloids (left). Trailing line whose color matches the dot on the colloids indicate trajectories over ~ 30 s, and color-matched arrows their velocities. Cluster detected (right). The colloids belonging to a given cluster are colored with the same color, and *solid triangles* are in green. It is interesting to note that proximity is not enough to define clusters. sup. mat. movie 3.

sliding fault appears in a cluster, with two sub-cluster going in opposite direction, but staying close to each other, we detect them as two different clusters. Another advantage of this method is that the polydispersity of the colloids is not a problem, while it makes the definition of an unequivocal l_c problematic at best.

The definition of clusters has three steps, first we look for all nearest neighbors, then we detect *solid triangles*, that is triangle of nearest neighbors whose shape is preserved through the motion, for ~ 1 s. Then we define the clusters as the connected components of adjacent solid triangles.

3.3.5.1 Delaunay triangulation.

From particles trajectories, we want to detect, in every frame, each colloid's nearest neighbors, that is all colloids that are closer to a given colloid than to any other colloid, except themselves, obviously. Doing this naively is a very lengthy process, with $O(n^2)$ operations, since we need to compute every pair of distances, which is quite hard since we have $n \sim 5 \cdot 10^3$, and $\sim 2 \cdot 10^3$ frames on which we need to make the analysis. A smart algorithm to find nearest neighbors has been proposed in 1934 by B. Delaunay, a Russian mathematician, his triangulation is the basis of the well-known Voronoi tessellation.

The Delaunay triangulation of an ensemble of points in the plane, is the ensemble of triangles whose vertices are the points in the plane, and whose circumcircles are empty, in the sense that for all triangles, no points lie inside the circumcircle, although they can lie on its perimeter. A given colloid is linked by edges to all its closest neighbors. The Delaunay triangulation exists, which is an important result. The tessellation being a local construction, it can be constructed in $O(n \log n)$ operations, using divide and conquer algorithms, which is much better than $O(n^2)$ (by a factor 10^3). We use the Qhull construction algorithm [120]. If four neighbors are arranged as a rectangle, the Delaunay triangulation is not unique. However, we have 5000 points, that are singles in memory, the probability of having a rectangle up to single digit precision is $\sim 2^{-80} \sim 10^{-24}$, an extremely small probability. Since we have $\sim 5 \cdot 10^6$ particles, this has less than $5 \cdot 10^{-18}$ occurrence probability. Better to play the lottery than this. However, we can still expect some triangles to change from one frame to the next, owing to detection errors that change particles' positions by about one pixel.

3.3.5.2 Graph of solid triangles

Once triangles of closest neighbors are defined, we remove all triangles whose edges are longer than $l_c = 5 \mu\text{m}$, to remove most isolated colloids, that are definitely not part of a cluster, and to diminish the number of candidate *solid triangles*.

A triangle is defined as a *solid triangle* if its edges do not change in length through time. To compensate for the small detection errors, we define solid triangles as triangles whose edges vary by less than $1 \mu\text{m}$ during a 2s time (it must exist for at least two seconds). The triangle keeps the same angles, and it will thus be easy to define its dynamic properties.

Triangles are defined as *adjacent* if they share one edge. We do not consider triangles that share a vertex as adjacent. This avoids colloids that rotate around another colloid. We then define the graph of all *adjacent solid triangles*. All triangles are the nodes of the graph, and nodes are linked by an edge if the triangles are adjacent. To represent this graph, we use the adjacency matrix:

$$A_{ij} = \begin{cases} 1 & \text{if } i \text{ and } j \text{ are adjacent.} \\ 0 & \text{if not.} \end{cases}$$

This matrix is symmetric since we defined adjacency as a symmetric relation.

3.3.5.3 Clusters of triangles

Clusters are defined as the connected components of this graph. Connected components of a graph are the ensembles of nodes \mathcal{E} that are connected to each other through a path, and not connected to a node outside \mathcal{E} . It is important to note that this definition allows some colloids (but not triangles) to belong to two clusters. This definition of clusters considers triangles and not colloids as its individual elements, which does not allow clusters smaller than three colloids. To compute the connected components of the graph, we use a quick algorithm, adapted from [121], probably from [122]. We define S the list of all the nodes of our graph, and W the list of connected components, that is a list of lists of nodes. We use a depth-first search, which explores all nodes of the graph. We use a list X of summits that have been visited, and Y of summits that have to be visited.

Algorithm: find connected component(S,A)

1. Initialize: $W = []$, $X = []$, and $Y = [S(1)]$
2. As long as $\exists x \in S$ and $x \notin W$,
3. As long as Y is not empty,
4. Remove the first element g in Y and add it to X .
5. Add to the beginning of Y all neighbors of g that do not belong to $X \cup Y$.
6. Append the cluster X to W .
7. return W .

This algorithm runs probably in $O(n \log n)$. The custom Matlab code for this analysis takes about 10^3 s to perform an analysis on a cluster assembly of $5 \cdot 10^3$ colloids through 10^3 time steps.

3.3.6 Cluster size distributions.

Using all the statistical might we gathered is useful to measure fine properties of the cluster, such as their size distribution. While it is extremely simple to see that the larger clusters are rarer than the smaller ones, the precise characterization of the distribution demands a lot of statistics. Measuring the size distribution of clusters might lead to hints as to the dynamical process by which cluster aggregate.

We measure the size N of every cluster, by counting the number of colloids inside every cluster. Due to our definition of the clusters,

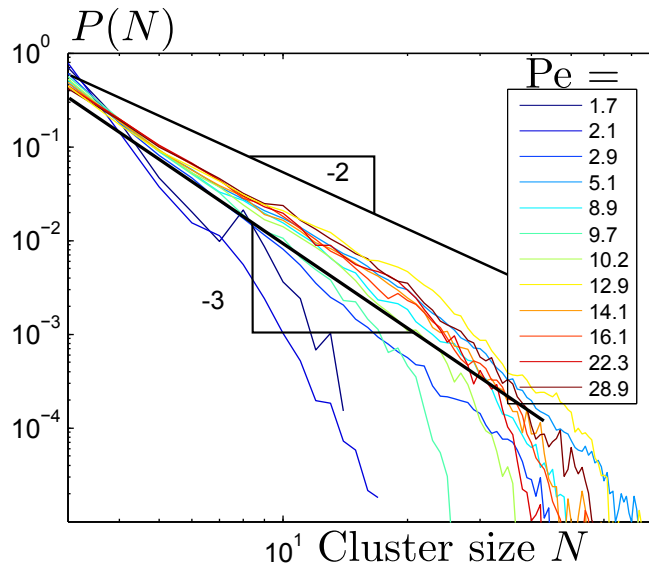


Figure 3.12: (color online) PDFs of cluster sizes for 12 different Péclets from 1.7 (Passive, dark blue) to 29 (highest activity, red), and density $\phi \sim 0.1 \pm 0.01$. The size of clusters increases with activity, and a notable feature is the power-law decay of cluster sizes, with exponent ~ -3 , except for very low activities.

the minimum size is $N = 3$, although we notice interesting two-particle behavior also observed by Ebbens *et al.* [123]. It is also important to note that our definition allows some microswimmers to belong to two clusters at the same time.

We count clusters over 50s, or 1000 frames, counting ~ 300 clusters per frame. This is enough statistics to get accurate measurements of the size distribution, except for larger clusters, which occur on average less than once per frame.

We show (see fig 3.12) the density probability functions (PDF) of cluster sizes, for 12 different activities, at density $\phi \sim 0.1$. There are many more small clusters than large clusters, and the PDFs of the cluster size is a power law with exponent ~ -3 . This means that the large cluster play a large part in the dynamics of the system, while still allowing to define a mean size. A -3 exponent, means $\langle N^2 \rangle \rightarrow \infty$, which implies a critical-like behavior, with large size fluctuations. This behavior is far from the exponential decay expected for the formation of micelles. New theoretical analysis are required to rationalize this power law decay.

It is important to note that no overall collapse of the system in a single cluster is observed, and that large clusters (up to 100units) break apart over very long timescales. What is the ingredient in our system that prevents the global collapse predicted in many simulations [55, 124]? The high mobility of the clusters rules out a dynamical freezing of the collapse. The clusters are colliding with each other constantly. Maybe

the polydispersity plays an important role as it allows higher mobility in dense parts of the system, by creating holes and structural defects inside the clusters, that could lead to a separation of the clusters.

The size distribution is stationary, and does not evolve through time, at least not over ~ 30 minutes. It would be interesting to see how it evolves over longer timescales, although this requires precautions to prevent fuel exhaustion, that would modify the size distribution. This supports the hypothesis that the assembly of Janus swimmers is a phase in the thermodynamical sense, and not an emulsion, bits of a dense phase suspended in a low density gas. Although large density fluctuations are present, it can be thought to have homogenous properties.

While it would have been easy to make up models for exponential decay, we have yet to propose a model to explain a power law distribution for the cluster sizes.

The average sizes computed for these different systems at slightly different densities $\phi = 0.1 \pm 0.02$, cannot be compared directly using the method proposed in sec. 3.3.2, because the densities are slightly different and it seems that the average size of clusters seems to depend on the history of the system, although more experiments are required to confirm this. We have not yet performed constant density experiments with the new analysis algorithm¹⁸. This is coherent with the KS model as after the initial cluster collapse, the dynamics of the cluster is much slower, and cluster might take a very long time to reach their equilibrium size. While this might cast a doubt on our measured distributions, one must not forget that they are stationary over ~ 10 minutes. Maybe over a few hours, a different distribution might arise¹⁹, but over intermediate times, the distributions we measure have meaning.

3.3.7 Conclusion

The assembly of clusters seems to behave as a thermodynamic phase with homogenous properties. Although locally inhomogeneous, we can define a cluster size distribution, an average density, a compressibility. The measurement of a temperature is more complicated and will be treated in the next chapter.

The mechanism of chemical attraction mediated by the consumption of a chemorepellent specie is in good quantitative agreement with the measured average cluster sizes.

¹⁸The constant density experiments done in sec. 3.3.2 could not be analyzed using the new algorithms, as they have been acquired at a low frequency, that precludes tracking.

¹⁹Observing those long times would also require, as mentioned before, a control system to ensure the amount of peroxide stays constant.

These experimental results rely on the development of experimental and analytical tools, to gather statistics on large sets of particles, and large areas. Fast tracking of ~ 5000 colloids is necessary. The points that needs to be studied in future work, is the evolution of the cluster size distribution as a function of activity, for short times. What is the dynamics of a size distribution change? Another interesting property is a direct study of the compressibility by changing the size of the container (see also next chapter).

3.4 Dynamic clusters

After the investigation of the static properties of clusters, the next question that naturally emerges is the question of their dynamical properties; we want to describe the motion of the clusters.

In this last experimental section, we report quantitative experimental measurement to be compared to numerical simulations and similar experiments. More precisely, we measure the dynamical properties of the clusters, how they translate and rotate, how they collide and exchange colloids, all the dynamical properties that make them so different from an equilibrium phase.

All 12 experiments presented here are done at surface density $\phi = 0.1 \pm 0.02$, but ~ 100 experiments have been performed at densities from $\phi=1\%$ to 0.4. They yield similar results, but we focus here on the effect of activity on the dynamical properties of clusters. So we only present results at constant ϕ .

3.4.1 Measuring cluster dynamics

From the measured velocities of the colloids, it is extremely simple to extract the clusters rotational and translational velocities.

We measure the translational velocity of the cluster Ψ by simply taking the average of all velocities in the cluster:

$$\mathbf{v}_{trans}^{\Psi}(t) = \langle \mathbf{v}_i(t) \rangle_{i \in \Psi},$$

i denoting average over each microswimmer inside the cluster. The angular velocity about the center of mass of cluster Ψ is:

$$\Omega^{\Psi} = \mathbf{I}^{-1} \sum_{i \in \Psi} (\mathbf{r}_i - \mathbf{r}_g) \times (\mathbf{v}_i - \mathbf{v}_{trans}^{\Psi}),$$

where \mathbf{I} is the Inertial tensor of the cluster Ψ : $\mathbf{I} = \sum_{i \in \Psi} (\mathbf{r}_i - \mathbf{r}_g)^2$. It reduces into a scalar quantity in two dimensions. These definitions assume

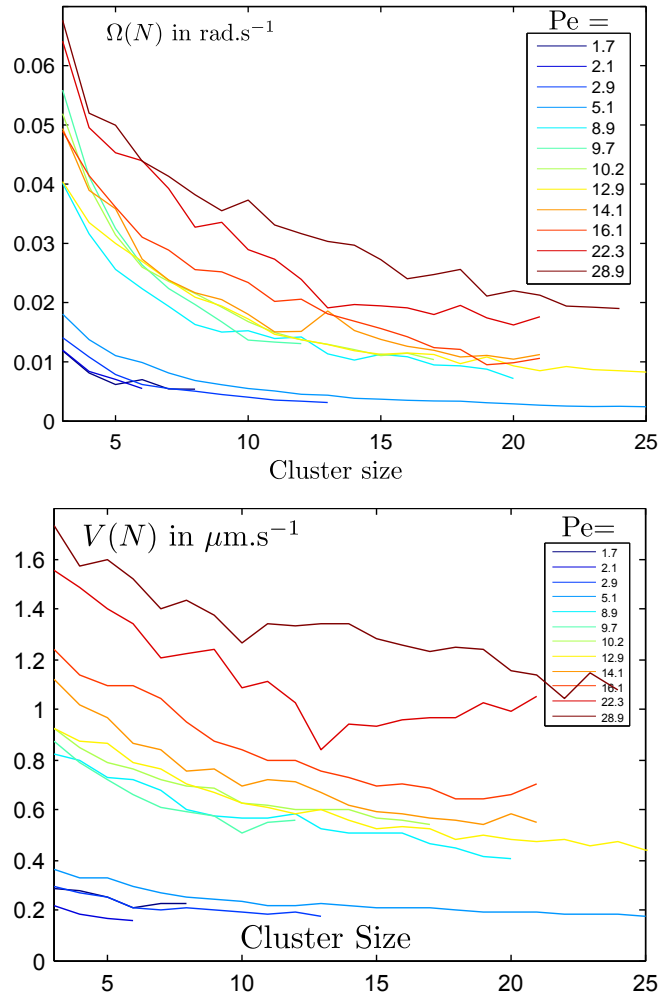


Figure 3.13: Rotational and translational velocities as a function of cluster size, for 12 different activities with Péclet number from 1.7 to 29, and $\phi = 0.1$. The velocities increase with activity, and decrease with cluster size. The decrease is very slow. For each curve ~ 500 clusters were analyzed during ~ 2 min.

that each colloid has the same unity mass. The error on these quantities is small, and comes mostly from bad cluster determinations. The errors are much smaller on \mathbf{v}^Ψ than on \mathbf{v} , because it is an averaged quantity over at least three colloids.

The measured translational and rotational velocities (see fig. 3.13) increase with activity, and decrease with cluster size. These velocities are measured over $2 \cdot 10^3$ time steps, counting $\sim 5 \cdot 10^2$ clusters at each time step, for activities from $\text{Pe}=1.7$ to 29, at area density $\phi = 0.1$.

The translational and rotational velocities have a similar behavior; they increase with Péclet, and decrease with cluster size. The slow decay is compatible with an algebraic decay, but also with a saturation, i.e. the velocity tends to a constant value. We do not have enough large clusters

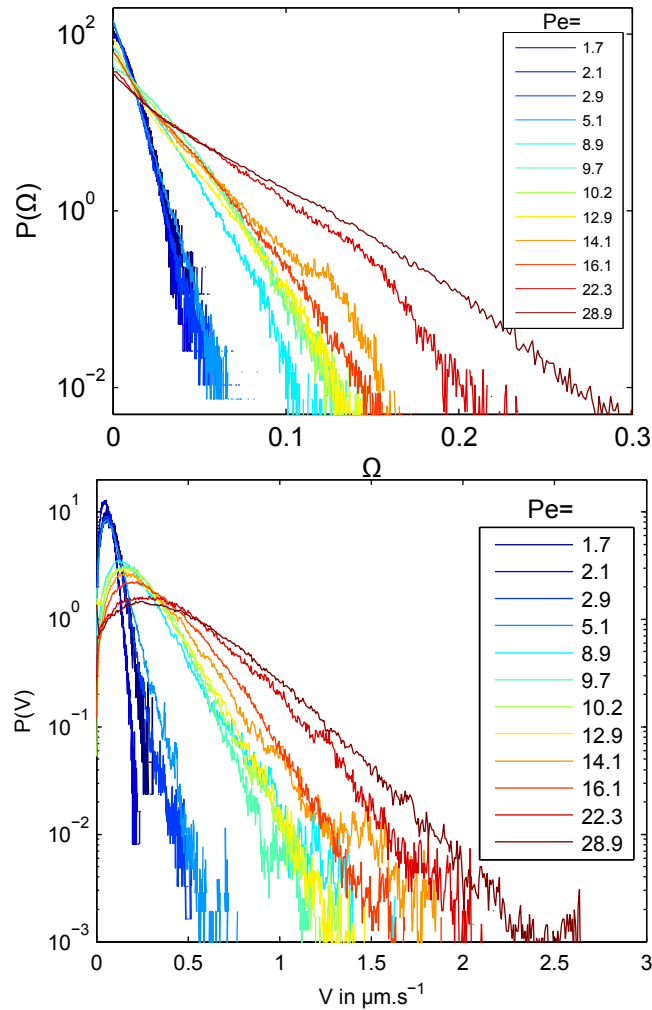


Figure 3.14: Probability density functions (PDFs) for rotational and translational velocities, for 12 different activities, and $\phi = 0.1$. The rotational and translational velocity PDFs decay exponentially.

to decide.

3.4.2 Velocities distribution

We compute the velocity distribution of clusters (see fig. 3.14). The rotational and translational velocity probability distribution functions (PDF) decay exponentially. This implies that the velocity are well defined, although their standard deviations have the same order of magnitude as the mean velocities themselves.

What is more interesting is that the translational velocity distribution of free colloids (not displayed here) has the same properties. Obviously, free colloids move at much higher velocities, and we cannot define rotational velocities for individual colloids. But the shape of the PDF is very similar, with an exponential decay. This hints at a very important

result: *the colloids that are inside clusters are the same*, in the sense that they have the same properties, *as those that are outside of clusters*. It is an important result, since we could imagine that two populations of swimmers exist, one with high velocities, and one with low velocities, very similarly to bacterial assemblies [79]. We could imagine slower particles would aggregate easily, while fast colloids would stay in the low density areas. The fact that the PDFs of translational velocities have the same exponential decay for clusters and isolated colloids, tends to indicate that there is no separation, and that colloids simply join and leave clusters without any activity or velocity selection.

3.4.3 Modeling velocities

The measured translation and rotation velocities are decreasing with cluster size, and increasing with Péclet number, that is the clusters move faster when the individual colloids move faster. This is not surprising since the driving “force²⁰” that moves the clusters comes from the individual swimmers. Increasing activity, implies an increase in the driving force.

To rationalize this slow decay of velocities, we use a very simple model. As the cluster size increases, the drag force felt by the cluster increases. The dynamical matrix can be written(see 2.7):

$$\begin{pmatrix} \mathbf{F} \\ \mathbf{M} \end{pmatrix} = \begin{pmatrix} A & B^T \\ B & C \end{pmatrix} \begin{pmatrix} \mathbf{u} \\ \boldsymbol{\Omega} \end{pmatrix}.$$

The B matrix gives the coupling between rotation and translation due to the possible non-chirality of the cluster. Very accurate measurement of the sizes of colloids inside the cluster, and a good theoretical understanding of the motility of assemblies of spheres could allow us to predict the exact values of A , B , and C . What is important, independently of the exact shape of the cluster, are the scaling relations adapted²¹ from Happel and Brenner [94]: $A \propto \eta R \sqrt{N}$ and $C \propto \eta R^3 N^{3/2}$, where N is the cluster size (the numbers of colloids inside the cluster) and R the colloid radius. The B coefficient depends non-trivially on cluster shape, we assume an non-chiral shape that leads to $N = 0$.

Translation velocities. The fact that the measured velocity of the clusters decreases with cluster size (see fig. 3.13), implies that the global

²⁰We should keep in mind that although individual swimmers swim without force, the interaction between swimmers can lead to an actual force exerted between the swimmer and an object, here the cluster.

²¹We take their scaling from the exact derivation of drag for a flat coin close to a surface.

propulsion force decreases with cluster size. We propose several possibilities to account for this effect, compatible with the measured velocities as a function of size.

1. Inside the cluster, we assume the orientations of the colloids as purely random, which would mean that the forces are also random. We assume that all colloids exert a force \mathbf{f}_i on the cluster whose orientation is random.

$$\mathbf{F} = \sum_{i=1}^N \mathbf{f}_i,$$

with \mathbf{F} the net force exerted on the cluster. For large N , $\mathbf{F} \sim \sqrt{N}\mathbf{f}_0$, from the central limit theorem by assuming a purely random independent orientation of the colloids. Of course, for small N , the net force would be higher. If we assume an exponential force distribution compatible with the exponential velocity distribution observed, $P(\mathbf{f}) = \alpha \frac{\mathbf{f}}{|\mathbf{f}|} \exp(-|\mathbf{f}|)$, with α a normalization parameter, we obtain a net force

$$\begin{aligned} \mathbf{F} &\underset{N \rightarrow 0}{\sim} f_0 N \\ \mathbf{F} &\underset{N \rightarrow \infty}{\sim} f_0 \sqrt{N} \end{aligned}$$

This predicts a saturation of the cluster translation velocity at high N , since

$$\begin{aligned} f_0 \sqrt{N} &\sim Au \\ u &\sim f_0 / \eta R, \end{aligned}$$

which is compatible with our observations.

2. Another possibility is that colloids inside the cluster lose their propulsion, owing to inter-colloid interactions and to fuel depletion. The propulsion force would then scale as $\sim n_0 \sqrt{N}$ for large clusters, the number of colloids at the periphery, n_0 giving a typical penetration length in colloids diameters. For small clusters, the force would be $\sim N$, since all colloids have enough access to fuel, since small clusters have only a periphery, and no interior. We can imagine a velocity behaving as:

$$v \sim \frac{f_0}{\eta R} \sqrt{\frac{N_0}{N} + 1},$$

where N_0 is the size of clusters affected by depletion²². This saturates

²²The minimum size at which clusters have an interior is 8 colloids.

for large sizes, again in qualitative agreement with our observations.

3. It is to be noted that experimentally, it is hard to make the difference between a velocity saturation, and simply a very slow decay. A theory giving a slow decay would be compatible with our observations.

Rotation velocities. The measured rotation velocities (see fig. 3.13) also increase with activity, which can be understood, as the driving force of each colloid increases with activity. The rotation velocity decreases with cluster size. To rationalize this slow decrease, we reuse, the two approaches previously studied. The rotational drag being always the same: $\mathbf{M} = C\boldsymbol{\Omega} \sim \eta R^3 N^{3/2} \boldsymbol{\Omega}$, the key factor is the motor of the rotation, that is the torque on the cluster. The two approaches give different resulting torque and thus different scaling for the rotational velocity.

1. Assuming random force orientations, the torque on the cluster is linked to the individual swimmer force by:

$$\mathbf{M} \sim \sum_{i=1}^N \mathbf{f}_0 \times \mathbf{r}_i,$$

Where \mathbf{r}_i is the position of colloid i with respect to the center of mass of the colloid. Then²³:

$$\mathbf{M} \sim \mathbf{f}_0 R N^{3/2}.$$

Since $\mathbf{M} = C\boldsymbol{\Omega} \sim \eta R^3 N^{3/2} \boldsymbol{\Omega}$, it yields:

$$\boldsymbol{\Omega} \sim \mathbf{f}_0 / \eta R^2.$$

2. The other approach neglect the activity of all colloids at the center, thus,

$$\begin{aligned} \mathbf{M} &\sim \sum_{i \in \text{periphery}} \mathbf{f}_0 \times \mathbf{r}_i \\ &\sim \mathbf{f}_0 \sqrt{N} \times R \sqrt{N} \\ &\sim R \mathbf{f}_0 N. \end{aligned}$$

Thus

$$\boldsymbol{\Omega} \sim \frac{\Omega_0}{\sqrt{N}},$$

²³A computation similar to that of the usual computation for moments of inertia, i.e. a continuum approximation of $\mathbf{M} \sim \sum_{i=1}^N \mathbf{f}_0 \times \mathbf{r}_i$, is: $\mathbf{M} \sim \int_0^{R\sqrt{N}} \frac{\pi}{R^2} u^2 \mathbf{f}_0$, that simplifies as the given formula.

again an algebraic decay, that is hard to differentiate experimentally from the simple saturation.

3.4.4 Other Dynamic

There are many other dynamical variables that we have not looked at. The lifetime of a cluster as a function of its size would be very interesting, as a way of characterizing what destroys the clusters, what causes cluster separation in smaller clusters. Indeed, although we understand how clusters form, we do not understand why their size remains constant over time. Fluctuations have to break the clusters, but it is hard to precisely understand how. Measuring the lifetime of clusters, that is the time between separations, would allow us to measure the dynamical matrix P_{kl} , the transition probability between clusters of size k and l . This would allow an understanding of which dynamical processes are in play in the formation/destruction of clusters.

A similar measurement would be the residence time of colloids inside clusters. Obviously, colloids at the center of large clusters stay longer inside a given cluster than those on the outside. However quantifying by how much would again allow insight at the mechanisms at play for cluster separation.

Similarly the orientation of colloids is a missing information. From our preliminary studies, some colloids that are about to leave are spinning very fast on themselves ($\Omega \sim 6\text{rad.s}^{-1}$). Could we correlate orientation fluctuations and cluster breaking?

3.5 Other Experiments and Models

During this thesis, the first experimental observation of collective behavior in a colloidal abiotic system have been performed. However, several experimental works have been published during the last three years, also showing collective behavior in abiotic systems, slightly different from our own, and which give interesting comparison points for our experiments. Comparing these to our results will help us answer the key question: *what are the physical ingredients necessary to observe the formation of clusters*. Several numerical and theoretical studies, whose models are very close to our own, or which give an interesting comparison point with our work, have also been published. In this section, I describe several recent papers. Since more than 40 papers specifically treating the matter of active particles have been published in 2013 alone, I will present only a very brief, review of articles focusing on those most closely related to our experimental system. Many articles, including interesting ones will not

be mentioned here, for want of room. A very brief recap is presented in Table 3.3.

3.5.1 Experimental contributions.

I first mention experimental works that are most closely related to our own. Special attention is paid to the possible mechanisms leading to the formation of clusters.

A first experiment, that unfortunately leaves more questions than it answers has been performed by Thutupalli *et al.* [125]. They study colloidal droplets of bromide inside an oil that does not mix with the aqueous colloids, but that reacts with it. The reaction on the colloid surface leads to propulsion owing to the Marangoni effect. Small clusters (~ 5 colloids) are observed, albeit only on short time scales as the fuel consumption is rather fast, on a ten minute scale at maximum. There is no proposed mechanism for the cluster formation, but local crowding is a plausible mechanism.

J. Palacci *et al.* published an experimental study [89] of an assembly of diffusiophoretic Janus particles, that are composed hematite (Fe_2O_3) and polymer Janus colloids. The fuel is also peroxide. An interesting property of the system is that the fuel consumption is done through a photocatalytic reaction, which could allow control through photo-patterning. The colloids are ferromagnetic, which allows control through magnetic fields. Dynamical clusters similar to ours do form in the system, and individual colloids have a random persistent motion. A notable feature is that the colloids are synthesized with remarkable monodispersity, creating nice, regularly crystalline clusters. The interparticle interaction is characterized, and an attractive interaction is observed, is interpreted in terms of diffusiophoretic attraction, and presented as the main cause for cluster aggregation. These experiments are similar to ours in many points, and indeed yield the same qualitative results for many aspects, such as dynamical properties. Quantitative comparisons still have to be made. The dynamic motion of clusters might be different, and the long term behavior of clusters over more than 10min is not known.

Another experimental contribution, by I. Buittoni *et al.* [126] studies Marangoni-effect driven Janus swimmers [127], powered by a local demixing of a binary subcritical fluid. Here, the authors show interaction between swimmers has no diffusiophoretic component. The interactions are then hard-spheres plus hydrodynamics. They observe colloidal clusters, similar to ours, and a striking feature is that they have the same average cluster size dependance as ours ($N^* \propto \text{Pe}$), although they have none of the ingredients we propose as an explanation. Indeed, while we

claim that phoretic attraction is the cause of cluster formation, leading to $N^* \propto Pe$, they experimentally rule out phoretic effects, and still observe the same dependance of cluster sizes.

The description of the proposed mechanism, supported by numerical simulations [128], allows a smooth transition towards numerical experiments.

3.5.2 Numerical simulations.

Many simulations of generic active particles have been performed, since the seminal works of Vicsek et al. [46]. Some are very generic describing active particles with minimal models, while some focus on a particular type of active particles, describing specifically bacterias, or even our Janus colloids.

A purely numerical study [55], by Fily *et al.* shows that clustering can occur in systems with purely repulsive interactions. Here the osmotic pressure of the surrounding gas of colloids is enough to ensure the cohesion of clusters. Their formation is done by an aggregation mechanism that is basically the following: when two swimmers collide, they repel themselves and decrease their velocity. This in turns means they have more chance to encounter another colloid. As the local density increases, each swimmer is hindered by all the swimmers in its vicinity, and its average velocity decreases, up to the point that its velocity relative to its neighbors becomes zero. A feature that is extremely similar to ours is the vanishing of the compressibility in the cluster phase. however, they observe a q^{-2} divergence, which tends to indicate there is still a difference. Also the clusters presented in this study all merge into a single cluster for long time scales.

Another numerical study, very detailed in the sense that it takes into account diffusiophoresis and hydrodynamics has been presented by I. Pagonabarag *et al.* at the 7th IDMRCS conference in 2013 [129], although yet unpublished, its main results are very interesting. Diffusiophoretic Janus microswimmers are modeled. They consume a chemorepellent in an asymmetric way, which propels them very much like the colloids used by Palacci *et al.*. The consumption of fuel is linked to propulsion, as mentioned in sec. 3.3.2. The formation of cluster is observed, but these clusters are different from ours in the sense that they are static (almost) and their size distribution of cluster is exponential.

As we have seen from both experiments and numerical simulations,

| Experiment | Proposed cause for cluster formation | Motile clusters? | global collapse? |
|---|--------------------------------------|------------------|------------------|
| Gold-Platinum Janus[17] | diffusiophoresis | yes | no |
| Hematite-Polymer Janus[89] | diffusiophoresis | yes | probably not |
| Thermal Janus[128, 126] | crowding decreases local velocity | yes (very slow) | yes |
| Marangoni swimmers[125] | ? | yes | ? |
| Diffusiophoretic swimmers (numeric)[130][129] | diffusiophoresis | no | no |
| Repulsive swimmers (numeric)[55] | crowding decreases local velocity | no | yes |
| Vicsek-like (numeric)[16][46] | explicit alignment | yes | depends |

Table 3.3: Summing up the main similarities and differences between this work and other experiments and simulations.

very similar behavior is observed with different proposed mechanisms. This either tells us that clustering is a general phenomenon, and that the similarities between our experiments are due to this general phenomenon, that the proposed explanations are simply facets of a generic theory, that remains to be discovered. For similarities in average cluster sizes, another possibility is that we are only probing short variations of N^* , which means we stay in the linear regime of N^* as a function of Péclet number. This questions the role of diffusiophoresis as the main cause of cluster formation in our experiments.

3.6 Conclusion

For the first time, collective behavior are observed at the colloidal scale, in model abiotic systems. The dynamical behavior of clusters is surprisingly rich, having very different time scales, and interesting spatial ordering.

We show in this chapter how powerful our experimental setup is, and what its limitations are, in terms of spatial and temporal resolution, that limit the available range of measurable time and space dynamics. We resolve quite well the positions of the particles over $\sim 5\text{min}$, with an accuracy of 200nm. We observe and quantify the static and dynamic behavior of clusters.

The Next step. As mentioned before, the most obvious and biggest impact experimental development we could have is the ability to observe the long-term behavior of the clusters, over a few hours rather than a few minutes.

We also want to characterize the dynamics of clusters that go beyond rotations and translations: what is their mean free path? what happens when they collide? How do they spontaneously break apart?

Can we do better to characterize the interparticle interaction?

Long term questions. How can we rationalize the power law distribution for the cluster sizes? Is it similar to critical phenomena?

We mentioned that the cluster phase has a diverging compressibility. How can we explain this? How can we measure it?

How does such a complex phase flow? Does it have a viscosity? This one should be fun as I'm betting density changes viscosity a lot, and very compressible fluids should be fun to play with. The low sound speeds imply that supersonic flows should be easy to observe.

Key ideas for this chapter

1. Clusters are ordered dense coherent ensembles of colloids moving around, rotating, exchanging colloids with other clusters, colliding and breaking apart over very different time scales.
2. The Keller-Segel description presents in good agreement with our experiments showing a linear increase of the average cluster size with activity.
3. A more detailed analysis shows that the cluster phase is less ordered than the passive solid phase and the active liquid phase; shows evidence of diverging compressibility, and has a power-law distribution of cluster sizes.
4. Rotation, and translation velocities are quantified; both decrease with increasing cluster size, and increase with activity. Quantitative data can help refine numerical experiments with realistic parameters.

Chapter 4

Sedimentation experiments

Colloidal systems have been used to prove experimentally major statistical mechanics predictions. From the existence of atoms, by the study of Brownian motion by Jean Perrin [131], to the direct observation of structure in glass transition [132, 133, 134], colloids have many advantages. They are large enough to be seen under a microscope, and small enough to feel thermal fluctuations. Their large size slows down dynamics such as crystallization or condensation so that they can be directly observed at the individual particle scale, which is impossible for atoms or molecules.

We would like to use all these characteristics to study, in an old-school classical thermodynamic fashion, the behavior of a far from equilibrium system. Sedimentation experiments have been used for a long time to probe the equation of state of colloidal systems. The main problem of classical thermodynamics (thermostatistics in this case might be better terminology [6]) is the problem of determining the state of a system undergoing a change under external constraints [7]. To describe the state of a thermodynamical system unequivocally, three intensive parameters, such as temperature, pressure, and density are enough¹. The relationship giving constraining the possible values of the intensive variables is called the equation of state (EOS):

$$f(P, T, \rho) = 0.$$

The existence of an equation of state implies equilibrium, or equilibrium-like behavior. In fact it implies stationarity, since the EOS has no time dependence, and the existence of a temperature requires the system to be at equilibrium, or since we can accept an effective temperature, to be in an equilibrium-like state.

For out of equilibrium, and far from equilibrium systems, equilibrium-

¹Depending on the nature of forces acting in the system, magnetization, charge density and many other parameters could be added. In simple cases, such as our own, T , P and ρ are enough to describe the system fully.

like state have been observed, for very dilute assemblies [64]. The persistent random walk of an isolated swimmer [66] or the exponential density distribution in a sedimentation experiment allow the definition of an effective temperature [64], for which the system obeys the fluctuation dissipation theorem.

After a short experimental description of the sedimentation experiments, we will focus on the measurement of density and pressure. Then, we present our “ideal gas thermometer” used to measure temperature in the system. After an in depth study of the dense phase, we conclude by showing that the system obeys an equation of state, compatible with a continuous phase transition between a low and high density phase.

4.1 Sedimentation experiments

For readers that have skipped the previous chapters, we remind that our active system [17] is purely abiotic, and uses phoretic effects to achieve self-propulsion [88]. The active particles we use are gold microspheres of radius $R = 1.1 \pm 1 \mu\text{m}$, with one half covered in platinum. When immersed in a hydrogen peroxide bath at volumetric concentrations C from 0 to $2 \cdot 10^{-4}$, the colloids become active. They behave as small batteries, disproportionation the peroxide into water and dissolved dioxygen. As they consume this fuel, they propel themselves at velocities from $1 \mu\text{m} \cdot \text{s}^{-1}$ to $15 \mu\text{m} \cdot \text{s}^{-1}$, the velocity increases as the concentration of fuel in the system increases. The interaction between the colloids are phoretic and hydrodynamic in nature (see sec. 3.2.3).

Following ideas put forward by Piazza *et al.* [135, 136] and Barrat *et al.* [137, 138], we study the sedimentation profiles of an assembly of colloids. Sedimentation experiments allow a measurement of the state of the system for continuously varying pressure. Indeed, in a sedimentation experiment, the density goes from 0 at the top of the system, to ρ_{max} at the bottom. Mechanical equilibrium imposes that the pressure at any given altitude z is equal to the effective mass² of all colloids above z . Thus measuring the density gives access to the pressure in the system. As the density is a positive, finite quantity, the pressure varies continuously and monotonically in the system.

To study the sedimentation of our active particle, the observation chamber is tilted by an angle $\theta \sim 10^{-3} \text{rad}$ creating a reduced gravity $g \sin \theta$. During one sedimentation experiment, about 10^6 Janus colloids sediment during one day into a 2D monolayer at the bottom of the observation chamber, a (6mm diameter, 8mm in height) cylindrical well, with a clear

²The effective mass of the system is its mass minus the mass of displaced water, to take into account Archimedes lift force.

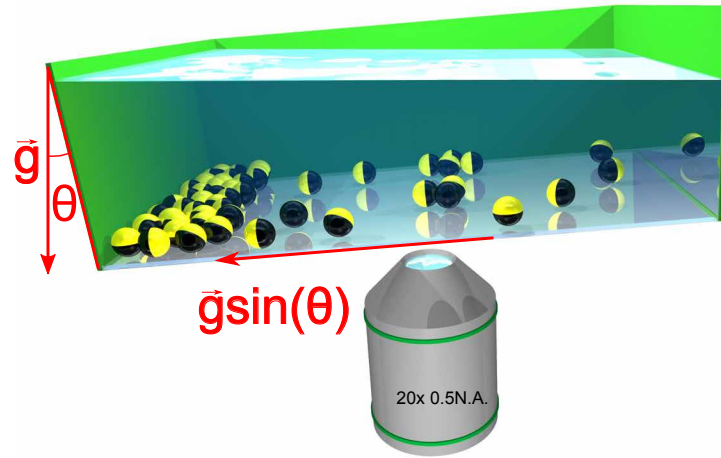


Figure 4.1: Schematics of a sedimentation experiment. The cell is tilted by a small angle $\theta \sim 10^{-3}$ rad, giving an effective gravity of order $\sim 10^{-2}$ m.s $^{-2}$. To control this tilt, we in fact tilt the whole microscope, by inserting paper sheets below it. The activity is controlled by modifying the amount of hydrogen peroxide in the system. We take films at all activities to measure the colloids velocities and the density profiles.

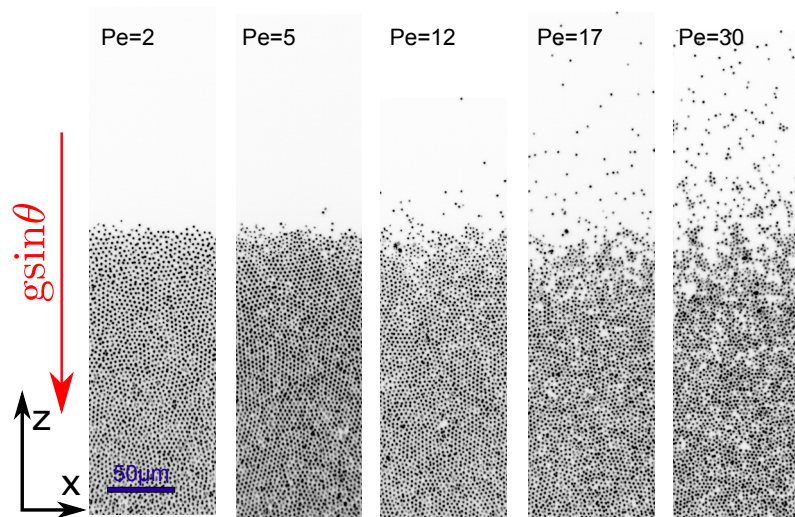


Figure 4.2: Sedimentation under effective gravity, for five different activities, measured by their Péclet Number. The interface between the dense phase and the gas widens with activity. Holes appear in the dense phase, allowing the motion of colloids, while its mean density increases. The scale bar is 50 μ m. See movie 9 in sup.mat.

bottom. We study the sedimentation in the direction parallel to the bottom plate of the observation chamber (see fig. 4.1). As mentioned before, this experiment is a way of continuously varying the pressure and the density along the z direction [136]. Tilting the cell is important to obtain an effective gravity much smaller than the standard gravity of $g = 9.81\text{m.s}^{-2}$. Indeed, the standard gravity yields a sedimentation length $l_g = \frac{mg}{k_B T} = 10\text{nm}$, where m is the mass of a colloid. With such a small sedimentation length, all colloids will be sedimented at the bottom of the observation chamber, without a possibility of measuring a sedimentation profile orthogonal to the cell surface.

To study the effect of activity on the sedimentation, we measure the density profiles at volumetric concentrations C in H_2O_2 from 0 to 2.10^{-4} . We study 21 different activities. After each increase in peroxide, we wait for 5 minutes to reach a stationary state inside the cell. Some resulting images are presented in fig 4.2. A classical way of studying phase transitions, is to use Clapeyron diagrams, or pressure-density profiles, that we display on fig. 4.3, and whose computation is presented below. All profiles, regardless of activity, show a low density zone at low pressure, and a high density solid at high pressure. The two zones are linked by a plateau, similar in aspect to the plateau of the classical Van der Waals liquid-gas transition [7]. However, this plateau is definitely not constant, which tends to exclude compatibility with a Maxwell construction [139, 7], and tends to indicate that the transition is a continuous phase transition.

4.2 From sedimentation profiles to osmotic pressure

From these images, we measure, as explained below, the density and osmotic pressure, that is the pressure exerted by the repeated chocs with the colloids³, and the temperature if it exists so as to compare our experiments with usual thermodynamics.

After recording a film, we measure particle positions and trajectories through time. We use standard detection and trajectory reconstruction algorithms [76].

To measure the area density, after measuring colloids positions, we perform a very basic form of coarse-graining the microscopic density by counting the number $n(x, z)$ of colloids in square boxes of side $l \sim 10\mu\text{m}$.

³In our two dimensional system, the pressure has units of force per unit length. The osmotic pressure is the force exerted on a line by the colloids. It is osmotic in that we do not take into account the fluid.

We compute the area density:

$$\phi(x, z) = \frac{n(x, z)\pi R^2}{l^2}.$$

And the number density:

$$\rho(x, z) = \frac{n(x, z)}{l^2}.$$

The size of discretization boxes is large when compared to colloid size, and has to be small when compared to the typical length scales for the density variation in order to get a proper coarse-graining of the density. While this is valid at high activities, since the density profiles vary over $\sim 100\mu\text{m}$, at the lowest activities this approach may fail, since the density changes brutally over $\sim 5\mu\text{m}$. The density profile $\phi(z)$ (z being the direction orthogonal to the interface) is computed by averaging in the x direction (parallel to the interface):

$$\rho(z) = \frac{1}{L} \int_0^L dx \rho(x, z).$$

We measure the pressure in a very simple way by assuming barometric equilibrium:

$$\Pi(z) = \Pi_0 + \frac{mg \sin \theta}{L^2} \int_0^L dx \int_z^L dz n(x, z), \quad (4.1)$$

where m is the average colloid mass, and $L = 350\mu\text{m}$ the size of the observation area, and Π_0 the pressure at the top of the observation cell. Factoring out the mean colloid mass requires that colloid the sedimentation is not affected by the polydispersity of colloids. While this is probably not the case in our system, we have to assume that this is a negligible effect. In order to compute the total pressure Π , we measure $\int_0^L dx \int_z^L dz n(x, z)$, by counting colloids; and Π_0 will be evaluated in the gas phase. We'll use the fact that in an ideal gas, Π_0 is the y-intercept of the $\frac{mg \sin \theta}{L^2} \int_0^L dx \int_z^L dz n(x, z)$ as a function of $\phi\rho$ curve. We will plot $\Pi(z)$ versus $\rho(z)$, to study the phase behavior of our active system. We are especially interested in the effect of activity on the sedimentation. This is why we describe in the next section how to use the $\Pi(z)$ versus $\rho(z)$ curves as a thermometer, that quantifies the effect of activity on the low density part of the sedimentation profiles.

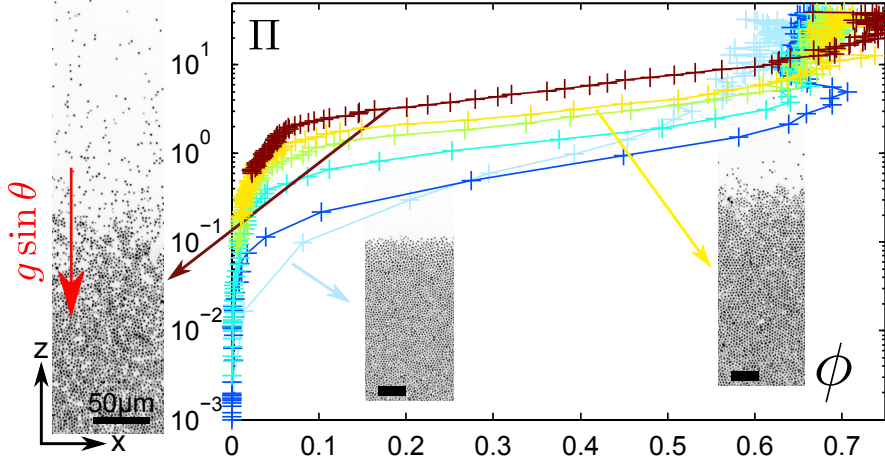


Figure 4.3: Sedimentation snapshots (left and inserts) : gravity causes a transition between a dense zone at the bottom of the observation area, and a low density gas phase at the top. Scale bars are $50 \mu\text{m}$. Osmotic pressure Π as a function of area density ϕ (right), for several activities (fuel peroxide volumetric concentration C from 0 to $2 \cdot 10^{-4}$). The osmotic pressure is measured from integration of the density profiles (see text). The transition pressure varies by one order of magnitude, and the density of the solid phase by 20%.

4.3 A thermal Gas phase.

In the most dilute part of the sample, which we define by $\phi < 5\%$, there are so few swimmers that the interaction between them becomes negligible. The osmotic pressure varies linearly with density (see fig 4.4), in agreement with the ideal gas model. The slope increases with activity, implying an effective temperature T_{eff} , that links the osmotic pressure and the number density:

$$\Pi = k_B T_{eff} \rho.$$

It is interesting to note that the low density limit of an active system behaves as an equilibrium system, while being very far from equilibrium [64]. Inspired by what is probably the oldest quantitative experiment in thermodynamics, the study of the thermoscope (a gas thermometer) by Galileo, at the end of the XVIth century, we use the gas phase as a thermometer to probe the activity of the system, i.e. by measuring T_{eff} . We first describe how we measure Π_0 . By counting colloids, we measure (see eq. 4.1) $\frac{1}{L^2} \int_0^L dx \int_z^L dz n(x, z) = (\Pi - \Pi_0) / mg \sin \theta$, where Π_0 is the pressure at the top of the cell, we define Π_0 as the y -intercept of the $(\Pi - \Pi_0) / mg \sin \theta$ as a function of ρ curve. This definition of Π_0 is used for the whole study and is valid even in the dense phase. We then measure T_{eff} up to a constant: $k_B T_{eff} / mg \sin \theta$. The effective temperature is a measure of the motility of individual microswimmers. Indeed, in the gas

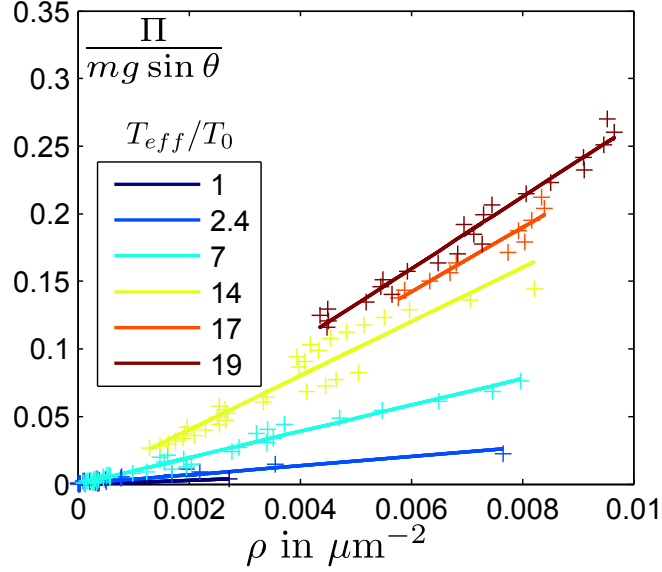


Figure 4.4: Ideal gas behavior of the active system at low density: Pressure versus area density for 6 different activities, and linear fits (lines). Π varies linearly with number density ρ , in good agreement with the ideal gas model. We measure the effective temperature T_{eff} from the shown linear fits to the data points (crosses), the values are given in the legend box in units of T_0 .

phase the lack of interparticle interactions implies that measuring the dynamical properties of particles gives the same result as the measure on individual isolated particles.

We must keep in mind that finding a ideal gas equation of state for the low density zone is not necessarily a sign of an usual equilibrium state⁴,

⁴Indeed, the linear relationship between Π and ρ is equivalent to saying that the density profile ρ decays exponentially. The sedimentation of active particles, has been studied for the case of bacterias, and is quite complicated[84]. The sedimentation profile

$$\rho(z) = \rho(0) \exp(-\kappa z),$$

where κ is the decay rate, is not determined simply by the Maxwellian expectation:

$$\kappa = -\frac{mg \sin \theta}{k_B T_{eff}},$$

as in the usual barometric equilibrium, with effective temperature, but by a more complex equation[62][140]:

$$\kappa \sim -\frac{v_s}{\tau_R} \frac{1}{(v^2 - v_s^2)},$$

where $v_s = \frac{mg \sin \theta}{6\pi\eta R} \sim 0.4 \mu\text{m.s}^{-1}$ is the sedimentation velocity due to the effective gravity, τ_R the rotational diffusion time, and v the translational active velocity of the colloids. This formula has been derived for the case of run and tumble bacterias with a tumbling rate $\alpha = 1/\tau_R$, but I think it is acceptable to extend its validity to the Janus microswimmers. Indeed, studies by Cates *et al.*[141] have shown that assuming that τ_R does not depend on v , implies an equivalence between tumbling bacterias and active swimmers that undergo rotational diffusion. In our case, $v_s \lesssim 0.4 \mu\text{m.s}^{-1}$; thus,

or even proof of a quasi equilibrium state, especially for low activities.

Another approach, complementary to this one is a kinetic approach. We could measure the kinetic pressure $p = m\rho(\mathbf{v} \cdot \mathbf{n})^2$, where \mathbf{n} is a vector normal to the surface on which we measure the pressure. This gives the pressure only in the gas phase, but is also a difficult quantity to compute for very low activities. The kinetic temperature is $k_B T_{eff}^c = m\langle v^2 \rangle$; measuring the kinetic temperature and kinetic pressure in the same way, that is directly from microscopic observation instead of averaged quantities, might allow an easier measurement of temperature. Since these measurements require ensemble averages, they are not very easy to compute, especially in the low density regions.

To conclude we use the low density gas phase as a thermometer, measuring effective temperature from⁵ $T_0 = 296\text{K}$, in the absence of activity, to $T_{eff} \sim 10^4\text{K}$ at maximal activity. We still have to be careful that the temperature we measure might be false for very low activities.

4.4 The dense phase.

At the high density limit, the system becomes solid. Owing to the polydispersity of the colloidal assembly, the solid phase is not crystalline, but rather glassy, as can be seen in the structure factor of the dense phase (see fig. 3.9).

However, activity changes the behavior of this solid phase in a non-trivial manner (See movie 8 in sup.mat.). The first and most obvious change is the fact that colloids are actually moving in the very dense assembly. This is due to the appearance of holes in the dense phase in which swimmers are more mobile than in the densest parts, and that somehow allow for the correlated motion of even the densest zones. Thus, the dense assembly is rather an active liquid than a solid, and sees correlated motion as in bacterial assemblies [113]. From now on I will call *dense phase* the high density assembly when the activity level does not matter; *solid phase* in the absence of activity and *active liquid phase* when active.

What is more surprising is a 20% increase in density from the passive to the highest activity solid. Indeed, while the mean nearest neighbor distance is $2.6\mu\text{m}$ in the absence of activity, it decreases to $2.2\mu\text{m}$ at

at high activity, since the propulsion velocity v is of order $5\mu\text{m}\cdot\text{s}^{-1}$, $\kappa \sim -\frac{v_s}{\tau_R v^2}$, thus the relationship between density decay and external gravity potential is linear, and we recover an equilibrium-like behavior. At low activity however, v_s and v are comparable, and the sedimentation decay is not linearly linked to the external potential, implying that the system is not in a Maxwell distribution.

⁵The T_0 is not measured by this experiment, but with a thermocouple, and T_{eff} is measured from this reference.

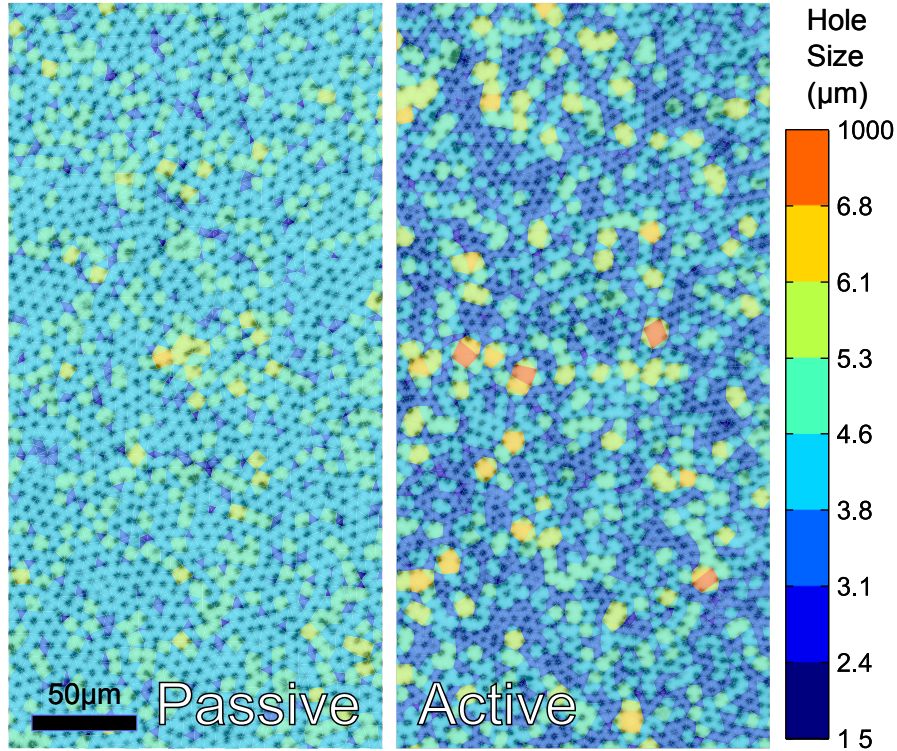


Figure 4.5: Images of the passive (left) and active dense phases. The passive phase is more ordered and less dense. The color overlay is a *hole size* map, that gives a measure of the local available space. The larger holes are larger in the active case, while small holes are smaller. While the average density increases with activity, the size of holes also increases. The scale bar is $50\mu\text{m}$. See movie 8 in sup.mat.

maximal activity. This effect may be due to the screening of the electrostatic repulsion (see sec. 3.2) between colloids caused by peroxide disproportionation. The maximum density of the active liquid phase increases accordingly ([17] and see Fig. 4.11).

This is surprising as, we usually think of density as increasing interactions, and thus decreasing the mobility of colloids. However, the density increase is coupled to an increase in the free space in the solid phase, that is the space the colloids are able to move through. The colloids get closer to each other, and at the same time, holes form, between clusters. To show this, we plot (see fig. 4.5) an image of the dense phase, with a “hole size” map overlay. The hole size is computed as follows : for each point in the plane, we compute the maximum distance between the three pairs of nearest neighbors. This map is drawn with transparency in order to see the colloids in the image below. The hole size increases with activity, as shown by the increase of the nearest neighbor standard deviation with effective temperature measured in the gas phase (fig. 4.7).

In the active liquid phase, the system dynamics is controlled by the

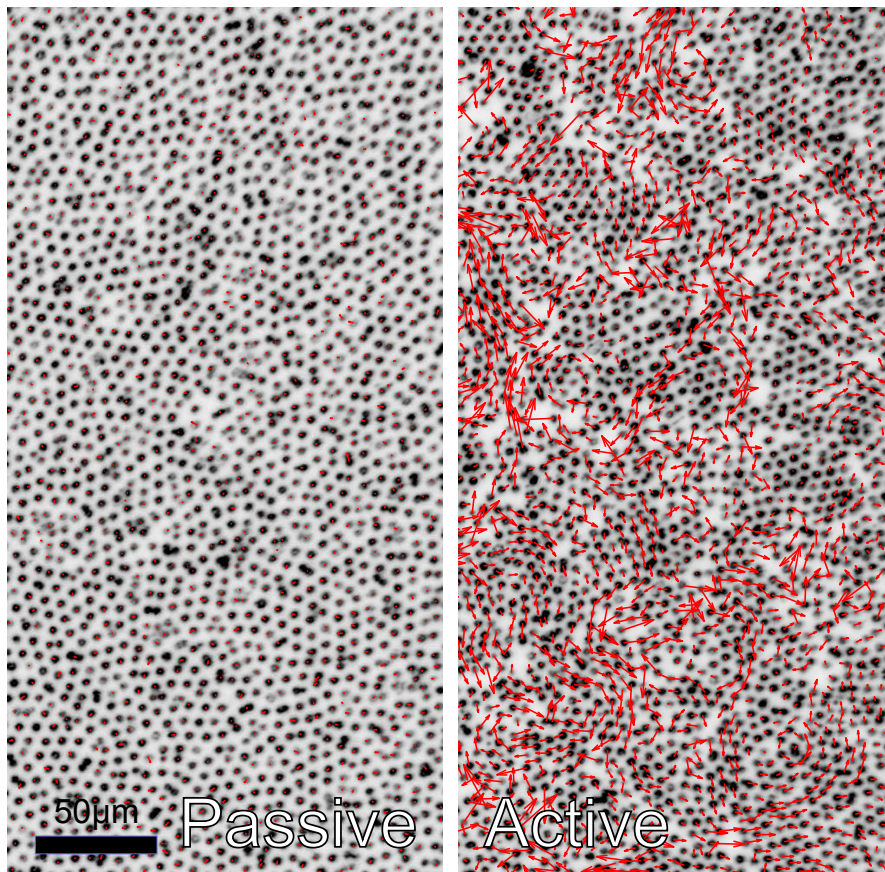


Figure 4.6: Images of the passive (left) and active dense phases. The passive phase is more ordered and less dense. Overlaid (red arrows) is a displacement map. The vectors correspond to the displacement of the colloids over 5s. The increase in displacement is huge, the displacement in the passive case are all below $.5\mu\text{m}$. The displacement follow the local structure of the active, the densest zones move in a correlated way. The scale bar is $50\mu\text{m}$. See movie 8 in sup.mat.

structure. Densely packed zones have correlated motion only, while disordered low density holes allow higher motion. We plot the displacement vector over 5s. The displacement of the colloids is orders of magnitude higher in the active solid when compared to the passive solid, which seems jammed [58]. Indeed using the same scale, the displacement vectors are hardly visible.

It is interesting to see that we can distinguish two different zones in the active liquid: the low density zones are very disordered zones, while the denser zones are more crystalline. While we have said that holes allow motion in the dense phase, on average, the displacement is the same in high and low density zones. The fastest colloids, with velocities $v \sim 5\mu\text{m}\cdot\text{s}^{-1}$, are always near holes, for they are the only zones that allow high displacement. However, because of the disorder, many colloids close to a hole are jammed and remain static over a few seconds until they reorient. In the densest zones, all colloids must move in the same direction, since there is no possible overlap (see fig 4.6 and sec. 3.2). Some of this very dense zones behave as clusters, and move within the dense phase with relatively velocities $v \sim 2\mu\text{m}\cdot\text{s}^{-1}$. The low density regions appear as defect zones in crystal, zones of low friction that allow the correlated motion of crystalline parts. These low density regions are constantly rearranging themselves, and dense zones can break apart and the newly created fault usually becomes a hole.

Preliminary experiments show that as the pressure increases, the density increases slightly, and the mobility of the particles is reduced, as the amount of free space decreases. Studying the behavior of this dense phase, and the transition from a jammed passive solid to an active liquid is a very novel type of phase transition that require further experimental and theoretical studies [57, 58].

4.4.1 Structure

To analyze the structure of the dense phase, we use the static structure factor $S(q)$, (see sec. 3.3.4). The structure factor is typical of glassy or liquid states, locally ordered, as can be seen by sharpness of the first few peaks, but without long range order, as can be seen by the decay of the peaks as $q \rightarrow \infty$. The cause of this lack of long-range order is twofold: the polydispersity plays a key role, but the activity also decreases the

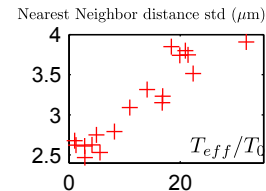


Figure 4.7: Standard deviation of the distance between nearest neighbors distribution, as a function of measured activity in the gas phase. The hole size increases with activity.

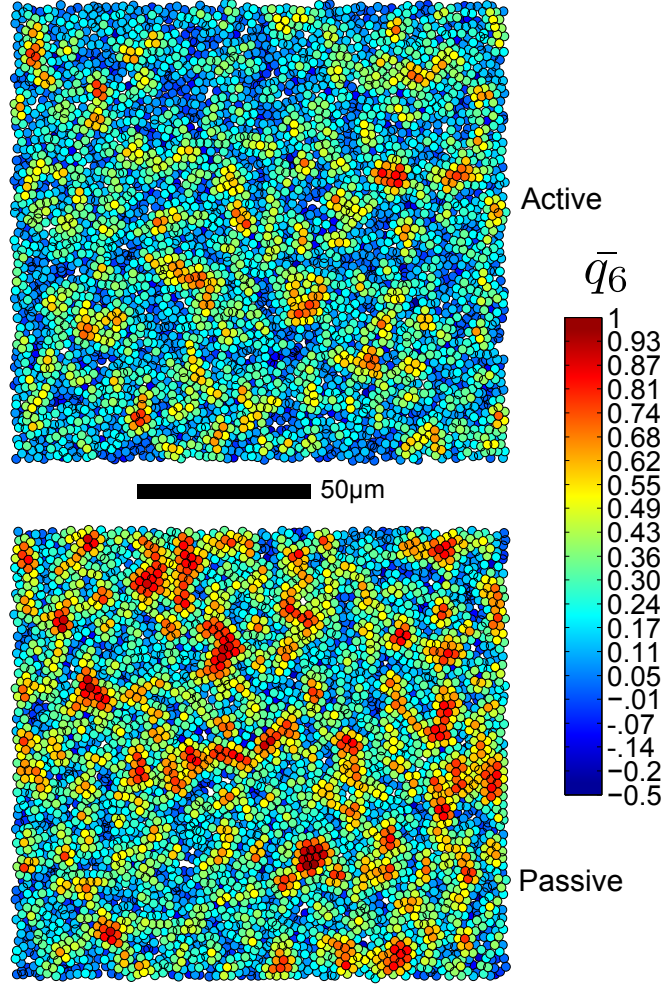


Figure 4.8: \bar{q}_6 map for the active (top) and passive (bottom) dense phases. Blue zones are disordered while red zones are highly ordered. The active liquid is more disordered than the passive solid phase.

ordering.

To better understand this, we use a measure of local order, the bond orientation parameter, defined for each colloid i :

$$q_6^i = \frac{1}{6} \sum_{j \in \mathcal{V}} \exp(-6i\pi\theta_{ij}),$$

where \mathcal{V} represents the i^{th} colloid nearest neighbors, and θ_{ij} is the angle $\widehat{\mathbf{r}_i - \mathbf{r}_j, \mathbf{e}_x}$. From this we define a real quantity:

$$\bar{q}_6^i = \text{Re} \left(\frac{1}{6} q_6^i \sum_{j \in \mathcal{V}} q_6^{j*} \right).$$

For each colloid, the \bar{q}_6 is equal to 1 if the local configuration is that of the compact hexagonal tiling, and can be negative if the neighbors are

really disordered. To compare our results with simulations, one has to be careful that polydispersity reduces the usual values of \bar{q}_6 . We also use a high magnification 60x objective to measure the positions of the particles with a higher accuracy.

From the \bar{q}_6 map (see fig. 4.8) we can see that the active phase is less ordered than the passive phase. An interesting thing is that even the highly ordered zones in the active dense phase are less ordered than their passive counterparts.

4.4.2 Conclusion

This dense active liquid phase has many interesting features, especially the fact that activity allows motion of colloids that would otherwise be jammed. The input of energy at the individual particle scale seems enough to break the structure of the dense phase, creating holes and defects that allow large-scale motion of colloids. Many interesting rheological properties need to be investigated.

4.5 Measuring an equation of state for an active system?

Now that we have characterized in details the low and high density limits of our system, we need to address a very important question: how does the system behave in-between. Can we describe all the intermediary states between the ideal gas and the dense phase?

The sedimentation experiment is ideal to study this question. As the density varies continuously and monotonically, so does the pressure. This could allow the reconstruction of an equation of state by plotting the osmotic pressure as a function of the area density.

We plot (see fig 4.11) the renormalized osmotic pressure $\Pi/\rho_{max}k_B T_{eff}$, the effective temperature is measured in the gas phase, with respect to the relative density ρ/ρ_{max} (see fig. 4.9). the inset shows the distribution of the same curves without the

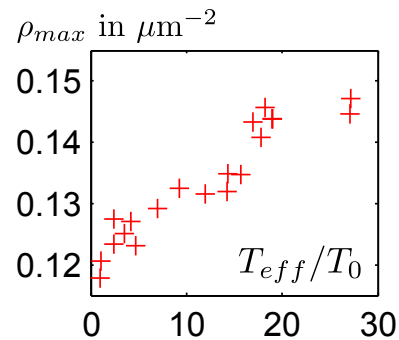


Figure 4.9: ρ_{max} in particles per square micrometer as a function of activity, measured by relative effective temperature T_{eff}/T_0 . The density in the solid phase increases almost linearly with effective temperature.

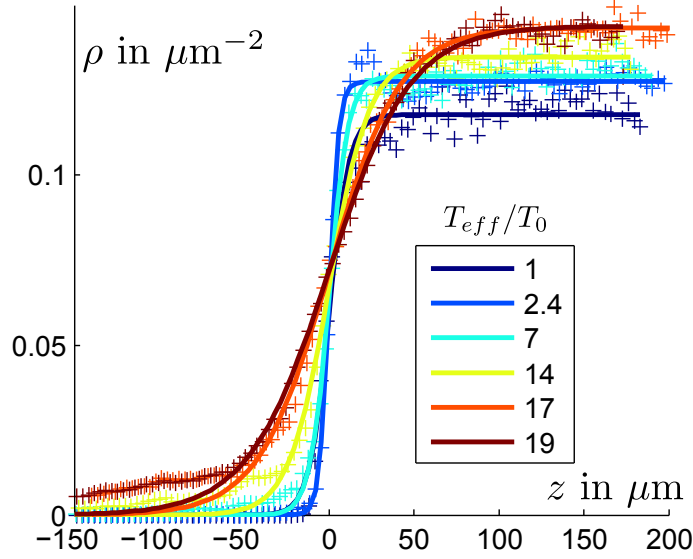


Figure 4.10: Experimental density profiles for 5 activities (crosses), and tanh fits to the data (continuous lines). The colors code the activity measured. The fits do not work very well in the low density region. The width of the interface increases with activity.

renormalization: $\Pi/k_B T_0$, where T_0 is the room temperature, the same for all experiments, as a function of ρ . To measure ρ_{max} , we fit the density profile $\rho(z)$ with a tanh profile (see fig. 4.10):

$$\rho(z) = \frac{1}{2} \rho_{max} (\tanh((z - z_0)/\xi) + 1),$$

z_0 representing the position of the gas-liquid interface, and ξ its width. The fit is acceptable, except in the low density region.

On fig. 4.11, the data from all 20 sedimentation profiles, obtained for different activities, collapses reasonably; the only curves whose collapse is questionable are the passive and lowest activity curves ($T_{eff}/T_0 < 3$). This could indicate that either our doubts on measuring temperatures at small activities are valid (see sec. 4.3) or simply that the nature of the transition changes between the simple passive hard-sphere transition and the active colloid phase transition, implying a different equation of state. Below a threshold effective temperature T_{eff}^0 , the transition would be a hard-sphere transition, while above this, it would become a the transition between an active gas and a high density active liquid, as we are observing.

The striking fact that all pressure-density curves collapse when renormalized, suggests that the active system, although far from equilibrium, follows an equation of state that depends linearly on the effective temperature. The range of effective temperature experimentally available is limited by bubble formation at high peroxide concentration, Different

transition regimes could occur at higher activity [124].

To investigate a possible equation of state for the system, we propose a heuristic equation of state:

$$\beta_{eff}\Pi/\rho_{max} = \frac{\rho/\rho_{max}}{(b\rho/\rho_{max} + 1)(1 - \rho/\rho_{max})^\alpha}.$$

With $\alpha = \frac{1}{2}$, and $b = 4$, this equation of state fits the data acceptably (except for low activity cases which have an equation of state closer to a hard sphere system), and is very different from the EOS proposed [109, 135] for hard disks :

$$\beta_{eff}\Pi/\rho_{max} = \frac{\rho/\rho_{max}}{(1 - \rho/\rho_{max})^2}.$$

The most striking differences are the divergence for the dense phase transition, with the exponent of the $1/(1-\rho/\rho_{max})$ changes from $-1/2$ to -2 . It may be due to the modification of the glass transition by activity [58, 59]. The term

$$(b.\rho/\rho_{max} + 1)^{-1}$$

is ad hoc, has no real physical justification, but is necessary to capture the medium-density behavior, in the range $0.05 < \rho/\rho_{max} < 0.5$.

The attentive reader might remark that we have mentioned in sec. 3.3.4 that the compressibility of the cluster phase (that is of the phase at intermediate densities) diverges. The experimental density profiles clearly do not show a divergence of compressibility for intermediate concentrations. This could be due to the inhomogeneity of the system, as the density varies sharply with respect to position. This leads to an inhomogeneous system, whose compressibility is not diverging. Indeed, a large volume is required to actually observe a divergence of the compressibility, while the cluster phase in our case is not larger than 100 μm . Further experiments could probe a system with slower density variations, by lowering the effective gravity.

This leads us to conclude that the density-transition from the ideal gas to the dense phase could follow an equation of state, even though we are very far from equilibrium. Moreover, this equation depends only linearly on the effective temperature. This is a very strong result, implying that the temperature measured from the gas phase is valid for all densities⁶,

⁶This is also compatible with a purely hard-disk transition, and an effective temperature that evolves with density following:

$$\beta_{eff}(\rho) = \beta_{eff}^{gas}(b\rho/\rho_{max} + 1)(1 - \rho/\rho_{max})^{\alpha-2}.$$

However, while formally equivalent, this conclusion is less physical. Indeed the temper-

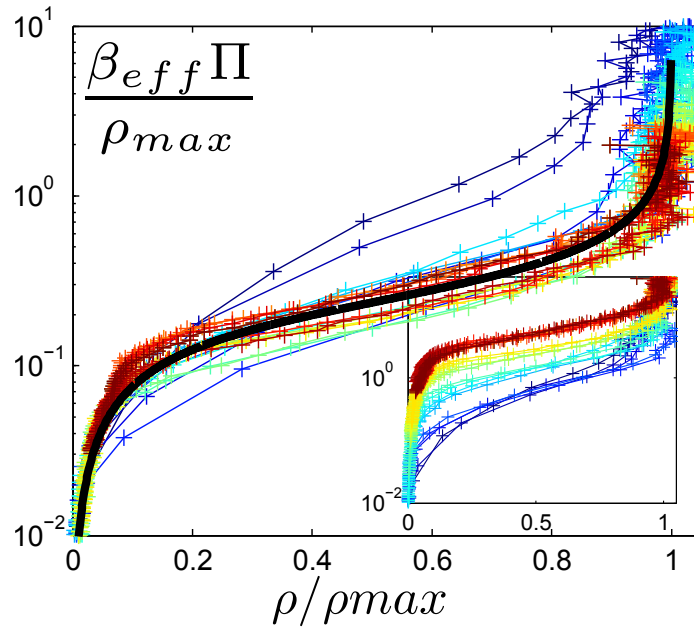


Figure 4.11: Equation of state for the active system : Rescaled osmotic pressure $\beta_{eff}\Pi/\rho_{max}$ as a function of normalized density ρ/ρ_{max} for all 21 sedimentation profiles, and solid density (ϕ_{max}) as a function of the effective temperature measured in the gas phase. The collapse for very different qualitative behavior, from low to very high activity, is compatible with an equilibrium-like phase transition, following an equation of state.

although the qualitative behavior is very different. A simple way to understand this is to postulate that the effective temperature, is not linked merely to the displacement of the particles – which changes with density – but directly to the energy dissipation by each particle, which is the actual parameter indicating how far from equilibrium the system is. The energy dissipation depends only on the rate of consumption of peroxide. This seems to indicate that swimmers immobilized inside the dense phase are consuming as much fuel as their free counterparts in the gas phase.

The success of a very simple thermodynamic model is very surprising, as thermodynamic is the science of equilibrium states, and our system is very far from equilibrium. For area densities higher than 10%, the system shows huge departure from equilibrium in the form of clusters and coordinated motion, and the dense active liquid also has properties that differ strongly from an equilibrium phase. The success of a quasi-equilibrium approach is again an evidence of the robustness of thermodynamics, and a small usual miracle of our everyday reductionist science.

ature goes to zero in the solid phase, while it should go to T_0 . I thus choose to assume a constant effective temperature in the sample. Maybe microscopic measurement could lead to a more accurate measurement of a local temperature.

4.6 Conclusion

The sedimentation experiment we presented is a very interesting way to probe the behavior of an assembly of Janus colloids. It allows a controlled and smooth evolution of the density and pressure. By using the gas phase as a thermometer, as a physicist of the 17th century, we can link the behavior of this intrinsically out of equilibrium system at all densities through an equation of state.

This is a very powerful result as it says that there is a phase transition, and this phase transition is continuous; and that the effective temperature, measured in the gas phase, is valid through all the range of densities.

The next step. Experimentally, a better control of the cell slope would be great, as well as long term tracking to follow the behavior of the solid phase, to measure a microscopic temperature and pressure.

Long term questions. The dense phase is probably the most interesting feature to investigate further. The relationship between the structure of the dense active liquid phase and its dynamic, that is the individual and collective motion of colloids is hard to determine. There is no obvious correlation between the velocity or the mean displacement of the colloids and local order parameters, such as density, \bar{q}_6 , nearest neighbor distance etc... The mean square displacement is very hard to measure, since the slowest colloids move very slowly, and measuring a MSD requires large displacements to be significant. The polydispersity of the colloids adds to the difficulty, by creating disordered zones, and density fluctuations, even in the absence of activity.

The spontaneous motion in the active fluid is reminiscent of negative viscosity active bacterial fluids [113], that show tangential stress in the absence of external shear. In a fluid-mechanics description the behavior of the dense phase is very far from that of a Newtonian fluid. It is thus interesting to investigate further the behavior of this dense active assembly under external stress. Can we imagine a rheometer⁷ that can probe efficiently the properties of this system? Does our system have a viscosity? a compressibility modulus?

⁷Something of a mix between [9] and [28] comes in mind.

Key ideas for this chapter

1. Cool use of sedimentation experiments to probe the phase behavior of our system
2. Low density ideal gas phase used as a thermometer.
3. High density active liquid with heterogeneous motion, transitions to jamming at low activity.
4. Continuous phase transition controlled by a simple equation of state, using the effective temperature measured in the gas.

Conclusion

During the past three years, I've developed an experiment aiming at finding the key elements causing collective behavior in assemblies of active particles. Although the experiments were performed on a colloidal abiotic system, the aim of the experiments is to give hints, on very different systems, from ant colonies, herds of sheep, flights of birds to bacterial assemblies. By using a statistical physics approach, I was able to characterize the collective effects in an assembly of gold-platinum Janus active colloids at both the microscopic and macroscopic level. We do not yet have a comprehensive picture allowing us to understand the key elements of collective effects, but this work is a small step towards a better understanding of how the interplay between activity and interactions creates collective effects.

One notable achievement of this thesis perhaps easy to overlook, is the fact that we were able to observe collective effects. This is not obvious at all, and many active systems, with interactions, do not lead to collective behavior. The main collective effect exhibited by our system is the formation of clusters that undergo directed motion. They probably have no polar ordering, which is coherent with our understanding of microscopic interactions as being mostly apolar for this system.

At the microscopic level, the dynamics of clusters are very rich, with particle exchange, cluster fusions, spontaneous breaking, and the quantitative measurements we perform will be compared to simulations and other similar experiments, to find the basic elements causing the collective behavior.

At the macroscopic level, the thermodynamic properties of the assembly of colloids are linked by an equation of state, using an effective temperature measured in the dense phase. The existence of an equation of state is already a surprise, pointing to the strength of thermodynamics ideas, that seem to be valid well beyond equilibrium.

I'd like to finish by pointing out possible next directions for this project, and the next questions it should try to answer. Maybe the most important question to validate the work that has already been done but not very exciting otherwise is the characterization of interparticle

interactions. Their measurement should enable us to describe accurate quantitative predictions for the collective behavior in the system. As optical tweezers experiments have failed, it might be possible to pin one of our Janus colloid onto an AFM tip, and then to approach another Janus and measure the exerted force with the AFM. While tricky to calibrate, it could give extremely accurate measurements.

The most interesting question, opening very rich possibilities is the study of the flowing of active matter. It surely is a fluid with very rich rheology. Moreover, and that in itself is motivation enough, the motion of an active fluid is already nice to watch, and the complications, the patterns introduced by external constraints might beautiful⁸. Building a rheometer for active fluids will probably be very fun; and although a direct measurement of forces is very difficult, microrheology approaches with tracers can be used.

⁸I'd very much like to see turbulent flows or high Reynolds instabilities of active matter.

Bibliography

- [1] A. Czirok, I. M. Janosi, and J. O. Kessler, “Bioconvective dynamics: dependence on organism behaviour,” *Journal of Experimental Biology*, vol. 203, no. 21, p. 3345–3354, 2000. [Online]. Available: <http://jeb.biologists.org/content/203/21/3345.short> 10, 38
- [2] T. J. Rudge, F. Federici, P. J. Steiner, A. Kan, and J. Haseloff, “Cell polarity-driven instability generates self-organized, fractal patterning of cell layers,” *ACS Synthetic Biology*, May 2013. [Online]. Available: <http://dx.doi.org/10.1021/sb400030p> 10, 36
- [3] P.-S. d. Laplace and A.-L. d. Lavoisier, *Mémoire sur la chaleur, lu à l’Académie royale des sciences, le 28 juin 1783, par Mrs Lavoisier et de La Place,...* Paris: Impr. royale, 1783. 11
- [4] J.-B.-J. Fourier, *Théorie analytique de la chaleur, par M. Fourier.* Paris: F. Didot père et fils, 1822. [Online]. Available: <http://gallica.bnf.fr/ark:/12148/bpt6k1045508v> 11
- [5] C. Truesdell, *The tragicomical history of thermodynamics, 1822-1854.* New York: Springer-Verlag, 1980. 11
- [6] ———, *Rational thermodynamics.* New York: Springer-Verlag, 1984. 11, 123
- [7] H. B. Callen and H. B. Callen, *Thermodynamics and an introduction to thermostatistics.* New York: Wiley, 1985. 12, 123, 126
- [8] J.-P. Hansen and I. McDonald, *Theory of Simple Liquids*, 3rd ed. Academic Press Inc, Feb. 2006. 12, 102, 106
- [9] L. Angelani, R. Di Leonardo, and G. Ruocco, “Self-starting micro-motors in a bacterial bath,” *Phys. Rev. Lett.*, vol. 102, no. 4, p. 048104, Jan. 2009. 12, 139
- [10] J. N. Wilking, V. Zaburdaev, M. D. Volder, R. Losick, M. P. Brenner, and D. A. Weitz, “Liquid transport facilitated by channels in bacillus subtilis biofilms,” *Proceedings of the National Academy of*

- Sciences*, vol. 110, no. 3, pp. 848–852, Jan. 2013, PMID: 23271809. [Online]. Available: <http://www.pnas.org/content/110/3/848> 12, 29
- [11] M. C. Marchetti, J. F. Joanny, S. Ramaswamy, T. B. Liverpool, J. Prost, M. Rao, and R. A. Simha, “Hydrodynamics of soft active matter,” *Reviews of Modern Physics*, vol. 85, no. 3, pp. 1143–1189, Jul. 2013. [Online]. Available: <http://link.aps.org/doi/10.1103/RevModPhys.85.1143> 26, 29, 30, 35, 42, 52
- [12] T. Vicsek and A. Zafeiris, “Collective motion,” *Physics Reports*, vol. 517, no. 3-4, pp. 71–140, Aug. 2012. [Online]. Available: <http://linkinghub.elsevier.com/retrieve/pii/S0370157312000968> 26, 39
- [13] K. Duke, *Bedtime*. London: Methuen Children’s, 1986. 26
- [14] P. M. Chaikin and T. C. Lubensky, *Principles of condensed matter physics*. Cambridge; New York, NY, USA: Cambridge University Press, 1995. 27, 84, 102, 105
- [15] J. L. Silverberg, M. Bierbaum, J. P. Sethna, and I. Cohen, “Collective motion of humans in mosh and circle pits at heavy metal concerts,” *Physical Review Letters*, vol. 110, no. 22, p. 228701, May 2013. [Online]. Available: <http://link.aps.org/doi/10.1103/PhysRevLett.110.228701> 28, 33
- [16] T. Vicsek and A. Zafeiris, “Collective motion,” *Physics Reports*, vol. 517, no. 3-4, pp. 71–140, Aug. 2012. [Online]. Available: <http://linkinghub.elsevier.com/retrieve/pii/S0370157312000968> 29, 40, 41, 121
- [17] I. Theurkauff, C. Cottin-Bizonne, J. Palacci, C. Ybert, and L. Bocquet, “Dynamic clustering in active colloidal suspensions with chemical signaling,” *Physical Review Letters*, vol. 108, no. 26, p. 268303, Jun. 2012. [Online]. Available: <http://link.aps.org/doi/10.1103/PhysRevLett.108.268303> 29, 121, 124, 131
- [18] J. D. Murray, *Mathematical biology. II*. New York: Springer, 2003. 29, 35, 101
- [19] V. Narayan, S. Ramaswamy, and N. Menon, “Long-lived giant number fluctuations in a swarming granular nematic,” *Science*,

- vol. 317, no. 5834, p. 105–108, 2007. [Online]. Available: <http://www.sciencemag.org/content/317/5834/105.short> 29
- [20] R. Kemkemer, V. Teichgräber, S. Schrank-Kaufmann, D. Kaufmann, and H. Gruler, “Nematic order-disorder state transition in a liquid crystal analogue formed by oriented and migrating amoeboid cells,” *The European Physical Journal E*, vol. 3, no. 2, pp. 101–110, Oct. 2000. [Online]. Available: <http://link.springer.com/article/10.1007/s101890070023> 29
- [21] T. J. Pitcher, A. E. Magurran, and J. I. Edwards, “Schooling mackerel and herring choose neighbours of similar size,” *Marine Biology*, vol. 86, no. 3, pp. 319–322, Jun. 1985. [Online]. Available: <http://link.springer.com/article/10.1007/BF00397518> 30, 31
- [22] M. Ballerini, N. Cabibbo, R. Candelier, A. Cavagna, E. Cisbani, I. Giardina, V. Lecomte, A. Orlandi, G. Parisi, and A. Procaccini, “Interaction ruling animal collective behavior depends on topological rather than metric distance: Evidence from a field study,” *Proceedings of the National Academy of Sciences*, vol. 105, no. 4, p. 1232–1237, 2008. [Online]. Available: <http://www.pnas.org/content/105/4/1232.short> 30, 33
- [23] C. Hohenegger and M. J. Shelley, “Stability of active suspensions,” *Physical Review E*, vol. 81, no. 4, p. 046311, Apr. 2010. [Online]. Available: <http://link.aps.org/doi/10.1103/PhysRevE.81.046311> 30, 94
- [24] A. Baskaran and M. C. Marchetti, “Statistical mechanics and hydrodynamics of bacterial suspensions,” *Proceedings of the National Academy of Sciences*, vol. 106, no. 37, p. 15567, 2009. 30, 35
- [25] D. Saintillan and M. J. Shelley, “Emergence of coherent structures and large-scale flows in motile suspensions,” *Journal of The Royal Society Interface*, vol. 9, no. 68, pp. 571–585, Jul. 2012, PMID: 21865254. [Online]. Available: <http://rsif.royalsocietypublishing.org/content/9/68/571> 30, 94
- [26] H.-S. Niwa, “Self-organizing dynamic model of fish schooling,” *Journal of Theoretical Biology*, vol. 171, no. 2, pp. 123–136, Nov. 1994. [Online]. Available: <http://www.sciencedirect.com/science/article/pii/S0022519384712185> 31
- [27] E. Altshuler, O. Ramos, Y. Núñez, J. Fernández, A. J. Batista-Leyva, and C. Noda, “Symmetry breaking in escaping ants.”

- The American Naturalist*, vol. 166, no. 6, pp. 643–649, Dec. 2005, ArticleType: research-article / Full publication date: December 2005 / Copyright © 2005 The University of Chicago. [Online]. Available: <http://www.jstor.org/stable/10.1086/498139> 31
- [28] J. Deseigne, O. Dauchot, and H. Chaté, “Collective motion of vibrated polar disks,” *Physical Review Letters*, vol. 105, no. 9, Aug. 2010. [Online]. Available: <http://link.aps.org/doi/10.1103/PhysRevLett.105.098001> 31, 42, 139
- [29] V. Narayan, N. Menon, and S. Ramaswamy, “Nonequilibrium steady states in a vibrated-rod monolayer: tetratic, nematic, and smectic correlations,” *Journal of Statistical Mechanics: Theory and Experiment*, vol. 2006, no. 01, pp. P01005–P01005, Jan. 2006. [Online]. Available: <http://stacks.iop.org/1742-5468/2006/i=01/a=P01005?key=crossref.338b94ad3e09bf3c31539a9e5cf8bfe3> 31
- [30] J. Deseigne, S. Léonard, O. Dauchot, and H. Chaté, “Vibrated polar disks: spontaneous motion, binary collisions, and collective dynamics,” *Soft Matter*, vol. 8, no. 20, pp. 5629–5639, May 2012. [Online]. Available: <http://pubs.rsc.org/en/content/articlelanding/2012/sm/c2sm25186h> 31, 42
- [31] L. Henderson, “On the fluid mechanics of human crowd motion,” *Transportation Research*, vol. 8, no. 6, pp. 509–515, Dec. 1974. [Online]. Available: <http://www.sciencedirect.com/science/article/pii/0041164774900276> 33
- [32] M. Moussaïd, N. Perozo, S. Garnier, D. Helbing, and G. Theraulaz, “The walking behaviour of pedestrian social groups and its impact on crowd dynamics,” *PLoS ONE*, vol. 5, no. 4, p. e10047, Apr. 2010. [Online]. Available: <http://dx.doi.org/10.1371/journal.pone.0010047> 33
- [33] F. Mondada, L. Gambardella, D. Floreano, S. Nolfi, J.-L. Deneubourg, and M. Dorigo, “The cooperation of swarm-bots: physical interactions in collective robotics,” *IEEE Robotics Automation Magazine*, vol. 12, no. 2, pp. 21–28, 2005. 33
- [34] R. Beckers, O. E. Holland, and J.-L. Deneubourg, “From local actions to global tasks: Stigmergy and collective robotics,” in *Artificial life IV*, vol. 181, 1994, p. 189. [Online]. Available: <http://www.eecs.harvard.edu/~rad/courses/cs266-fall04/papers/beckers-alife94.pdf> 33
- [35] G. Egan, *Schild’s ladder*. London: Gollancz, 2008. 33

- [36] ———, *Diaspora*. London: Gollancz, 2008. 33
- [37] I. Banks and I. Banks, *The hydrogen sonata*, 1st ed., ser. Culture novel. New York: Orbit, 2012. 33
- [38] M. Masár and E. Pajorová, “Cooperative mobile agents for swarm behavior simulation,” in *Cooperative Design, Visualization, and Engineering*, ser. Lecture Notes in Computer Science, Y. Luo, Ed. Springer Berlin Heidelberg, Jan. 2013, no. 8091, pp. 128–136. [Online]. Available: http://link.springer.com/chapter/10.1007/978-3-642-40840-3_19 33
- [39] V. Schaller, C. Weber, C. Semmrich, E. Frey, and A. R. Bausch, “Polar patterns of driven filaments,” *Nature*, vol. 467, no. 7311, pp. 73–77, Sep. 2010. [Online]. Available: <http://www.nature.com/nature/journal/v467/n7311/abs/nature09312.html> 35
- [40] K. Drescher, R. E. Goldstein, N. Michel, M. Polin, and I. Tuval, “Direct measurement of the flow field around swimming microorganisms,” *Physical Review Letters*, vol. 105, no. 16, p. 168101, Oct. 2010. [Online]. Available: <http://link.aps.org/doi/10.1103/PhysRevLett.105.168101> 35, 94
- [41] E. PURCELL, “LIFE AT LOW REYNOLDS-NUMBER,” *AMERICAN JOURNAL OF PHYSICS*, vol. 45, no. 1, pp. 3–11, 1977. 35
- [42] E. Lauga and T. R. Powers, “The hydrodynamics of swimming microorganisms,” *Reports on Progress in Physics*, vol. 72, no. 9, p. 096601, Sep. 2009. [Online]. Available: <http://iopscience.iop.org/0034-4885/72/9/096601> 35, 78
- [43] J. Saragosti, V. Calvez, N. Bournaveas, A. Buguin, P. Silberzan, and B. Perthame, “Mathematical description of bacterial traveling pulses,” *PLoS Comput Biol*, vol. 6, no. 8, p. e1000890, Aug. 2010. [Online]. Available: <http://dx.doi.org/10.1371/journal.pcbi.1000890> 37
- [44] J. Palacci, B. Abécassis, C. Cottin-Bizonne, C. Ybert, and L. Bocquet, “Colloidal motility and pattern formation under rectified diffusiophoresis,” *Physical Review Letters*, vol. 104, no. 13, p. 138302, Apr. 2010. [Online]. Available: <http://link.aps.org/doi/10.1103/PhysRevLett.104.138302> 37
- [45] M. Ibele, T. E. Mallouk, and A. Sen, “Schooling behavior of light-powered autonomous micromotors in water,” *Angewandte*

- Chemie International Edition*, vol. 48, no. 18, p. 3308–3312, 2009. [Online]. Available: <http://onlinelibrary.wiley.com/doi/10.1002/anie.200804704/abstract> 37, 84
- [46] T. Vicsek, A. Czirok, E. Ben-Jacob, I. Cohen, and O. Shochet, “Novel type of phase transition in a system of self-driven particles,” *Phys. Rev. Lett.*, vol. 75, no. 6, p. 1226–1229, Aug. 1995. 39, 40, 120, 121
- [47] A. Czirók, H. E. Stanley, and T. Vicsek, “Spontaneously ordered motion of self-propelled particles,” *Journal of Physics A: Mathematical and General*, vol. 30, p. 1375, 1997. 39
- [48] H. Chaté, F. Ginelli, G. Grégoire, and F. Raynaud, “Collective motion of self-propelled particles interacting without cohesion,” *Physical Review E*, vol. 77, no. 4, p. 046113, Apr. 2008. [Online]. Available: <http://link.aps.org/doi/10.1103/PhysRevE.77.046113> 39, 40
- [49] G. Grégoire and H. Chaté, “Onset of collective and cohesive motion,” *Physical Review Letters*, vol. 92, no. 2, p. 025702, Jan. 2004. [Online]. Available: <http://link.aps.org/doi/10.1103/PhysRevLett.92.025702> 39, 40
- [50] V. Lobaskin and M. Romenskyy, “Collective dynamics in systems of active brownian particles with dissipative interactions,” *Physical Review E*, vol. 87, no. 5, p. 052135, May 2013. [Online]. Available: <http://link.aps.org/doi/10.1103/PhysRevE.87.052135> 40
- [51] M. Aldana, H. Larralde, and B. Vázquez, “On the emergence of collective order in swarming systems: a recent debate,” *International Journal of Modern Physics B*, vol. 23, no. 18, pp. 3661–3685, Jul. 2009. [Online]. Available: <http://www.worldscientific.com/doi/abs/10.1142/S0217979209053552?journalCode=ijmpb> 40
- [52] G. Baglietto and E. V. Albano, “Finite-size scaling analysis and dynamic study of the critical behavior of a model for the collective displacement of self-driven individuals,” *Physical Review E*, vol. 78, no. 2, p. 021125, Aug. 2008. [Online]. Available: <http://link.aps.org/doi/10.1103/PhysRevE.78.021125> 40
- [53] F. Ginelli, F. Peruani, M. Bär, and H. Chaté, “Large-scale collective properties of self-propelled rods,” *Physical Review Letters*, vol. 104, no. 18, p. 184502, May 2010. [Online]. Available: <http://link.aps.org/doi/10.1103/PhysRevLett.104.184502> 40

- [54] J. Galanis, D. Harries, D. L. Sackett, W. Losert, and R. Nossal, “Spontaneous patterning of confined granular rods,” *Physical Review Letters*, vol. 96, no. 2, p. 028002, Jan. 2006. [Online]. Available: <http://link.aps.org/doi/10.1103/PhysRevLett.96.028002> 40
- [55] Y. Fily and M. C. Marchetti, “Athermal phase separation of self-propelled particles with no alignment,” *arXiv:1201.4847*, Jan. 2012. [Online]. Available: <http://arxiv.org/abs/1201.4847> 40, 42, 110, 120, 121
- [56] D. Grossman, I. S. Aranson, and E. B. Jacob, “Emergence of agent swarm migration and vortex formation through inelastic collisions,” *New Journal of Physics*, vol. 10, no. 2, p. 023036, Feb. 2008. [Online]. Available: <http://iopscience.iop.org/1367-2630/10/2/023036> 41, 42
- [57] Y. Fily, S. Henkes, and M. C. Marchetti, “Freezing and phase separation of self-propelled disks,” *arXiv preprint arXiv:1309.3714*, 2013. [Online]. Available: <http://arxiv.org/abs/1309.3714> 42, 133
- [58] L. Berthier and J. Kurchan, “Non-equilibrium glass transitions in driven and active matter,” *Nature Physics*, vol. 9, no. 5, pp. 310–314, May 2013. [Online]. Available: <http://www.nature.com/nphys/journal/v9/n5/full/nphys2592.html> 42, 133, 137
- [59] S. Henkes, Y. Fily, and M. C. Marchetti, “Active jamming: Self-propelled soft particles at high density,” *Physical Review E*, vol. 84, no. 4, p. 040301, 2011. [Online]. Available: <http://pre.aps.org/abstract/PRE/v84/i4/e040301> 42, 137
- [60] E. Bertin, M. Droz, and G. Grégoire, “Boltzmann and hydrodynamic description for self-propelled particles,” *Physical Review E*, vol. 74, no. 2, p. 022101, Aug. 2006. [Online]. Available: <http://link.aps.org/doi/10.1103/PhysRevE.74.022101> 42
- [61] J. Toner and Y. Tu, “Flocks, herds, and schools: A quantitative theory of flocking,” *Physical Review E*, vol. 58, no. 4, p. 4828, 1998. [Online]. Available: http://pre.aps.org/abstract/PRE/v58/i4/p4828_1 42
- [62] J. Tailleur and M. E. Cates, “Statistical mechanics of interacting run-and-tumble bacteria,” *Physical Review Letters*, vol. 100, no. 21, p. 218103, May 2008. [Online]. Available: <http://link.aps.org/doi/10.1103/PhysRevLett.100.218103> 43, 129
- [63] A. Baskaran and M. C. Marchetti, “Hydrodynamics of self-propelled hard rods,” *Physical Review E*, vol. 77, no. 1, p. 011920,

2008. [Online]. Available: <http://pre.aps.org/abstract/PRE/v77/i1/e011920> 43
- [64] J. Palacci, C. Cottin-Bizonne, C. Ybert, and L. Bocquet, "Sedimentation and effective temperature of active colloidal suspensions," *Physical Review Letters*, vol. 105, no. 8, Aug. 2010. [Online]. Available: <http://link.aps.org/doi/10.1103/PhysRevLett.105.088304> 45, 51, 75, 84, 86, 89, 100, 101, 124, 128
- [65] W. F. Paxton, P. T. Baker, T. R. Kline, Y. Wang, T. E. Mallouk, and A. Sen, "Catalytically induced electrokinetics for motors and micropumps," *Journal of the American Chemical Society*, vol. 128, no. 46, pp. 14 881–14 888, Nov. 2006. [Online]. Available: <http://dx.doi.org/10.1021/ja0643164> 45, 46, 73, 94, 95
- [66] J. Howse, R. Jones, A. Ryan, T. Gough, R. Vafabakhsh, and R. Golestanian, "Self-motile colloidal particles: From directed propulsion to random walk," *Physical Review Letters*, vol. 99, no. 4, Jul. 2007. [Online]. Available: <http://link.aps.org/doi/10.1103/PhysRevLett.99.048102> 45, 49, 75, 84, 86, 89, 124
- [67] G. Miño, T. E. Mallouk, T. Darnige, M. Hoyos, J. Dauchet, J. Dunstan, R. Soto, Y. Wang, A. Rousselet, and E. Clement, "Enhanced diffusion due to active swimmers at a solid surface," *Physical Review Letters*, vol. 106, no. 4, p. 048102, Jan. 2011. [Online]. Available: <http://link.aps.org/doi/10.1103/PhysRevLett.106.048102> 46
- [68] W. F. Paxton, K. C. Kistler, C. C. Olmeda, A. Sen, S. K. Angelo, Y. Cao, T. E. Mallouk, P. E. Lammert, and V. H. Crespi, "Catalytic nanomotors: autonomous movement of striped nanorods," *J. Am. Chem. Soc.*, vol. 126, no. 41, p. 13424–13431, 2004. 46, 75
- [69] R. Laocharoensuk, J. Burdick, and J. Wang, "Carbon-nanotube-induced acceleration of catalytic nanomotors," *ACS Nano*, vol. 2, no. 5, pp. 1069–1075, May 2008. [Online]. Available: <http://dx.doi.org/10.1021/nm800154g> 46
- [70] S. Michelin, E. Lauga, and D. Bartolo, "Spontaneous autophoretic motion of isotropic particles," *arXiv:1211.6935*, Nov. 2012. [Online]. Available: <http://arxiv.org/abs/1211.6935> 46
- [71] D. V. Goia and E. Matijevi, "Tailoring the particle size of monodispersed colloidal gold," *Colloids and Surfaces A: Physicochemical and Engineering Aspects*, vol. 146, no. 1-3, p. 139–152, 1999. 47

- [72] B. Abécassis, C. Cottin-Bizonne, C. Ybert, A. Ajdari, and L. Bocquet, “Boosting migration of large particles by solute contrasts,” *Nature Materials*, vol. 7, no. 10, pp. 785–789, Aug. 2008. [Online]. Available: http://74.125.155.132/scholar?q=cache:6BFwe_aKnIsJ:scholar.google.com/+Abecassis+et+al,+Nature+Materials,+2008&hl=fr&as_sdt=0,5 52, 96
- [73] J. L. Anderson and D. C. Prieve, “Diffusiophoresis: Migration of colloidal particles in gradients of solute concentration,” *Separation & Purification Reviews*, vol. 13, no. 1, pp. 67–103, 1984. [Online]. Available: <http://www.tandfonline.com/doi/abs/10.1080/03602548408068407 54>
- [74] J. L. Anderson, “Colloid transport by interfacial forces,” *Annual Review of Fluid Mechanics*, vol. 21, no. 1, p. 61–99, 1989. 54, 95, 96, 100
- [75] C. Bendicks, “Improved 3-d particle tracking velocimetry with colored particles,” *Journal of Signal and Information Processing*, vol. 02, no. 02, pp. 59–71, 2011. [Online]. Available: <http://www.scirp.org/journal/PaperDownload.aspx?DOI=10.4236/jsip.2011.22009 59>
- [76] J. C. Crocker and D. G. Grier, “Methods of digital video microscopy for colloidal studies,” *Journal of colloid and interface science*, vol. 179, no. 1, p. 298–310, 1996. [Online]. Available: <http://crocker.seas.upenn.edu/CrockerGrier1996b.pdf 59, 62, 126>
- [77] T.-W. Su, L. Xue, and A. Ozcan, “High-throughput lensfree 3D tracking of human sperms reveals rare statistics of helical trajectories,” *Proceedings of the National Academy of Sciences*, vol. 109, no. 40, pp. 16 018–16 022, Feb. 2012. [Online]. Available: <http://www.pnas.org/content/109/40/16018 61>
- [78] A. V. Mikheev and V. M. Zubtsov, “Enhanced particle-tracking velocimetry (EPTV) with a combined two-component pair-matching algorithm,” *Measurement Science and Technology*, vol. 19, no. 8, p. 085401, Aug. 2008. [Online]. Available: <http://stacks.iop.org/0957-0233/19/i=8/a=085401?key=crossref.74ec5e97919ac0bd54a3ebfb7bb354a1 61>
- [79] V. A. Martinez, R. Besseling, O. A. Croze, J. Tailleur, M. Reufer, J. Schwarz-Linek, L. G. Wilson, M. A. Bees, and W. C. K. Poon, “Differential dynamic microscopy: A high-throughput method for characterizing the motility of microorganisms,” *Biophysical Journal*,

- vol. 103, no. 8, pp. 1637–1647, Oct. 2012. [Online]. Available: [http://www.cell.com/biophysj/abstract/S0006-3495\(12\)00972-1](http://www.cell.com/biophysj/abstract/S0006-3495(12)00972-1) 63, 91, 103, 115
- [80] L. Wilson, V. Martinez, J. Schwarz-Linek, J. Tailleur, G. Bryant, P. Pusey, and W. Poon, “Differential dynamic microscopy of bacterial motility,” *Physical Review Letters*, vol. 106, no. 1, Jan. 2011. [Online]. Available: <http://link.aps.org/doi/10.1103/PhysRevLett.106.018101> 63
- [81] M. Reufer, V. A. Martinez, P. Schurtenberger, and W. C. K. Poon, “Differential dynamic microscopy for anisotropic colloidal dynamics,” *Langmuir*, vol. 28, no. 10, pp. 4618–4624, Mar. 2012. [Online]. Available: <http://pubs.acs.org/doi/abs/10.1021/la204904a> 63
- [82] R. Cerbino and V. Trappe, “Differential dynamic microscopy: Probing wave vector dependent dynamics with a microscope,” *Physical Review Letters*, vol. 100, no. 18, p. 188102, May 2008. [Online]. Available: <http://link.aps.org/doi/10.1103/PhysRevLett.100.188102> 63
- [83] P. D. Kaplan, V. Trappe, and D. A. Weitz, “Light-scattering microscope,” *Applied Optics*, vol. 38, no. 19, pp. 4151–4157, Jul. 1999. [Online]. Available: <http://ao.osa.org/abstract.cfm?URI=ao-38-19-4151> 63
- [84] W. C. K. Poon, “From clarkia to escherichia and janus: the physics of natural and synthetic active colloids,” *arXiv e-print*, Jun. 2013, proceedings of the International School of Physics "Enrico Fermi", Course CLXXXIV "Physics of Complex Colloid", eds. C. Bechinger, F. Sciortino and P. Zihlerl, IOS, Amsterdam: SIF, Bologna (2013), pp. 317-386. [Online]. Available: <http://arxiv.org/abs/1306.4799> 63, 74, 78, 88, 129
- [85] Y. Wang, R. M. Hernandez, D. J. Bartlett, J. M. Bingham, T. R. Kline, A. Sen, and T. E. Mallouk, “Bipolar electrochemical mechanism for the propulsion of catalytic nanomotors in hydrogen peroxide solutions,” *Langmuir*, vol. 22, no. 25, pp. 10 451–10 456, Dec. 2006. [Online]. Available: <http://dx.doi.org/10.1021/la0615950> 73, 75, 77
- [86] S. Fournier-Bidoz, A. C. Arsenault, I. Manners, and G. A. Ozin, “Synthetic self-propelled nanorotors,” *Chemical Communications*, no. 4, pp. 441–443, Jan. 2005. [Online]. Available: <http://pubs.rsc.org/en/content/articlelanding/2005/cc/b414896g> 73

- [87] P. Dhar, T. M. Fischer, Y. Wang, T. E. Mallouk, W. F. Paxton, and A. Sen, "Autonomously moving nanorods at a viscous interface," *Nano Letters*, vol. 6, no. 1, pp. 66–72, Jan. 2006. [Online]. Available: <http://pubs.acs.org/doi/abs/10.1021/nl052027s> 73, 89
- [88] J. L. Moran and J. D. Posner, "Electrokinetic locomotion due to reaction-induced charge auto-electrophoresis," *Journal of Fluid Mechanics*, vol. 680, pp. 31–66, Jun. 2011. [Online]. Available: http://www.journals.cambridge.org/abstract_S0022112011001327 74, 76, 93, 95, 100, 124
- [89] J. Palacci, S. Sacanna, A. P. Steinberg, D. J. Pine, and P. M. Chaikin, "Living crystals of light-activated colloidal surfers," *Science*, vol. 339, no. 6122, pp. 936–940, Jan. 2013. [Online]. Available: <http://www.sciencemag.org/cgi/doi/10.1126/science.1230020> 75, 119, 121
- [90] W. M. Haynes, D. R. Lide, and B. , *CRC handbook of chemistry and physics: a ready-reference book of chemical and physical data*. Boca Raton, Fla.; London: CRC, 2012. 76
- [91] E. Lauga, "Les houches 2012 lecture notes." [Online]. Available: <http://maeresearch.ucsd.edu/lauga/references/leshouches12.pdf> 78
- [92] L. D. Landau and E. M. Lifshitz, *Fluid mechanics*. Amsterdam: Elsevier/Butterworth-Heinemann, 2004. 78
- [93] A. T. Chwang and T. Y. Wu, "Hydromechanics of low-reynolds-number flow. part 2. singularity method for stokes flows," *J. Fluid Mech*, vol. 67, no. Part 4, p. 787, 1975. [Online]. Available: <http://journals.cambridge.org/production/action/cjoGetFulltext?fulltextid=373308> 78, 79
- [94] J. Happel and H. Brenner, *Low Reynolds Number Hydrodynamics: with special applications to particulate media*, 1st ed. Springer, Aug. 1973. 78, 115
- [95] J. D. Jackson, *Classical electrodynamics*. New York: Wiley, 1999. 79
- [96] L. Durlofsky, J. F. Brady, and G. Bossis, "Dynamic simulation of hydrodynamically interacting particles," *Journal of Fluid Mechanics*, vol. 180, pp. 21–49, 1987. 79
- [97] T. Ishikawa and T. Yamaguchi, "Shear-induced fluid-tracer diffusion in a semidilute suspension of spheres," *Physical*

- Review E*, vol. 77, no. 4, Apr. 2008. [Online]. Available: <http://link.aps.org/doi/10.1103/PhysRevE.77.041402> 79
- [98] R. Golestanian, T. B. Liverpool, and A. Ajdari, “Designing phoretic micro-and nano-swimmers,” *New Journal of Physics*, vol. 9, p. 126, 2007. 79, 100
- [99] R. Huang, I. Chavez, K. M. Taute, B. Lukić, S. Jeney, M. G. Raizen, and E.-L. Florin, “Direct observation of the full transition from ballistic to diffusive brownian motion in a liquid,” *Nature Physics*, vol. 7, no. 7, pp. 576–580, Jul. 2011. [Online]. Available: <http://www.nature.com/nphys/journal/v7/n7/full/nphys1953.html> 84
- [100] J. Palacci, “Manipulation of colloids by osmotic forces,” Ph.D. dissertation, Université Claude Bernard - Lyon I, Oct. 2010. [Online]. Available: <http://tel.archives-ouvertes.fr/tel-00597477> 88
- [101] R. Di Leonardo, D. Dell’Arciprete, L. Angelani, and V. Iebba, “Swimming with an image,” *Physical Review Letters*, vol. 106, no. 3, p. 038101, Jan. 2011. [Online]. Available: <http://link.aps.org/doi/10.1103/PhysRevLett.106.038101> 90
- [102] K. Martens, L. Angelani, R. Leonardo, and L. Bocquet, “Probability distributions for the run-and-tumble bacterial dynamics: An analogy to the lorentz model,” *The European Physical Journal E*, vol. 35, no. 9, Sep. 2012. [Online]. Available: http://epje.epj.org/index.php?option=com_article&access=standard&Itemid=129&url=/articles/epje/abs/2012/09/10189_2012_Article_9761/10189_2012_Article_9761.html 92
- [103] J. G. Berryman, “Definition of dense random packing,” *Advances in the Mechanics and the Flow of Granular Materials*, edited by M. Shahinpoor (Trans-Tech, Clausthal, Germany, 1983), vol. 1, p. 1–18, 1983. 93
- [104] E. Helfand, H. L. Frisch, and J. L. Lebowitz, “Theory of the two- and One-Dimensional rigid sphere fluids,” *The Journal of Chemical Physics*, vol. 34, no. 3, pp. 1037–1042, Mar. 1961. [Online]. Available: http://jcp.aip.org/resource/1/jcpsa6/v34/i3/p1037_s1?isAuthorized=no 93
- [105] M. Clusel, E. I. Corwin, A. O. N. Siemens, and J. Brujić, “A ‘granocentric’ model for random packing of jammed emulsions,” *Nature*, vol. 460, no. 7255, pp. 611–615, Jul. 2009. [Online]. Available: <http://www.nature.com/nature/journal/v460/n7255/full/nature08158.html> 93

- [106] A. Mulero, I. Cachadiña, and J. Solana, “The equation of state of the hard-disc fluid revisited,” *Molecular Physics*, vol. 107, no. 14, pp. 1457–1465, 2009. [Online]. Available: <http://www.tandfonline.com/doi/abs/10.1080/00268970902942250> 93
- [107] M. López de Haro, A. Santos, and S. B. Yuste, “Simple equation of state for hard disks on the hyperbolic plane,” *The Journal of Chemical Physics*, vol. 129, no. 11, pp. 116 101–116 101–2, Sep. 2008. [Online]. Available: http://jcp.aip.org/resource/1/jcpsa6/v129/i11/p116101_s1 93
- [108] T. Boublík, “Equation of state of hard disk and 2D convex bodies,” *Molecular Physics*, vol. 109, no. 12, pp. 1575–1580, 2011. [Online]. Available: <http://www.tandfonline.com/doi/abs/10.1080/00268976.2011.573508> 93
- [109] W. R. Smith and D. Henderson, “Analytical representation of the percus-yevick hard-sphere radial distribution function,” *Molecular Physics: An International Journal at the Interface Between Chemistry and Physics*, vol. 19, no. 3, p. 411, 1970. 93, 137
- [110] J. S. Guasto, K. A. Johnson, and J. P. Gollub, “Oscillatory flows induced by microorganisms swimming in two dimensions,” *Physical Review Letters*, vol. 105, no. 16, p. 168102, Oct. 2010. [Online]. Available: <http://link.aps.org/doi/10.1103/PhysRevLett.105.168102> 94
- [111] J. Leach, H. Mushfique, R. d. Leonardo, M. Padgett, and J. Cooper, “An optically driven pump for microfluidics,” *Lab on a Chip*, vol. 6, no. 6, pp. 735–739, May 2006. [Online]. Available: <http://pubs.rsc.org/en/content/articlelanding/2006/lc/b601886f> 94
- [112] D. Saintillan and M. J. Shelley, “Instabilities and pattern formation in active particle suspensions: Kinetic theory and continuum simulations,” *Physical Review Letters*, vol. 100, no. 17, p. 178103, Apr. 2008. [Online]. Available: <http://link.aps.org/doi/10.1103/PhysRevLett.100.178103> 94
- [113] H. H. Wensink, J. Dunkel, S. Heidenreich, K. Drescher, R. E. Goldstein, H. Löwen, and J. M. Yeomans, “Meso-scale turbulence in living fluids,” *Proceedings of the National Academy of Sciences*, vol. 109, no. 36, pp. 14 308–14 313, Apr. 2012, PMID: 22908244. [Online]. Available: <http://www.pnas.org/content/109/36/14308> 94, 130, 139

- [114] A. Sokolov, I. Aranson, J. Kessler, and R. Goldstein, “Concentration dependence of the collective dynamics of swimming bacteria,” *Physical Review Letters*, vol. 98, no. 15, Apr. 2007. [Online]. Available: <http://link.aps.org/doi/10.1103/PhysRevLett.98.158102> 94
- [115] L. Petitjean, M. Reffay, E. Grasland-Mongrain, M. Poujade, B. Ladoux, A. Buguin, and P. Silberzan, “Velocity fields in a collectively migrating epithelium,” *Biophysical journal*, vol. 98, no. 9, p. 1790–1800, 2010. 99
- [116] E. F. Keller and L. A. Segel, “Initiation of slime mold aggregation viewed as an instability,” *Journal of Theoretical Biology*, vol. 26, no. 3, p. 399–415, 1970. 99, 100
- [117] M. Brenner, L. Levitov, and E. Budrene, “Physical mechanisms for chemotactic pattern formation by bacteria,” *Biophysical Journal*, vol. 74, no. 4, p. 1677–1693, 1998. 99
- [118] J. L. Moran, P. M. Wheat, and J. D. Posner, “Locomotion of electrocatalytic nanomotors due to reaction induced charge autoelectrophoresis,” *Physical Review E*, vol. 81, no. 6, p. 065302, Jun. 2010. [Online]. Available: <http://link.aps.org/doi/10.1103/PhysRevE.81.065302> 100
- [119] J.-L. Barrat and J.-P. Hansen, *Basic Concepts for Simple and Complex Liquids*. Cambridge University Press, Mar. 2003. 102, 106
- [120] C. B. Barber, D. P. Dobkin, and H. Huhdanpaa, “The quickhull algorithm for convex hulls,” *ACM Trans. Math. Softw.*, vol. 22, no. 4, p. 469–483, Dec. 1996. [Online]. Available: <http://doi.acm.org/10.1145/235815.235821> 108
- [121] G. Bisson, “Algorithmique des graphes,” Ecole des Mines de Nancy, Tech. Rep., 2010. [Online]. Available: <http://www.normalesup.org/~bisson/tea/pepites-graph.pdf> 109
- [122] S. Dasgupta, C. H. Papadimitriou, and U. V. Vazirani, *Algorithms*. Boston: McGraw-Hill Higher Education, 2008. 109
- [123] S. Ebbens, R. A. L. Jones, A. J. Ryan, R. Golestanian, and J. R. Howse, “Self-assembled autonomous runners and tumblers,” *Physical Review E*, vol. 82, no. 1, p. 015304, Jul. 2010. [Online]. Available: <http://link.aps.org/doi/10.1103/PhysRevE.82.015304> 110

- [124] G. S. Redner, M. F. Hagan, and A. Baskaran, “Structure and dynamics of a phase-separating active colloidal fluid,” *Physical Review Letters*, vol. 110, no. 5, p. 055701, Jan. 2013. [Online]. Available: <http://link.aps.org/doi/10.1103/PhysRevLett.110.055701> 110, 137
- [125] S. Thutupalli, R. Seemann, and S. Herminghaus, “Swarming behavior of simple model squirmers,” *New Journal of Physics*, vol. 13, no. 7, p. 073021, Jul. 2011. [Online]. Available: <http://stacks.iop.org/1367-2630/13/i=7/a=073021?key=crossref.81eae01f6973b3eea70282ef7213e2aa> 119, 121
- [126] I. Buttinoni, J. Bialké, F. Kümmel, H. Löwen, C. Bechinger, and T. Speck, “Dynamical clustering and phase separation in suspensions of self-propelled colloidal particles,” *Physical Review Letters*, vol. 110, no. 23, p. 238301, Jun. 2013. [Online]. Available: <http://link.aps.org/doi/10.1103/PhysRevLett.110.238301> 119, 121
- [127] G. Volpe, I. Buttinoni, D. Vogt, H.-J. Kümmerer, and C. Bechinger, “Microswimmers in patterned environments,” *Soft Matter*, vol. 7, no. 19, pp. 8810–8815, Sep. 2011. [Online]. Available: <http://pubs.rsc.org/en/content/articlelanding/2011/sm/c1sm05960b> 119
- [128] J. Bialké, H. Löwen, and T. Speck, “Microscopic theory for the phase separation of self-propelled repulsive disks,” *EPL (Europhysics Letters)*, vol. 103, no. 3, p. 30008, Aug. 2013. [Online]. Available: <http://iopscience.iop.org/0295-5075/103/3/30008> 120, 121
- [129] I. Pagonabarraga, “7th IDMRCS presentation, barcelona, 2013.” 120, 121
- [130] F. Alarcón and I. Pagonabarraga, “Spontaneous aggregation and global polar ordering in squirmer suspensions,” *Journal of Molecular Liquids*, vol. 185, pp. 56–61, Sep. 2013. [Online]. Available: <http://www.sciencedirect.com/science/article/pii/S0167732212004552> 121
- [131] J. Perrin, F. Perrin, and F. Perrin, *Les atomes*. Alcan, 1913. 123
- [132] P. N. Pusey and W. van Meegen, “Observation of a glass transition in suspensions of spherical colloidal particles,” *Physical Review Letters*, vol. 59, no. 18, pp. 2083–2086, Nov. 1987. [Online]. Available: <http://link.aps.org/doi/10.1103/PhysRevLett.59.2083> 123

- [133] E. R. Weeks, J. C. Crocker, A. C. Levitt, A. Schofield, and D. A. Weitz, “Three-dimensional direct imaging of structural relaxation near the colloidal glass transition,” *Science*, vol. 287, no. 5453, pp. 627–631, Jan. 2000, PMID: 10649991. [Online]. Available: <http://www.sciencemag.org/content/287/5453/627> 123
- [134] L. Berthier, G. Biroli, J.-P. Bouchaud, L. Cipelletti, D. E. Masri, D. L’Hôte, F. Ladieu, and M. Pierno, “Direct experimental evidence of a growing length scale accompanying the glass transition,” *Science*, vol. 310, no. 5755, pp. 1797–1800, Dec. 2005, PMID: 16357256. [Online]. Available: <http://www.sciencemag.org/content/310/5755/1797> 123
- [135] R. Piazza, T. Bellini, and V. Degiorgio, “Equilibrium sedimentation profiles of screened charged colloids: A test of the hard-sphere equation of state,” *Physical Review Letters*, vol. 71, no. 25, pp. 4267–4270, Dec. 1993. [Online]. Available: <http://link.aps.org/doi/10.1103/PhysRevLett.71.4267> 124, 137
- [136] R. Piazza, S. Buzzaccaro, and E. Secchi, “The unbearable heaviness of colloids: facts, surprises, and puzzles in sedimentation,” *Journal of Physics: Condensed Matter*, vol. 24, no. 28, p. 284109, Jul. 2012. [Online]. Available: <http://iopscience.iop.org/0953-8984/24/28/284109> 124, 126
- [137] J.-L. Barrat, T. Biben, and J.-P. Hansen, “Barometric equilibrium as a probe of the equation of state of colloidal suspensions,” *Journal of Physics: Condensed Matter*, vol. 4, no. 1, p. L11, 1999. [Online]. Available: <http://iopscience.iop.org/0953-8984/4/1/003> 124
- [138] T. Biben, J.-P. Hansen, and J.-L. Barrat, “Density profiles of concentrated colloidal suspensions in sedimentation equilibrium,” *The Journal of Chemical Physics*, vol. 98, no. 9, p. 7330, 1993. [Online]. Available: <http://link.aip.org/link/JCPSA6/v98/i9/p7330/s1&Agg=doi> 124
- [139] L. D. Landau and E. M. Lifshic, *Statistical Physics*. Oxford: Pergamon Press., 1978. 126
- [140] R. W. Nash, R. Adhikari, J. Tailleur, and M. E. Cates, “Run-and-tumble particles with hydrodynamics: Sedimentation, trapping, and upstream swimming,” *Physical review letters*, vol. 104, no. 25, p. 258101, 2010. 129
- [141] M. E. Cates and J. Tailleur, “When are active brownian particles and run-and-tumble particles equivalent? consequences for

motility-induced phase separation,” *EPL (Europhysics Letters)*, vol. 101, no. 2, p. 20010, Jan. 2013. [Online]. Available: <http://iopscience.iop.org/0295-5075/101/2/20010> 129